Vision System-based Multi-rate State Estimation and Control for Electric Vehicles

(ビジョンシステムを利用した電気自動車の
マルチレート状態推定と制御)

A Doctoral Dissertation Submitted to
The Department of Electrical Engineering
at the University of Tokyo
for the Degree of Doctor of Philosophy

By

Yafei Wang

Supervisors

Professor Yoichi Hori

Professor Hiroshi Fujimoto

Department of Electrical Engineering
The University of Tokyo
March 2013

Abstract

This work focuses on two objectives: 1) develop new and practical state estimation methodologies based on Kalman filter for systems with multi-rate and delayed measurements; 2) apply the multi-rate Kalman filter to vision-based control systems for electrical vehicles (EVs).

Vehicle electrification has become a world-widely recognized solution to the oil shortage and emission problems brought by engines-driven vehicles. Besides trying to build EVs that can be comparable with conventional vehicles, it should also be critical to have a deep understanding of the advantages and challenges brought by EVs. It is widely known that motors can response hundreds of times faster than engines and hydraulic systems. In fact, the inherent merits of EVs provide opportunities to realize advanced active safety control systems as have been already studied thoroughly during the last decade. However, motion control-related issues brought by EVs should also be emphasized for performance enhancement.

For motion control systems, real-time feedback of vehicle information is indispensible. While many vehicle states can be measured directly from cheap sensors, some of them are not readily available and therefore need to be estimated using information from the other sensors. However, different sensors may have different sampling rates and some of them are delayed. Therefore, direct fusion of different sensors may be problematic. Lots of conventional research simply down-sample the fast rate sensors to adapt slow-rate ones. On the other hand, from the viewpoint of EV control, fast feedback is preferable because the control periods of electric motors are short. Thus, unlike traditional vehicles with slower control input, multi-rate measurements can be a specific problem for EVs. Moreover, sensor measurement delays (constant or random) should also be considered in the estimator design.

Regarding the multi-rate problem, two solutions can be employed: 1) down-sample fast-rate sensors to adapt slow-rate device; 2) design multi-rate estimation algorithm without changing sensor sampling times. Although method 1 is simple and straightforward, it has to reduce the sampling rate of the whole system. In contrast, method 2 allows better estimation accuracy by full utilization of sensor information and provides faster updating rate that can match with the control periods of electric motors. The system's open-loop stability margin

can thus be increased. Meanwhile, inter-sample residuals should be considered into the estimator design to guarantee the inter-sampling convergence. For constant or uneven delays, they can be included into the estimator using augmentation method or the proposed residual estimation method. The proposed approaches can be applied to a variety of multi-rate and delay-related applications such as chemical process estimation and control, vision-based estimation and control, GPS-based estimation and control, etc.

Considering the multi-rate and delay issues, two vision-based estimation and control systems for EVs are studied with the proposed estimation algorithm: 1) body slip angle estimation and control, 2) vehicle position estimation for integrated vehicle lateral control. Vehicle body slip angle is considered as one of the key enablers for vehicle safety control. However, due to the high cost of direct measurement, estimation approach needs to be investigated. In this dissertation, a combined vehicle-vision model is proposed for body slip angle estimation using multi-rate Kalman filter, and the estimation result is more robust against vehicle parameter uncertainties compared with the traditional bicycle model-based method. With the multi-rate estimator, a two-degree-of-freedom controller is designed for body slip angle control. In the second application, using the same vehicle-vision model, vehicle lateral position to the lane marker is estimated using the proposed observer, and it is then utilized together with yaw rate for integrated vehicle lateral control. Moreover, the two applications are implemented in simulation and experiments to verify the effectiveness of the proposed approaches.

This dissertation is mainly organized into three parts: backgrounds are given from Chapter 1 to Chapter 3; the multi-rate Kalman filter theories are explained in Chapter 4; in Chapter 5 and Chapter 6, vision-based vehicle state estimation and control applications are discussed. In the Appendices, the experimental vehicle and image processing techniques for lane detection are introduced.

Acknowledgements

Three years ago, I sent an E-mail to Professor Yoichi Hori inquiring the possibility to carry out my doctoral study at his laboratory. Professor Hori kindly gave me a chance to take the entrance examination, and patiently helped me to get the VISA to Japan. Professor Hori's kindness affected me even before I met him. After entering the doctoral course, with his patient guidance, kind encouragement and critical critiques, I was able to accomplish this research and realize this dissertation. Not only on my research, Professor Hori also taught me a lot on how a good researcher and how a man should be. Here, I would like to express my infinite and deepest gratitude to Professor Yoichi Hori. In fact, I can never image how my doctoral life would be without Professor Hori's excellent advises and constant support. Most importantly, I appreciate Professor Hori for gave me the opportunity to realize my dream to further my study and to see how far I can go. Dreams, no matter big or small, are very important for young people. I do appreciate.

Meanwhile, I would like to express my sincere appreciation to another supervising professor of mine, Professor Hiroshi Fujimoto. I first met Professor Fujimoto on the first day I started my life in Japan. From then on, I benefited a lot from his advices, encouragement and critiques. He taught me not only by words, but also by the way he works. I can never forget the days he worked until mid-nights to give advices to the students; also, I cannot forget the critiques and smiles he gave to us. Just as Professor Hori, Professor Fujimoto always offers the first priority to his students with constant love. Actually, my doctoral research can hardly be realized without Professor Fujimoto's advices, and I really appreciate.

Then, I want to thank ALL of the members in Hori-Fujimoto Laboratory. However, it is very difficult to list them one by one as "Hori-Fujimoto Lab family" is huge. Thanks so much for the discussions on research, care on my life... I find it difficult to express all of my thanks to you all. Specially, I would like to thank blue-COMS team members, Binh Minh Nguyen and Palakon Kotchapansompote, for the cooperation and friendship. Moreover, I want to give my sincere thanks to the alumni of the laboratory such as Professor Chengbin Ma, Dr. Sehoon Oh, Dr. Kiyotaka Kawashima, Dr. Dejun Yin, Professor Cong Geng, Dr. Valerio Salvucci, Dr. Ryo Minaki, Dr. Kanghyun Nam, Dr. Alexander Viehweider, …, for their kind help before and during my doctoral study. Thanks so much.

Also, I want to express my appreciation to Professors Katsushi Ikeuchi, Takashi Kubota, Hiroyuki Ohsaki, and Takafumi Koseki of the University of Tokyo, who are the members of

the judging committee of my doctoral degree together with Professors Yoichi Hori and Hiroshi Fujimoto. Their constructive comments and advices in the pre-defense meeting helped me a lot to improve my research. Thank you very much.

Moreover, I would like to thank all the members of the Global Center of Excellence (GCOE) office, Electrical Engineering office and office of International Students of The University of Tokyo, for the financial support and all kinds of help. Especially, I would like thank Ms. Yoko Inoue of the GCOE office, for her kind help and care these three years. I will never forget.

Finally, I want to thank my father Wang Qi and mother Chen Yuxia. They gave me birth and love, and always encourage me to follow my heart and respect my decisions. I would like to dedicate this work to them.

Yafei Wang
Hori-Fujimoto Laboratory
The University of Tokyo
December 2012

Contents

1. Introduction 1
1.1 Research Background 1
1.1.1 Multi-rate and Delay Issues in State Estimation and Control Systems 2
1.1.2 Vision-based States Estimation and Control for EVs 6
1.2 Motivation 11
1.3 Dissertation Outline 11
2. Vehicle Lateral Dynamics and Vision System Modeling 15
2.1 Introduction 15
2.2 Vehicle Kinematic Model Considering Visual Information 16
2.3 Combined Vehicle Dynamics and Vision Kinematics-based Model 19
2.3.1 Two-degree-of-freedom Bicycle Model 19
2.3.2 Visual Model Based on Geometry 22
2.3.3 Combined Vehicle Dynamics and Vision Kinematics Model 24
2.4 Chapter Summary 25
3. State Estimation and Motion Control for Electric Vehicles 27
3.1 Introduction 27
3.2 Control Approaches 28
3.2.1 Two-degree-of-freedom (2DOF) Control 28
3.2.2 Disturbance Observer (DOB) 30
3.3 Vehicle Motion with Active Lateral Control 32
3.3.1 Active Front Steering Control 32
3.3.2 Differential Torque Control 37
3.4 Vehicle State Estimation Based on Kalman Filter 38
3.5 Stability of Kalman Filter-based Control System 39
3.6 Constrains of Observer-based Motion Control for Electric Vehicles 42
3.7 Considerations on Performance Requirements 43
3.8 Chapter Summary 44

4. Multi-rate Kalman Filter Design Considering Time Delay 45
4.1 Introduction 45
4.2 Discretizaion of Continuous Model 46
4.3 Problems Statement 48
4.3.1 Multi-rate Sampling 49
4.3.2 Time-delay 50
4.4 Multi-rate Kalman filter Design Considering Constant Measurement Delay 52
4.4.1 Augmentation of Constant Measurement Delay 52
4.4.2 Multi-rate Kalman Filter Design Based on Inter-sample Residual Estimation 55
4.4.3 Convergence Analysis 60
4.5 Multi-rate Kalman filter Design Considering Uneven Measurement Delay 62
4.5.1 Measurement Reconstruction 63
4.5.2 Inter-sample Residual Estimation 64
4.5.3 Convergence Analysis 65
4.6 Chapter Summary 69
5. Vision-based Multi-rate Estimation for Vehicle Body Slip Angle Control 71
5.1 Introduction 71
5.2 Sensor Configurations for Body Slip Angle Estimation 72
5.2.1 Traditional Sensor Configuration 1: Gyro Sensor 72
5.2.2 Traditional Sensor Configuration 2: Gyro and Lateral Acceleration Sensors 74
5.2.3 Proposed Sensor Configuration: Gyro Sensor and Vision System 74
5.3 Multi-rate Kalman Filter Design with Constant Delay Compensation for Vehicle Body Slip Angle Estimation 76
5.3.1 Augmentation of Delayed Visual Measurements 76
5.3.2 Design of Multi-rate Kalman Filter 78
5.4 Body Slip Angle Controller Design with Multi-rate Feedback 80
5.4.1 Desired Body Slip Angle 81
5.4.2 Design of 2DOF Controller 81
5.4.3 Torque Distribution Law (TDL) 82
5.5 Simulations and Experiments 83
5.5.1 Body Slip Angle Estimation 83
5.5.2 Body Slip Angle Control 86

5.6 Chapter Summary 90
6. Vision-based Multi-rate Estimation for Integrated Vehicle Lateral Control 91
6.1 Introduction 91
6.2 Infrequent and Random Delayed Visual Information 93
6.3 Multi-rate Kalman Filter Design with Uneven Delay Compensation for Integrated Vehicle Lateral States Estimation 94
6.3.1 Measurement Reconstruction 94
6.3.2 Design of Multi-rate Kalman Filter 95
6.4 Integrated Vehicle Lateral Controller with Multi-rate Feedback 98
6.4.1 Vehicle Lateral Position Controller 98
6.4.2 Yaw Motion Controller 99
6.5 Simulations and Experiments 99
6.5.1 Vehicle Lateral Position Estimation 101
6.5.2 Integrated Vehicle Lateral Control 102
6.6 Chapter Summary 105
7. Conclusions and Future Works 107
7.1 Conclusions 107
7.1.1 Multi-rate Estimation Considering Measurement Delay 108
7.1.2 Vision-based Multi-rate Estimation and Control for EVs 108
7.2 Future Works 109
Appendix A Experimental Electrical Vehicle Introduction 111
Appendix B Image Processing Techniques for Lane Detection 115
Bibliography 121
List of Publications 131

List of Figures

Fig.1. 1 A general digital control system with state estimator considering multi-rate and measurement delay issues.....2

Fig.1. 2 Electric vehilces in Hori-Fujimoto lab and in-wheel-motors.....7

Fig.1. 3 Typical onboard sensors.....8

Fig.1. 4 Commercial sensors for body slip angle measurement.....9

Fig.1. 5 Onboard vision system.....9

Fig.1. 6 Dissertation structure.....14

Fig.2. 1 Vehicle lateral kinematics model.....16

Fig.2. 2 Single track vehicle model.....19

Fig.2. 3 Bicycle model considering differential torque.....20

Fig.2. 4 Combined vehicle and vision models.....23

Fig.3. 1 General control structure for EVs.....26

Fig.3. 2 One degree of freedom (1DOF) controller.....27

Fig.3. 3 Two degree of freedom controller (Feed-forward representation).....28

Fig.3. 4 Disturbance observer structure.....30

Fig.3. 5 Equivalence representation of DOB.....30

Fig.3. 6 Frequency response of γ at different vehicle speeds (steering input).....32

Fig.3. 7 Frequency responsse of β at different vehicle speeds (steering input).....32

Fig.3. 8 Frequency responsse of y_l at different vehicle speeds (steering input).....33

Fig.3. 9 Frequency responsse of β at different vehicle speeds (differential torque input).....34

Fig.3. 10 Frequency responsse of γ at different vehicle speeds (differential torque input).....35

Fig.3. 11 Frequency responsse of y_l at different vehicle speeds (differential torque input).....35

Fig.4. 1 System sampling sequence (primary measurement with random delay).....50

Fig.4. 2 System sampling sequence (primary measurement with constant delay).....51

Fig.4. 3 Operating principle of the inter-sample residual estimation.....59

Fig.4. 4 Measurement reconstruction 63
Fig.5. 1 System sampling sequence (multi-rate and constant delay)..... 75
Fig.5. 2 Controller structure with body slip angle estimator. 79
Fig.5. 3 Simulation comparison of the body slip angle estimation based on different estimation methods (without model discrepancy). 82
Fig.5. 4 Simulation comparison of the body slip angle estimation based on different estimation methods (with model discrepancy). 82
Fig.5. 5 Estimation method comparisons based on experimental data. 84
Fig.5. 6 Simulation comparison of the controller performance based on single-rate and multi-rate Kalman filters. 85
Fig.5. 7 Experimental comparison of the controller performance 87
Fig.6. 1 Measurement sequence. 93
Fig.6. 2 Integrated lateral controller for EVs 95
Fig.6. 3 Estimation comparison in simulation. 98
Fig.6. 4 Estimation comparison based on experimental data. 99
Fig.6. 5 Steering angle input comparison. 101
Fig.6. 6 Yaw moment input for yaw rate control. 101
Fig.6. 7 Steering angle input for vehicle position control. 102
Fig.6. 8 Steering angle input for vehicle position control. 102
Fig.A. 1 Experimental vehicle COMS 108
Fig.A. 2 Structure of the experimental vehicle 109
Fig.B. 1 Structure of the experimental vehicle 112
Fig.B. 2 Geometric relationship among camera, image plane and road 113
Fig.B. 3 View from different of image plane axes 113
Fig.B. 4 Original and mapped view of the road. 115
Fig.B. 5 Image processing results 116

List of Tables

Table 1. 1 Sampling period comparisons between traditional vehicle and EV 10

Table 3. 1 Applications and Control Approaches..... 43

Table 5. 1 Stability Margin Comparison 80

Table A. 1 Vehicle Parameters..... 110

Chapter 1

Introduction

This dissertation aims at developing new state estimation methodologies that are practical for systems with multi-rate and delayed (constant or random) measurements, as well as exploring new applications of onboard vision system for electric vehicles (EVs).

In this chapter, research backgrounds of related theories and applications are first introduced thoroughly. Then, Motivations of this research are explained. Finally, outline of this dissertation is provided.

1.1 Research Background

In many engineering applications, online information of system states is a prerequisite for system health monitoring, fault diagnostics, dynamics control, etc. However, some of the states are not measurable or are too costly to be measured. Cost effective estimation approaches are therefore desired. A widely employed technique is model-based estimation method using available sensor information as measurements. Yet, in some cases, sampling rates of different sensors do not match and some of the sensor data are delayed due to processing or/and transmission, which render the state estimation not straightforward. Multi-rate and delay issues, although can be independent, exist together in many systems.

On the other hand, onboard vision devices are utilized more and more for vehicle state estimation and control systems. Meanwhile, EVs are gaining an increasing concern from both industry and research fields nowadays. Nevertheless, the sampling rate of a normal camera is much slower compared to that of the other onboard sensors and electric motors, and image processing brings delay into the visual measurements. The multi-rate and delay problems need to be addressed in the estimation and control algorithms for vision-based EV system. This chapter will introduce the backgrounds of multi-rate and delay issues, motion control systems for EV and vision-based applications for vehicles.

1.1.1 Multi-rate and Delay Issues in State Estimation and Control Systems

A general digital control system with feedback from a state estimator is shown in Fig. 1.1, where $P(s)$ is a continuous time plant with n output signals measured by different sensors, $C(z)$ is a digital controller designed for reference tracking, and $O(z)$ is an observer for immeasurable state estimation. As plants are usually affected by disturbances and sensor measurements are contaminated by noises, $d(t)$ and $w_i(t)$ (i=1,2,…) are introduced to model input disturbance and measurement noises, respectively. As a discrete control system, three time periods exit: T_r, T_u and T_y, where T_r is the reference holder, T_u is the control input holder generally decided by the speed of the actuators, the D/A converters, or the CPU loads, and T_y is the measurement holder determined by the speed of the sensors or the A/D converters [1]. In this dissertation, only T_u and T_y are considered due to the reason that T_r usually does not have restrictions. As can be seen in Fig. 1.1, in case of n measurements, more than one T_y exist, and some of them are different from T_u; this is known as the multi-rate problem [1].

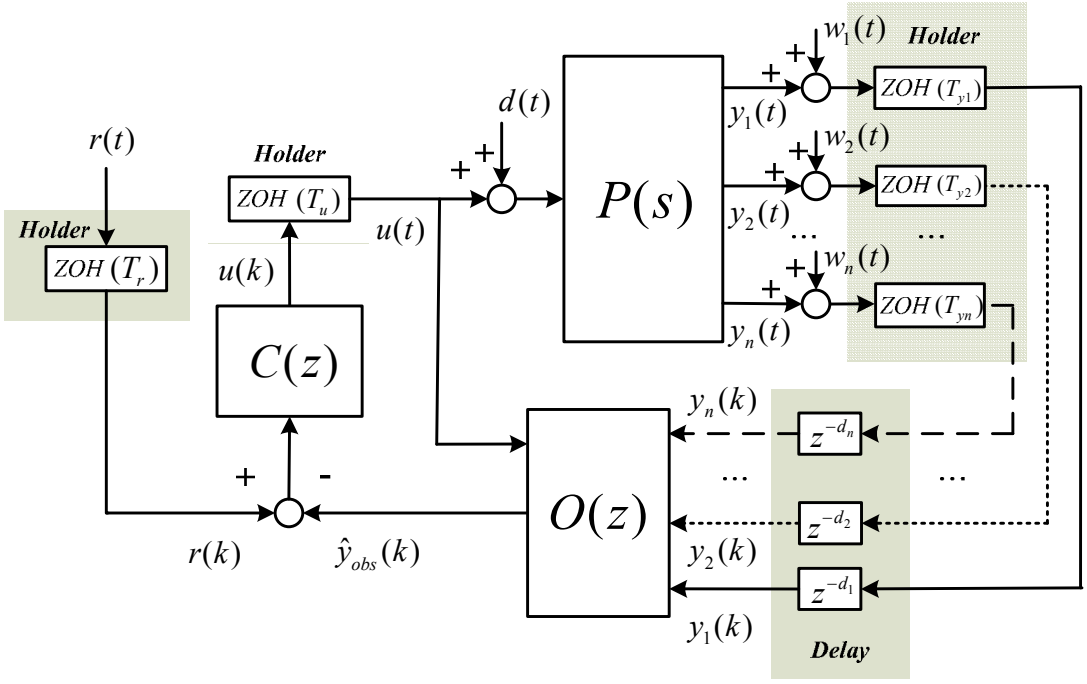

Fig.1. 1 A general digital control system with state estimator considering multi-rate and measurement delay issues.

Assume that $T_{y1} < T_{y2} < \ldots < T_{yn}$, then T_{y1} can be selected as a base and the multi-rate ratios N_i can be defined as

$$N_i = T_{yi} / T_{y1} \tag{1.1}$$

where $1 < i \le n$. Moreover, some sensor data are delayed due to the time present on communication or/and data processing. Generally, the time-delays are also different from sensor to sensor (some of them are small and hence can be neglected). In practical, the time-varying delays are assumed to be in a given finite set as

$$d_i \in \{0,1,2,...d_{\max}\} \tag{1.2}$$

where d_i=0 means no delay.

Multi-rate issue:

Multi-rate estimation and control are significant research areas motivated by engineering applications, and they have been studied for decades [2-11]. In [2], the history of the multi-rate control theory and applications were reviewed. One of the typical multi-rate examples is hard disk, where the sampling frequency of position error signal is limited. To achieve smoother control input and higher control bandwidth, Tomizuka *et al.* developed a serial of methods by redesigning the state estimator [3-7]. Under the framework of Kalman filter, they redesigned the steady state Kalman gain F_s at time step $j \cdot r$ as

$$F_s = M_s \cdot C_{T_c}^T \cdot \left(C_{T_c} \cdot M_s \cdot C_{T_c}^T + V \right)^{-1} \tag{1.3}$$

where C_{Tc} is the measurement matrix discretized by sampling time T_c, V is the measurement noise covariance, and M_s is the positive definite solution of the algebraic Riccati equation 1.4. Detailed explanations of the parameters in equation 1.4 can be found in [4].

$$\begin{aligned} M_s = {} & A_{T_c}^r \cdot M_s \cdot \left(A_{T_c}^r \right)^T + \sum_{i=0}^{r-1} A_{T_c}^i \cdot B_{wT_c} \cdot W \cdot B_{wT_c}^T \cdot \left(A_{T_c}^T \right)^T \\ & - A_{T_c}^r \cdot M_s \cdot C_{T_c}^T \cdot \left(C_{T_c} \cdot M_s \cdot C_{T_c}^T + V \right)^{-1} \cdot C_{T_c} \cdot M_s \cdot \left(A_{T_c}^r \right)^T \end{aligned} \tag{1.4}$$

In [8], Tomizuka summarized the advantages of multi-rate estimation and control for motion control systems. Meanwhile, Fujimoto and Hori *et al.* proposed Perfect Tracking Control (PTC) approach which focuses on the multi-rate reformulation of feed-forward

controller [9-11]. More recently, multi-rate theory-based hard disk control was further developed by Al-Mamun *et al* [12], Fujimoto *et al* [13] and Sato *et al* [14]. In some practical applications, the information of position and acceleration are both needed for observer design, and the position signal is usually slower compared with the acceleration one. In [15], a multi-rate-based sensor fusion algorithm is developed for motor states estimation. Interestingly, an application to civil health monitoring is studied with slow position sensor and fast acceleration sensor [16]. In addition, some chemical processes are in the scope of multi-rate estimation and control. For example, Ravindra *et al* designed an adaptive multi-rate estimator for both state and parameter estimation with application to a bioreactor [18]. Vision-based industrial robot control is another application of multi-rate theory, and it was intensively studied in [19-21]. Nowadays, GPS is becoming more and more popular in vehicles, and the sampling rate of GPS is very slow. Some research studied multi-rate-based navigation and vehicle dynamics controller [22-23]. Recently, the multi-rate theory was also expanded and applied to precise stage positioning and piezo scanner control [24-25].

Measurement delay issue:

Due to hardware restrictions, measurement delay is an inevitable problem for both estimator and controller design, and a number of methods have been proposed in the literatures [26-11]. Based on the length, delay can be categorized into constant delay and uneven delay; based on the ways for delay handling, solutions can be divided into state-augmentation type and non-augmentation type. State-augmentation methods rely on augmenting the current state with appropriate past information required for fusing the lagged measurements. One of the well-documented state-augmentation methods is fix-lag approach that stores all the past states information is for augmentation [26]. This method, although simple and straightforward, is quite computation intensive and only convenient for constant and small time delays [27]. Another state-augmented method is measurement augmentation. Instead of augmenting all the previous states, only the delayed measurements are utilized to augment with the current state for the previous time steps [28]. This method is also computational consuming if the delayed steps are large. In addition to the state-augmentation approach, some techniques latency compensation at the measurements arriving time were proposed [29-31]. The simplest way is to ignore the fact that the sensor measurements are lagged, and a normal estimator can be designed with the delayed information [29]. Obviously, this method has poor performance. Initially designed by Alexander [30] and further developed by Larsen *et al.* [31], the estimation accuracy can be improved by designing suitable filter covariance. This method requires the measurement sensitivity matrix and the observation noise covariance matrix to

be available. Assume that the measurement is taken at step l and is only available at step s, the filter covariance is then updated at time l as if the measurement is already available. This leads the measurements in the delay period to be fused as if the measurement had been fused at step l. At step s, when the measurement really becomes available, incorporating the measurement correctly is then simplified by modifying the Kalman gain as M given in equation 1.5.

$$M = \prod_{i=0}^{N-1} \left(I - K'_{k-i} \cdot C_{k-i} \right) \cdot A_{k-i-1} \tag{1.5}$$

where N is the delayed steps and K' represents the Kalman gain calculated with the covariance of the delayed measurement at step l. This implies that the covariance estimates of the filter will be wrong before the delayed measurement arrives, causing normal non-delayed measurements during this period to be fused sub-optimally. However, after the addition of correction with the modified Kalman gain given in equation 1.5, the filter state and covariance will once again be optimal. Such algorithm requires minimal computational effort and can also be used for time varying delays; an equivalent technique can be found in [32], which was designed for GPS delay compensation. Some other research compensated the delay using disturbance observer by considering the time-varying communication delays as disturbances [33].

Interestingly, another type of estimation method named predicting observer can solve the delay issue inherently [109], and it was utilized for motor control using information from a camera [17]. Unlike current type observer that uses the current measurement for current estimation correction, the predictive type observer uses measurement sampled one step before to correct the estimation. Therefore, measurement delay does not have effect on this kind of observer as only previous sampled data are used. However, it should be noted that the estimation is likely to be less accurate than correction by the current type observer [109]. It should be noticed that, Kalman filter belongs to the current type observer.

Combined multi-rate and delay issue:

Although not as many as research on multi-rate and time-delay separately, some studies addressed the multi-rate and delay issues together [34]-[35]. In fact, vision-based applications involve both multi-rate and delay issues. In [34], a vision-based satellite state estimation using multi-rate Kalman filter was developed, but the inter-sampling performance was not addressed; the image processing delay, although discussed in somehow, was not included.

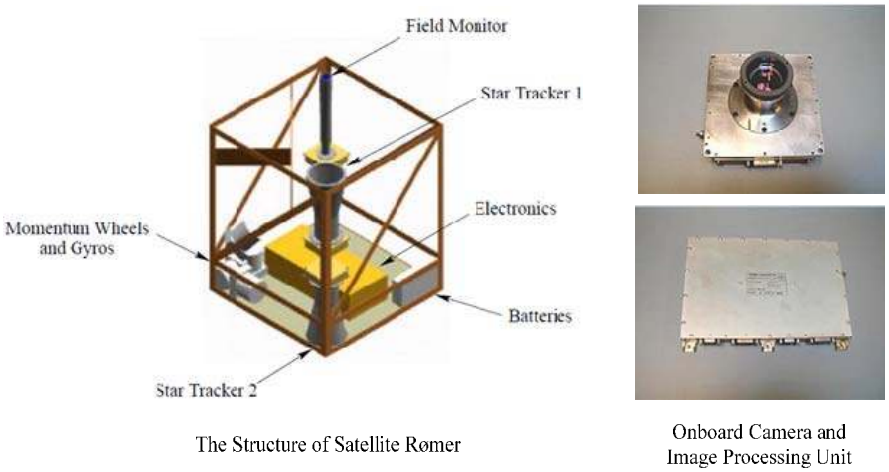

Fig.1. 2 The sattelite Rømer and its onboard vision system.

The satellite and its onboard vision system are shown in Fig. 1.2, the sampling time of the star-track camera is 332 ms and the image processing unit takes 170 ms to process one frame [34]. Gopalakrishnan *et al* summarized literatures on state estimation considering multi-rate or/and delay, and applied some of them to chemical process estimation [35]. One latest paper was published by Bavdekar *et al*, a moving window Ensemble Kalman Filter (EnKF) was developed by considering appropriate matrix covariance [36]. The moving window EnKF does not need state augmentation and therefore reduces the computation burden. To ensure that the estimate updates do not exceed the physical limits, a constrained moving horizon EnKF was also proposed. The use of a moving window of measurements guarantees that the delayed measurements can be appropriately placed in the window and hence be used along with the fast rate measurements for state estimation. However, this method is complex for implementation.

Generally speaking, the combined multi-rate and delay issue can be solved in two ways: 1) augment the system state with delayed information and then apply multi-rate estimation algorithm; 2) treat multi-rate and delay as a whole and design the estimator in a one step manner. The two methods will be further explained in the following chapters.

1.1.2 Vision-based State Estimation and Control for EVs

Estimation and control technologies have been intensively studied for vehicle applications during the last few decades due to the desire for performance, comfort and economy.

Considering the uniqueness of EVs such as fast control period, vision-based estimation and control for body slip angle and vehicle lateral motion are studied in this dissertation. Two basic concepts relate to the applications that are studied in this dissertation: 1) motion control; 2) sensing and estimation.

Motion control technologies for EVs:

Nowadays, actuators such as active steering system (AFS), four wheel steering (4WS), four wheel driving (4WD) and differential braking are available in more and more vehicles. Using these actuators, a variety of functions for vehicle stabilization can be achieved: anti-lock brake system (ABS), electronic stability control (ESC), traction control system (TCS), lane keeping control (LKC) and so on.

In case of EVs with in-wheel-motors (IWMs), many safety control systems can be realized more effectively and conveniently. From the viewpoint of motion control, EVs' advantages have been summarized as four points [38]-[40]: 1) motor torque response is tens to hundreds times faster than that of an internal combustion engine and hydraulic actuators. This feature enables high performance tire adhesion controls such as anti-slip control and traction force control; 2) motor torque can be measured easily by observing motor current, and it can be used for road condition and driving force estimation; 3) since an electric motor is compact and inexpensive, it can be equipped in each wheel, which realizes high performance lateral motion control systems including roll stability control, yaw stability control and integrated control system; 4) there is no difference between acceleration and deceleration control, which means the wheels can be controlled freely to generate desired motion. Fig. 1.3 shows some of the EVs in Hori-Fujimoto laboratory and an image of an in-wheel-motor.

Fig.1. 3 Electric vehilces in Hori-Fujimoto laboratory and an in-wheel-motor.

Utilizing the aforementioned advantages of IWMs, control algorithms have been developed in areas such as safety, drivability and economy. For example, in [41], a controller is designed to operate the vehicle at a desired yaw rate, and it was verified by field test. More recently, range extension system (RECS) that controls the IWMs at some specific operation ranges is developed in practice [42]-[43]. In some other research, considering the multiple actuators, control allocation approaches [46]-[50] and fault detection and tolerance control systems [44]-[45] are gaining an increasing interest lately.

Sensing and estimation:

To realize motion control system, on-line information of vehicle states and parameters is indispensable. Therefore, along with the development of semiconductor industry, onboard sensors such as gyro sensor, acceleration sensor, encoders can be found in more and more vehicles. Fig. 1.4 shows some typical sensors available for vehicles.

While many vehicle states can be readily obtained from inexpensive sensors, some of the states are too expensive to be measured directly, and body slip angle is one of them. Body slip angle is defined as the difference between the direction that the car is heading and direction that it is travelling, and it is useful in many vehicle stability control systems [51]-[60]. Unfortunately, the costs of commercial sensors to measure body slip angle such as

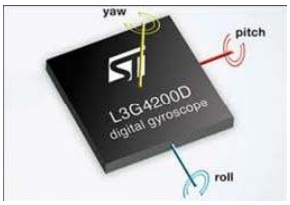

Gyro Sensor: from ST

Steering Angle Sensor: from Nissan

GPS: from JRC

Wheel Encoder: from Oxford Technical Solutions

Fig.1. 4 Typical onboard sensors.

Optical Sensor: from Datron Dynamics　　DGPS-based Sensor: from VBOX

Fig.1. 5 Commercial sensors for body slip angle measurement.

Onboard Camera: from Nissan　　Onboard Stereo Camera: from Subaru　　Night Vision System: from BMW

Fig.1. 6 Onboard vision system.

optical sensor and DGPS-based device (as shown in Fig. 1.5) are very high. Therefore, a variety of methods have been developed using the information from cheap sensors for body slip angle estimation. Basically, estimation involves three aspects: sensor configuration, estimation model, and estimation method. Sensor configuration means the combination of different kinds of available sensors to estimate the unknown information. In fact, to estimate one piece of information, several kinds of sensor combination can be employed. Estimation model can be kinematic, dynamic or the combination of them. It is a concept related to sensor configuration, i.e., if system model is selected, the sensor configuration is fixed in somehow. Estimation method is the algorithm to implement estimator, for example, it can be Lunberger observer, Kalman filter, particle filter, and so on.

In addition to know the status of the vehicle itself, surrounding information also plays key role for vehicle safety and stability. Onboard vision system is one of the effective ways to

obtain information around the vehicle, and most of them are developed for lane departure warning, automatic driving, collision avoidance, and so on [61]-[64]. Nowadays, cameras can be easily found in many vehicles of all levels. Fig. 1.6 shows some of the onboard vision system. For example, Subaru employed stereo vision systems to assist the driver for safe driving such as automatic obstacle avoidance.

Vision-based estimation and control for EVs:

As introduced above, estimation and control of traditional vehicles using onboard camera have been intensively studied. Unfortunately, vision-based estimation and control considering multi-rate and delay issues can hardly be found in the exiting literatures. Meanwhile, just like traditional vehicles, onboard vision systems are important for EV motion control applications. The sampling time comparisons between traditional vehicle and EV are given in Table 1.1, where T_u is the control input period, T_{y_normal} is the sampling time of normal onboard sensors such as gyroscope and encoder, and $T_{y\_caemera}$ is the sampling time of onboard camera. In case of traditional vehicle, as the control period is relatively long, the feedback signals just need to be adapted to it [63]. On the other hand, the control period of EV is short and the sampling discrepancy among camera, normal onboard sensors and motors have to be considered for estimator and controller implementation.

As look-ahead cameras have increasingly become popular in vehicles, investigating other applications other than lane keeping or collision avoidance using the onboard vision system is desirable. This dissertation investigates a vision-based body slip angle estimation method, and the visual model is independent of the uncertain parameters of the vehicle, such as cornering stiffness. Moreover, vehicle position measurement from the vision system is very accurate [61]. Therefore, incorporating visual information can increase the estimator's design freedom without introducing uncertainties into it. In addition, traditional lane keeping or yaw motion control only cannot satisfy the demand for driving safety, and an integrated vehicle lateral motion stabilizing system is desired. Both of the above two applications have to consider the multi-rate and delay (constant or random) issues.

Table 1. 1 Sampling period comparisons between traditional vehicle and EV

	T_u	T_{y_normal}	T_{y_camera}
Traditional Vehicle	*Long*	*Short*	*Long*
EV	*Short*	*Short*	*Long*

1.2 Motivation

As aforementioned, multi-rate and delay issues are very common in various engineering applications. However, many of the existing solutions are only designed for multi-rate or delay problem independently. Some of the methods that deal with both issues are very complicated or have high computation costs. One of the objectives of this dissertation is to construct a new and computational efficient algorithm for practical implementations.

Look-ahead cameras have increasingly become popular in vehicles, and most of the studies focus on lane keeping or collision avoidance. Investigating other applications using onboard vision system is desirable. Meanwhile, as stated in 1.1.2, real time vehicle state information such as body slip angle is of particular importance for vehicle control system. However, traditional vehicle dynamic model-based observers are not robust against model uncertainties. The first application investigated in this dissertation is vision-based body slip angle estimation method. The vision model is independent of the uncertain parameters of the vehicle, such as cornering stiffness. Moreover, vehicle position measurement from the vision system is very accurate [61]. Therefore, incorporating visual information can increase the estimator's design freedom without introducing uncertainties into it. To compensate the multi-rate and delayed visual measurements, inter-sample residual estimation methodology is applied.

In addition, as traditional lane keeping or yaw motion control only cannot satisfy the demand for driving safety (explained in Chapter 6), an integrated vehicle lateral stabilizing system is desired. The second application considered in this dissertation is a vision-based integrated vehicle lateral control system that considers position and motion together. As the position and motion feedback are of different rates, just as the previous application, multi-rate and delay issues are also addressed in the estimation and control design.

1.3 Dissertation Outline

The outline of this dissertation is illustrated in Fig. 1.7. It covers multi-rate estimation and control theory, as well as vision-based estimation and control applications for EVs. The details of this dissertation are summarized as follows:

1) **Research background**:

In Chapter 1, background of the research on both multi-rate and delay theories, as well as vision-based state estimation and control for EVs were described, and relevant literatures are categorized and reviewed. Dissertation motivation and structure are also explained.

In Chapter 2, a kinematic model is first introduced, and then, a combined vehicle and vision model is developed and analyzed. The kinematic exhibits good performance at low speed, and the combined model works better at high speed.

In Chapter 3, control approaches such as two-degree-of-freedom control, disturbance observer are introduced, and then, vehicle motions with different actuators are analyzed. Then, Kalman filter is introduced as an effective method for vehicle state estimation. Finally, constrains of observer-based control and performance requirements for EV motion control systems are explained.

2) **Estimation theories considering multi-rate and delayed measurements**:

In Chapter 4, a residual estimation technique is developed for state estimation with multi-rate and delay issues. First, the system discretization method is introduced. Then, multi-rate Kalman filter based on state augmentation is designed for estimation with multi-rate and constant delayed measurements, and the convergence performance is analyzed. And then, the multi-rate Kalman filter considering uneven delay is studied using measurement reconstruction method and inter-sample residual estimation algorithm and, the convergence performance is also analyzed. This chapter provides a general solution to the state estimation with multi-rate and delay problems.

3) **Vision-based estimation and control applications for EVs**:

In Chapter 5, a new sensor configuration for body slip angle estimation is investigated. As the visual model is accurate and increases observer's design freedom, the combined model-based estimator proposed in Chapter 2 can provide more accurate estimation result compared with the traditional bicycle model-based one. However, two issues are raised by the combined vehicle and vision models: 1) image processing introduces delay into the visual measurements and 2) the sampling time of a normal camera is much longer than that of other onboard sensors. For electric vehicles, the control period of motors is much shorter than the sampling time of a

normal camera. Considering the above-mentioned delay and multi-rate problems, a multi-rate Kalman filter with inter-sample compensation is designed. Then, a 2DOF controller is designed using the estimated body slip angle as feedback for reference tracking. With the proposed multi-rate estimator, the controller achieves better tracking performance than the single-rate method.

In Chapter 6, considering the importance of vehicle lateral control, an integrated control system that addressing both vehicle motion and position is proposed. However, the feedback signals of vehicle position and motion have different rates. How to unify the sampling rates of the two feedback loops becomes a problem. Employing the multi-rate Kalman filter developed in Chapter 4, an estimator that can update vehicle position more frequently is designed, and the updating rate can match with the rate of control input. Finally, the estimated vehicle lateral offset and yaw rate are controlled using an integrated motion and position controller..

4) **Conclusions and appendices**:

In Chapter 7, dissertation summary and future works are stated. Additionally, the experimental setups are introduced in Appendix A, and image processing techniques for lane detection are elaborated in Appendix B.

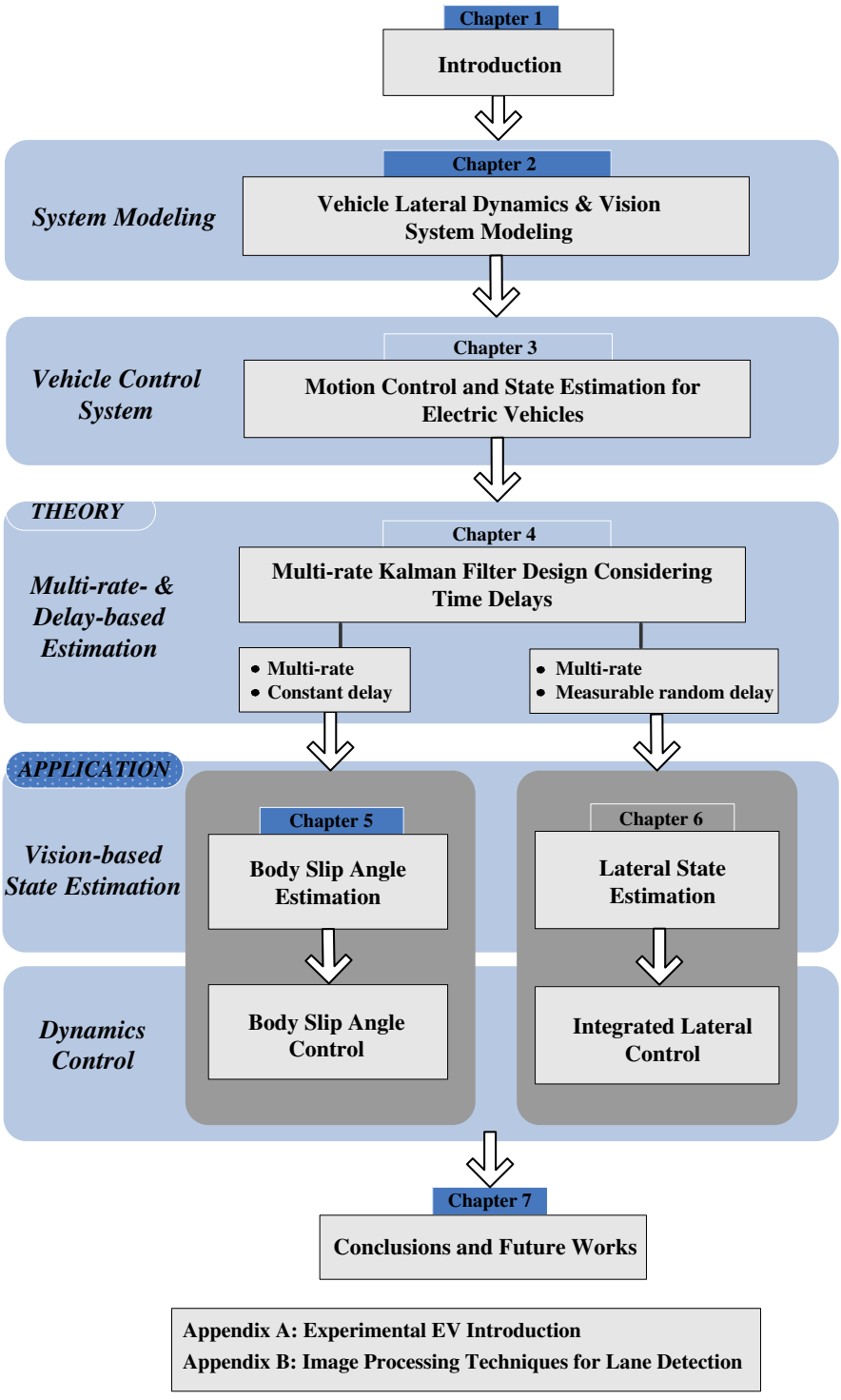

Fig.1. 7 Dissertation structure.

Chapter 2

Vehicle Lateral Dynamics and Vision System Modeling

This chapter covers modeling of vehicle lateral dynamics and vision system for estimator and controller design. After introduction of current available models for vehicle system, a nonlinear vehicle kinematic model including visual information is introduced. Then, a more suitable linear model for high speed application is described. The second model is a combination of vehicle dynamics and vision kinematics. Finally, this chapter is summarized briefly.

2.1 Introduction

Vehicle lateral model mainly address the vehicle motion and onboard vision system model describes the relationship between vehicle and the road (vehicle position with reference to the road). Both of them have their own characteristics. However, as they work as a system, for the benefits of state estimation and control, a combined model is required. Modeling of vehicle and vision system is quite mature, and a variety of models have been developed based on different assumptions for different kinds of applications.

Generally, the available vehicle models can be categorized into two groups based on the purpose. The first kind of models tries to include all the relevant characteristics of vehicle lateral dynamics, and they are developed to approximate the vehicle plant for estimator/controller performances evaluation. However, although this kind of models describes true plant very well, they are usually too complex to be implemented in real time. Instead, another kind of models simplifies complex models and only captures the essential features of the vehicle lateral dynamics, and therefore can be applied for on-line estimation/control.

On the other hand, a four wheels vehicle can be modeled that the two front and two rear

wheels are considered as one single front and one single rear wheel. This type of models is known as a single track model or bicycle model [65]-[66]. Based on this concept, it is possible to further design both kinematic and dynamic vehicle models. This chapter will explain the two types of models, and both of them cover dynamics/kinematics for vehicle and vision system. That is, the models not only deal with the vehicle itself, but also address the interaction between the vehicle and the road. These models can therefore broaden the concept of vehicle motion control in comparison with the traditional bicycle ones.

2.2 Vehicle Kinematic Model Considering Visual Information

Kinematic model describes vehicle motion on a planar geometrically without considering the affection of forces. When vehicle run at small velocities, the lateral forces generated by the tires are very small; it is then reasonable to neglect tire forces by assuming zero tire slip angles. Consider a front steering vehicle in Cartesian coordinates (X, Y) with camera mounted

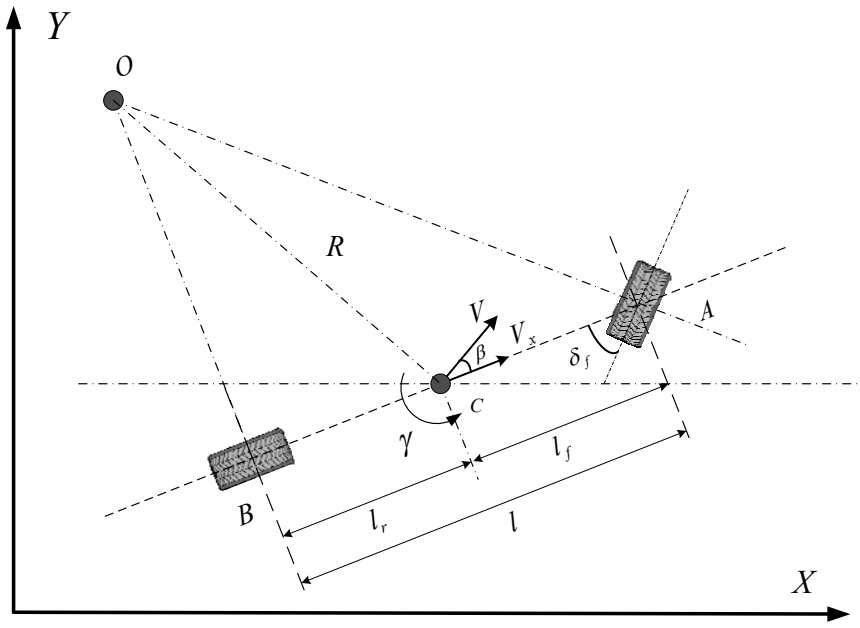

Fig.2. 1 Vehicle lateral kinematics model.

in the vehicle's center of gravity (CoG) as shown in Fig. 2.1, three coordinates are required to describe the motion of the vehicle: X, Y and Ψ, where (X, Y) are inertial coordinates of the CoG and Ψ represents the heading angle of the vehicle. The velocity at the CoG of the vehicle and the longitudinal velocity are denoted as V and V_x, respectively, and the body slip angle β is defined as the angle between the two vectors. The front steering angle is denoted by δ_f, and it is the angle between the wheel pointing and the longitudinal axis of the vehicle of the front wheel. The point O is the instantaneous rotation center of the vehicle, and it is defined by the intersection of the lines AO and BO, which are perpendicular to the orientations of the front and rear wheels. R is defined as the vehicle's traveling radius which equals to the length of the line OC, and V is perpendicular to the line OC as can be observed in the figure.

With the simplified kinematic model, governing equations can be derived as below. First, based on geometry, the vehicle's longitudinal motion and lateral motion in the Cartesian coordinates can be described as Equations 2.1 and 2.2.

$$\dot{X} = V \cdot \cos(\beta + \psi) \tag{2.1}$$

$$\dot{Y} = V \cdot \sin(\beta + \psi) \tag{2.2}$$

Then, according to the triangle sine theorem, equation 2.3 can be obtained for the triangle OCA.

$$\begin{aligned} \frac{l_f}{R} &= \frac{\sin\left(\delta_f - \beta\right)}{\sin\left(\pi/2 - \delta_f\right)} \\ &= \frac{\sin\left(\delta_f\right) \cdot \cos\left(\beta\right) - \cos\left(\delta_f\right) \cdot \sin\left(\beta\right)}{\cos\left(\delta_f\right)} \\ &= \tan\left(\delta_f\right) \cdot \cos\left(\beta\right) - \sin\left(\beta\right) \end{aligned} \tag{2.3}$$

Similarly, equation 2.4 can be derived for the triangle OCA.

$$\frac{l_r}{R} = \sin\left(\beta\right) \tag{2.4}$$

Adding equations 2.3 and 2.4 yields equation 2.5.

$$\frac{l_f + l_r}{R} = \frac{l}{R} = \tan\left(\delta_f\right) \cdot \cos\left(\beta\right) \tag{2.5}$$

Assume that the R changes slowly due to the low vehicle speed, then the yaw rate of the vehicle is equal to the angular velocity of the vehicle, which is given as

$$\dot{\psi} = \frac{V}{R} \tag{2.6}$$

As equation 2.6 contains R which is usually not measurable, considering the body slip angle β is small, equation 2.7 can be got from equations 2.5 and 2.6 as below

$$\dot{\psi} = \frac{V}{l}\tan\left(\delta_f\right) \tag{2.7}$$

Combining equations 2.1, 2.2 and 2.7 yields a nonlinear continuous state space equation given in equation 2.8. As can be observed, this model is very simple and the tire forces are not included in the formulation.

$$\begin{bmatrix} \dot{X} \\ \dot{Y} \\ \dot{\psi} \end{bmatrix} = \begin{bmatrix} V \cdot \cos(\beta + \psi) \\ V \cdot \sin(\beta + \psi) \\ \dfrac{V}{l}\tan\left(\delta_f\right) \end{bmatrix} \tag{2.8}$$

The vehicle kinematic model can be discretized for extended Kalman filter design. In this model, the vehicle position information is included, and therefore can be directly utilized for combined motion and position estimation and control applications. An example is elaborated in [67] for robot navigation.

A velocity encoder can be mounted on the vehicle drive shaft for measurement of wheel speed (not vehicle speed). The two values are unequal if the wheels are spinning or skidding. To compensate for some of these effects a wheel radius state can be added to the state vector as studied by [105].

2.3 Combined Vehicle Dynamics and Vision Kinematics-based Model

At high speed region, the lateral forces at each wheel can no longer be neglected. Moreover, as stated before, in case of EVs with IWMs, the differential forces generated by left and right wheels can be utilized for EV motion control. However, it is not straightforward to include differential torques the in the kinematic model described in section 2.2 (transformation from yaw moment to vehicle heading angle or steering angle is needed). In this case, instead of a kinematic model, a dynamics-based model to better describe vehicle lateral motion should be considered. In fact, the model given here is combined of vehicle lateral dynamics and visual kinematics.

2.3.1 Two-degree-of-freedom Bicycle Model

Again, the bicycle model mentioned before is utilized for derivation of the vehicle dynamics-based model. For lateral dynamics representation, two freedoms are considered: vehicle lateral motion and yaw motion. The two-degree-of-freedom model is shown in Fig. 2.2, where γ is the yaw rate at CoG, V_y is the lateral velocity at CoG, F_{yf} and F_{yr} represent the lateral forces on the front and rear wheels, respectively, α_f and α_r denote the tire slip angles of the front and rear wheels, respectively. The other parameters are the same as the ones in the previous section.

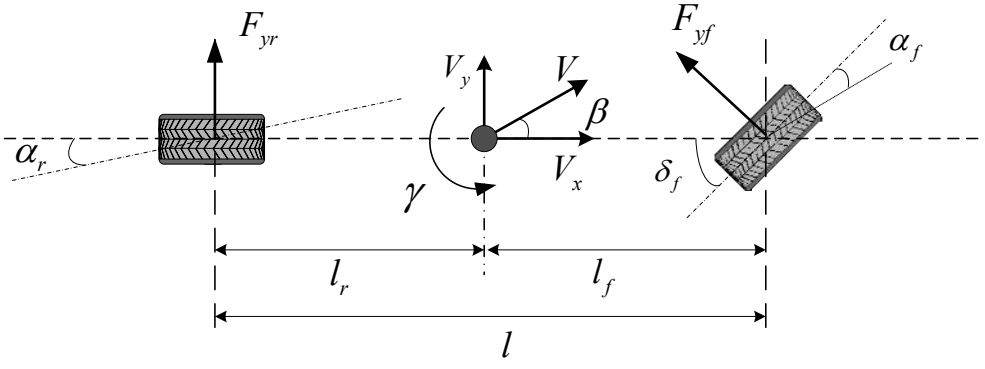

Fig.2. 2 Single track vehicle model.

The governing equations of lateral and yaw motions are given as

$$m \cdot a_y = F_{yf} + F_{yr} \tag{2.9}$$

$$I_z \cdot \dot{\gamma} = l_f \cdot F_{yf} - l_r \cdot F_{yr} \tag{2.10}$$

Where a_y is the lateral acceleration at CoG, and I_z is the yaw inertial of the vehicle. The lateral acceleration a_y can be given as equation 2.11.

$$a_y = V \cdot \left(\dot{\beta} + \gamma \right) \tag{2.11}$$

Then, the lateral forces at each axis need to be obtained for further derivation. Some assumptions need to be made before moving on: 1) tire side slip angles are small and the lateral tire forces are therefore proportional to the side slip angles; 2) vehicle velocity is approximately constant and the body side slip angle at the CoG is small; 3) lateral load transfer due to lateral acceleration is neglected.

Based on the above assumptions, the lateral forces are modeled as

$$F_{yf} = -2 \cdot C_f \cdot \alpha_f \tag{2.12}$$

$$F_{yr} = -2 \cdot C_r \cdot \alpha_r \tag{2.13}$$

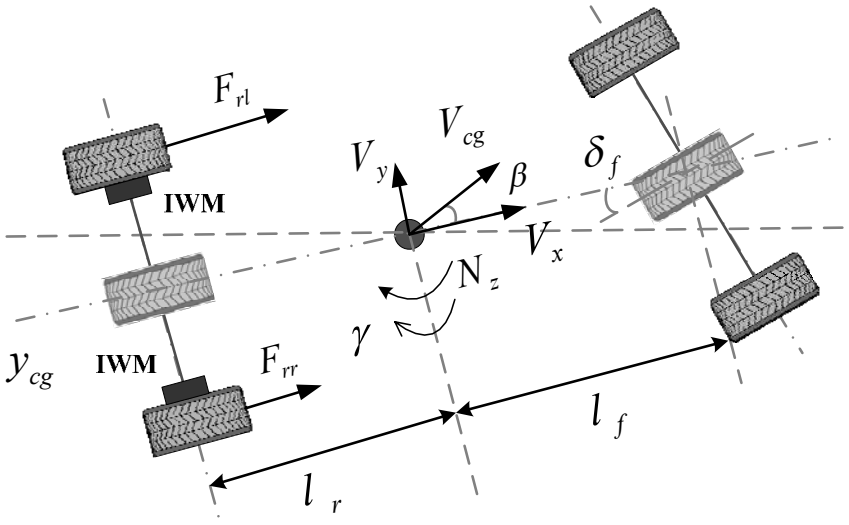

Fig.2. 3 Bicycle model considering differential torque.

where C_f and C_r are the cornering stiffness of the front and rear tires, respectively. The front tire side slip angle α_f and rear tire side slip angle α_r are given as equations 2.14 and 2.15.

$$\alpha_f = \frac{l_f \cdot \gamma + V_y}{V} - \delta_f = \beta + \frac{l_f \cdot \gamma}{V} - \delta_f \tag{2.14}$$

$$\alpha_r = \beta - \frac{l_r \cdot \gamma}{V} \tag{2.15}$$

Combining equations from 2.9 to 2.15, the bicycle model on a planar can be obtained:

$$m \cdot V \cdot \left(\dot{\beta} + \gamma\right) = -2 \cdot C_f \cdot \left(\beta + \frac{l_f \cdot \gamma}{V} - \delta_f\right) - 2 \cdot C_r \cdot \left(\beta - \frac{l_r \cdot \gamma}{V}\right) \tag{2.16}$$

$$I_z \cdot \dot{\gamma} = -2 \cdot C_f \cdot \left(\beta + \frac{l_f \cdot \gamma}{V} - \delta_f\right) \cdot l_f + 2 \cdot C_r \cdot \left(\beta - \frac{l_r \cdot \gamma}{V}\right) \cdot l_r \tag{2.17}$$

However, it should be noticed that, in case of EVs with IWMs as illustrated in Fig. 2.3, the differential torque should also be included. Equation 2.17 then becomes

$$I_z \cdot \dot{\gamma} = -2 \cdot C_f \cdot \left(\beta + \frac{l_f \cdot \gamma}{V} - \delta_f\right) \cdot l_f + 2 \cdot C_r \cdot \left(\beta - \frac{l_r \cdot \gamma}{V}\right) \cdot l_r + N_z \tag{2.18}$$

where N_z is the differential torque generated by left and right wheels, and it works as control input for vehicle stabilization.

Equations 2.16 and 2.18 can be formulated in the state space form in equation 2.19. This model is usually employed to construct observers for body slip angle estimation [56]-[59].

$$\begin{bmatrix} \dot{\beta} \\ \dot{\gamma} \end{bmatrix} = \begin{bmatrix} -\frac{2 \cdot \left(C_f + C_r\right)}{m V_x} & -1 - \frac{2 \cdot \left(C_f l_f - C_r l_r\right)}{m V_x^{\,2}} \\ \frac{2 \cdot \left(C_r \cdot l_r - C_f \cdot l_f\right)}{I_z} & -\frac{2 \cdot \left(C_f l_f^2 + C_r l_r^2\right)}{I_z \cdot V_x} \end{bmatrix} \cdot \begin{bmatrix} \beta \\ \gamma \end{bmatrix} + \begin{bmatrix} \frac{2 \cdot C_f}{m \cdot V_x} & 0 \\ \frac{C_f \cdot l_f}{I_z} & \frac{1}{I_z} \end{bmatrix} \cdot \begin{bmatrix} \delta_f \\ N_z \end{bmatrix} \tag{2.19}$$

For the observation model, as yaw rate information can be obtained from gyroscope which is very cheap, a generally utilized observation model is as equation 2.20.

$$\gamma = \begin{bmatrix} 0 & 1 \end{bmatrix} \cdot \begin{bmatrix} \beta \\ \gamma \end{bmatrix} \tag{2.20}$$

Another measurement model not only use yaw rate, but also employ the lateral acceleration information, i.e., two measurements are available in the observation model. This model is shown in equation 2.21. This model can increase design of freedom of the observer due to the adding of one additional measurement. Moreover, unobservability issue can be avoided by using this model which will be discussed in Chapter 5. However, as can be seen, model uncertainties such as cornering stiffness are also included which may influence the final estimation results.

$$\begin{bmatrix} \gamma \\ a_y \end{bmatrix} = \begin{bmatrix} 0 & 1 \\ -\dfrac{2 \cdot \left(C_f + C_r \right)}{m} & -\dfrac{2 \cdot \left(C_f l_f - C_r l_r \right)}{m V_x} \end{bmatrix} \cdot \begin{bmatrix} \beta \\ \gamma \end{bmatrix} + \begin{bmatrix} 0 & 0 \\ \dfrac{2 \cdot C_f}{m} & 0 \end{bmatrix} \cdot \begin{bmatrix} \delta_f \\ N_z \end{bmatrix} \tag{2.21}$$

2.3.2 Visual Model Based on Geometry

The vehicle dynamic model is independent of road reference, whereas the vision model is obtained from the geometric relationship between the vehicle and the road. The vision model is schematically illustrated in Fig. 2.4, where the camera is located at the vehicle's CoG, l_{pre} is the fixed preview distance of the vision system that needs to be calibrated beforehand, y_l is the lateral offset at that preview point, ψ denotes the heading angle, y_{cg} is the lateral offset at the vehicle's CoG, and the gray borders are the lane makers. In this model, assumptions that the vehicle travels along a straight road and that the onboard vision system detects the lane and provides relative position information were made.

Compared with bicycle model, several new parameters are added. Among them, an important one is the preview distance l_{pre}, and it works as a damping factor for control systems such as lane keeping [68]. The information detected by the onboard vision system are y_l (lateral distance at the preview point) and ψ (vehicle heading angle). In case of zero preview distance, y_l equals the lateral distance to lane at the vehicle's CoG (y_{cg}). The effects of preview distance on vehicle control performances were studied by [106]-[107].

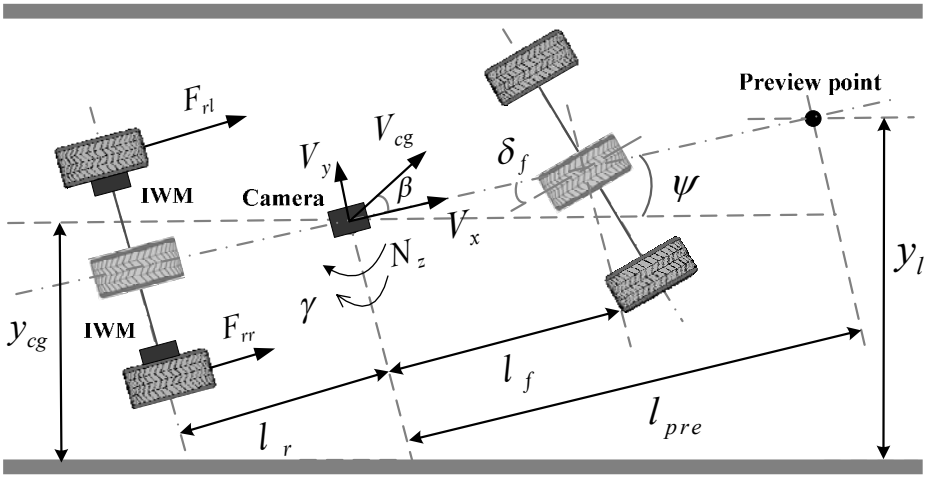

Fig.2. 4 Combined vehicle and vision models.

To derive the vision model, ψ and β are assumed to be small. Based on Fig. 2.4, y_l is approximated as

$$\begin{aligned} y_l &= y_{cg} + l_{pre} \cdot \sin\psi \\ &\approx y_{cg} + l_{pre} \cdot \psi \end{aligned} \tag{2.22}$$

Then, y_{cg} is derived as equation 2.23 based on geometry.

$$\begin{aligned} \dot{y}_{cg} &= V_{cg} \cdot \sin(\beta + \psi) \\ &= V_x / \cos(\beta) \cdot \sin(\beta + \psi) \\ &\approx V_x \cdot (\beta + \psi) \end{aligned} \tag{2.23}$$

The final equation that describes the body slip angle, yaw rate, and heading angle is obtained by taking the derivative of equation 2.22 and substituting equation 2.23 into it.

$$\dot{y}_l = V_x \cdot \beta + l_{pre} \cdot \gamma + V_x \cdot \psi \tag{2.24}$$

From equation 2.24, it can be known that, the derivative of offset at the preview point, i.e., lateral velocity at that point, comprises three parts: the lateral velocity of CoG, the components of yaw rate, and the component of longitudinal speed (resulted from vehicle heading angle).

Heading angle ψ can be simply modeled as the integration of the yaw rate as equation 2.25.

$$\dot{\psi} = \gamma \tag{2.25}$$

Here, it should be noticed that the course angle c and heading angle are different concepts, and the course angle is defined as equation 2.26 [69]-[70].

$$c = \psi + \beta \tag{2.26}$$

Although curved roads are not considered here, the system can still be modeled in the same manner by taking the curvature into account [68]. That is, this research can be expanded to all roads with lane markers.

2.3.3 Combined Vehicle Dynamics and Vision Kinematics Model

Equations 2.16, 2.18, 2.24 and 2.25 yield a new system that is represented in a continuous state space form as equation 2.27. The first two states are modeled by the vehicle model, and the latter two are modeled by the vision model. Clearly, the vision model contains much fewer uncertainties compared with the bicycle model. In the combined vehicle and vision models, the measurable outputs are yaw rate, vehicle heading angle, and lateral offset at the preview point. The body slip angle is still observable using only visual information, which provides estimation redundancy.

$$\begin{aligned} \dot{x} &= A \cdot x + B \cdot u \\ y &= C \cdot x \end{aligned} \tag{2.27}$$

where

$$B = \begin{bmatrix} \dfrac{2C_f}{mV_x} & \dfrac{2C_f l_f}{I} & 0 & 0 \\ 0 & \dfrac{1}{I} & 0 & 0 \end{bmatrix}^T, \quad C = \begin{bmatrix} 0 & 1 & 0 & 0 \\ 0 & 0 & 1 & 0 \\ 0 & 0 & 0 & 1 \end{bmatrix},$$

$$x = \begin{bmatrix} \beta & \gamma & \psi & y_l \end{bmatrix}^T, \quad u = \begin{bmatrix} \delta_f & N_z \end{bmatrix}^T, \quad y = \begin{bmatrix} \gamma & \psi & y_l \end{bmatrix}^T,$$

$$A = \begin{bmatrix} -\frac{2(C_f + C_r)}{m V_x} & -1 - \frac{2(C_f l_f - C_r l_r)}{m V_x^2} & 0 & 0 \\ -\frac{2(C_f l_f - C_r l_r)}{I} & -\frac{2(C_f l_f^2 + C_r l_r^2)}{I V_x} & 0 & 0 \\ 0 & 1 & 0 & 0 \\ V_x & l_{pre} & V_x & 0 \end{bmatrix}.$$

In case of curved roads, the road curvature can be included into the system as an additional term. For state estimation and controller design, it can be considered as a disturbance. Related research can be referred in [63], [68].

2.4 Chapter Summary

This chapter introduced two models addressing vehicle lateral motion and visual information:

- Pure vehicle kinematic model;
- Combined vehicle dynamics and vision kinematics model.

The first model considers vehicle lateral motion on a planar and provides three equations of motion purely based on geometric relationships. In terms of state estimation, since there are only three states, the calculation burden is not high. Yet, it is only useful for very low speed applications. The second model discussed in this chapter is based on vehicle dynamics and vision kinematics, and it can better describe the vehicle behavior at high speed region. The two models can be employed for vision-based vehicle state estimation and control systems such as lateral speed estimator, vehicle lateral position and heading angle estimation, lane keeping control, etc. Moreover, the combined model can be applied to vehicle lateral dynamics control.

Chapter 3

State Estimation and Motion Control for Electric Vehicles

This chapter first explains the general structure of EV control system which includes upper layer control, lower layer control and signals feedback. Then, two effective control approaches are introduced. And then, vehicle motion controls in terms of actuators are analyzed followed with introduction to state estimation. Constrains of observer-based feedback and vehicle performance requirements are then explained. Finally, this chapter is summarized briefly.

3.1 Introduction

As a dynamic system subject to all kinds of disturbances, vehicle behaviors change from time to time and it is very difficult for drivers to handle all the situations. Therefore,

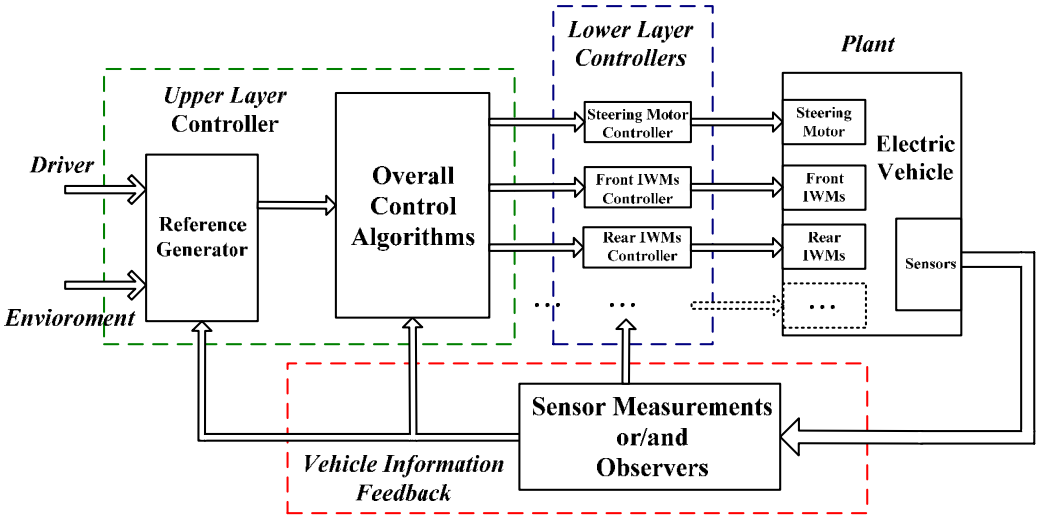

Fig.3. 1 General control structure for EVs.

control systems for driver assistance are commonly recognized to be indispensible. A general control structure for EV applications is shown in Fig. 3.1. Three parts exist in the control structure for EVs in general: 1) upper layer controller which defines reference behavior, control law (includes individual actuator behavior, actuators coordination, control efforts, etc.); 2) lower layer controllers which comprise the local controllers for each actuator; 3) feedback loop which includes sensor measurements or/and estimations from observers.

3.2 Control Approaches

The control structure in Fig. 3.1 can be employed by various applications such as anti-lock control and yaw motion control. No matter what kind of control targets to be realized, the basic performance criteria are in common: fast response, moderate overshoot and minimal steady-state error. In this section, two simple and effective control approaches are briefly introduced.

3.2.1 Two-degree-of-freedom (2DOF) Control

The degree of freedom of a control system is defined as the number of closed-loop transfer functions that can be adjusted independently [71]. First, consider a conventional feedback control system that is subjected to input disturbance $d(s)$ and measurement noise $n(s)$ as shown in Fig. 3.2.

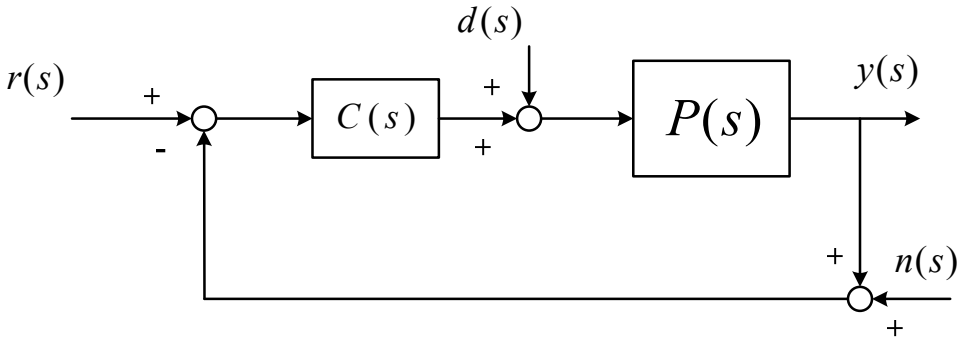

Fig.3. 2 One degree of freedom (1DOF) controller.

As is well known, three closed-loop transfer functions can be obtained as

$$G_{yr1}(s)=\frac{y(s)}{r(s)}=\frac{P(s)\cdot C(s)}{1+P(s)\cdot C(s)} \tag{3.1}$$

$$G_{yd1}(s)=\frac{y(s)}{d(s)}=\frac{P(s)}{1+P(s)\cdot C(s)} \tag{3.2}$$

$$G_{yn1}(s)=\frac{y(s)}{n(s)}=\frac{-P(s)\cdot C(s)}{1+P(s)\cdot C(s)} \tag{3.3}$$

where the subscript *1* represents one degree of freedom (1DOF) which will be explained below.

Obviously, equations 3.1 and 3.3 can be determined by each other. Multiply $P(s)$ to equation 3.1 and then add it to equation 3.2, equation 3.4 can be derived.

$$G_{yr1}(s)\cdot P(s)+G_{yd1}(s)=P(s) \tag{3.4}$$

This equation shows explicitly that for a given plant, $G_{yr1}(s)$ is uniquely determined if $G_{yd1}(s)$ is fixed, and vice versa. Therefore, such control structure is called one degree of freedom [71]. This approach, although simple, has to make compromise between disturbance response and reference response.

In addition to the feedback path, it is possible to move portions of these control actions to the feed-forward path. In fact, several representations are available for this concept

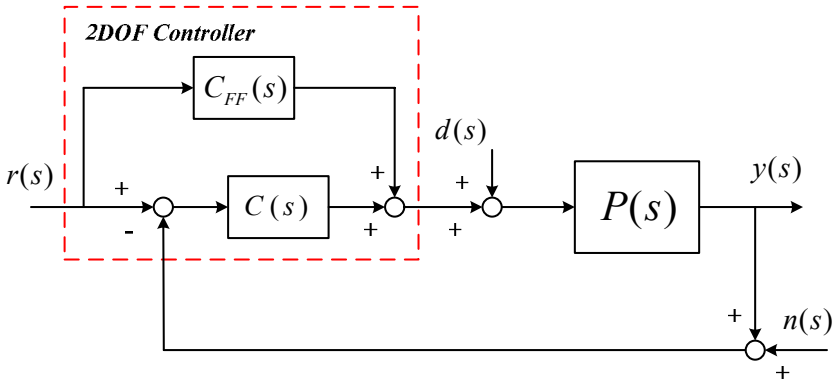

Fig.3. 3 Two degree of freedom controller (Feed-forward representation).

such as feed-forward expression, feedback expression, etc. Here, let's consider a feed-forward type which is given in Fig. 3.3, the below closed-loop transfer functions can be derived

$$G_{yr2}(s)=\frac{y(s)}{r(s)}=\frac{P(s)\cdot C(s)}{1+P(s)\cdot C(s)}+\frac{P(s)\cdot C_{FF}(s)}{1+P(s)\cdot C(s)} \tag{3.5}$$

$$G_{yd2}(s)=\frac{y(s)}{d(s)}=\frac{P(s)}{1+P(s)\cdot C(s)} \tag{3.6}$$

$$G_{yn2}(s)=\frac{y(s)}{n(s)}=\frac{-P(s)\cdot C(s)}{1+P(s)\cdot C(s)} \tag{3.7}$$

Compared to the 1DOF case, it can be found that the disturbance responses and output to noise relationship of the two approaches are the same; the reference tracking equation of the 2DOF system has an additional term. Therefore, 2DOF controller can be designed to have better reference tracking performance without deteriorate the disturbance rejection loop. Moreover, the feedback and feed-forward loops can be adjusted independently. Usually, the feed-forward controller can be selected to be the inverse of the plant [72]-[73].

3.2.2 Disturbance Observer (DOB)

The above 2DOF controller is designed based on the modeled plant. However, the plant cannot be modeled exactly. An actual system can be expressed as

$$P(s)=\mathrm{P}_n(s)\cdot\left(1+\Delta(s)\right) \tag{3.8}$$

where $P(s)$ is the actual plant, $P_n(s)$ is the nominal model, and $\Delta(s)$ is the multiplicative modeling error. In this case, it is desirable to implement an inner loop that can reject model uncertainties as well as disturbances in addition to the 2DOF controller mentioned above.

DOB is an effective method to achieve robustness against model error and disturbances [74]-[75]. A basic DOB block diagram is shown in Fig. 3.4. Basically, it consists two blocks: inverse plant block and Q filter block.

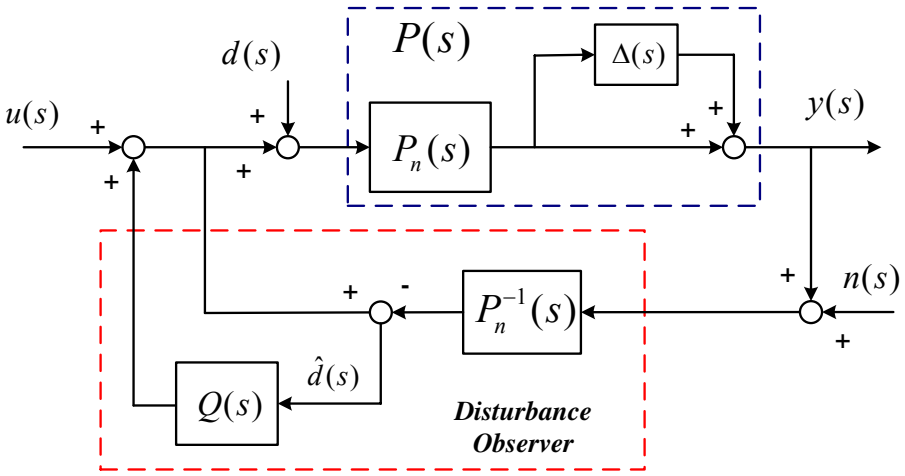

Fig.3. 4 Disturbance observer structure.

The inverse plant module is designed based on the nominal plant. After recalculation of the "control input" with the measured output, disturbance can be obtained by subtracting the recalculated control input from the desired one. The inverse of nominal plant may not be proper in many cases, and the key factor of DOB design is relied on Q filter selection. In control systems, disturbances often dominate at low frequencies while high frequencies are dominated by sensor noises, hence, Q filter is designed to be a low pass filter with unity DC gain [75]. In addition to the structure in Fig. 3.3, DOB can be transformed into the other representations such as the one shown in Fig. 3.5, which has an equivalent block diagram to 2DOF control [76].

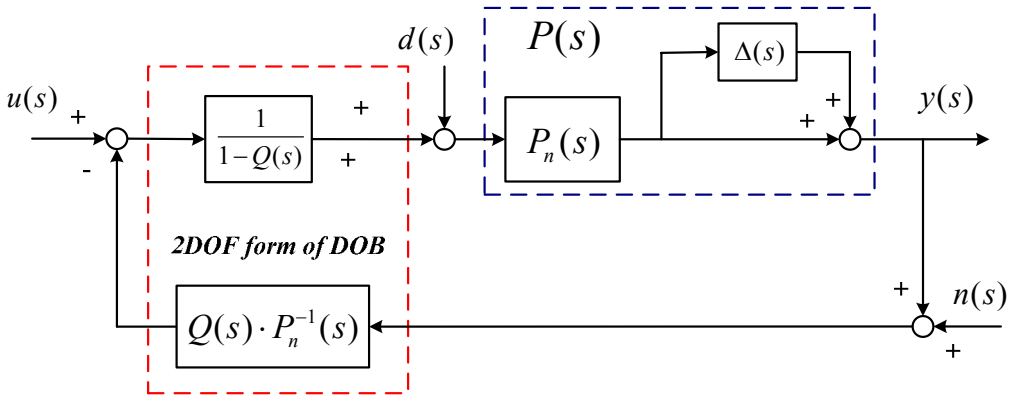

Fig.3. 5 Equivalence representation of DOB.

Then, the closed loop transfer functions can be derived as

$$G_{yr}(s)=\frac{y(s)}{r(s)}=\frac{P(s)\cdot P_n(s)}{Q(s)\cdot\left(P(s)-P_s(s)\right)+P_n(s)} \tag{3.9}$$

$$G_{yd}(s)=\frac{y(s)}{d(s)}=\frac{P(s)\cdot P_n(s)\cdot\left(1-Q(s)\right)}{Q(s)\cdot\left(P(s)-P_s(s)\right)+P_n(s)} \tag{3.10}$$

$$G_{yn}(s)=\frac{y(s)}{n(s)}=\frac{P(s)\cdot Q(s)}{Q(s)\cdot\left(P(s)-P_s(s)\right)+P_n(s)} \tag{3.11}$$

At low frequency when disturbance dominate, $Q(s) \approx 1$, and equations 3.9 – 3.11 become

$$G_{yr}(s)\approx\frac{P(s)\cdot P_n(s)}{P(s)}=P_n(s),\ \ G_{yd}(s)\approx 0,\ \ G_{yn}(s)\approx 1. \tag{3.12}$$

The disturbance rejection principle can then be explained using equation 3.12. It should be noticed that DOB is only used for disturbance rejection, and an outer control loop such as 2DOF controller is still necessary for desired performance realization.

3.3 Vehicle Motion with Active Lateral Control

To intervene the vehicle motion through active control, actuator effects need to be investigated. The most widely used actuators in EVs are active front steer and IWMs [77]. In essence, they take effect on vehicle motion by means of changing the tire forces of the vehicle. For the applications studied in this dissertation, the representative states of vehicle motion are yaw rate, body slip angle and vehicle lateral position; this section will discuss the effects of different actuators on them.

3.3.1 Active Front Steering Control

Vehicle lateral motion is very sensitive to steering system, because the steer wheels change the lateral forces of the vehicle directly. Moreover, vehicle speed influences vehicle motion characteristics heavily.

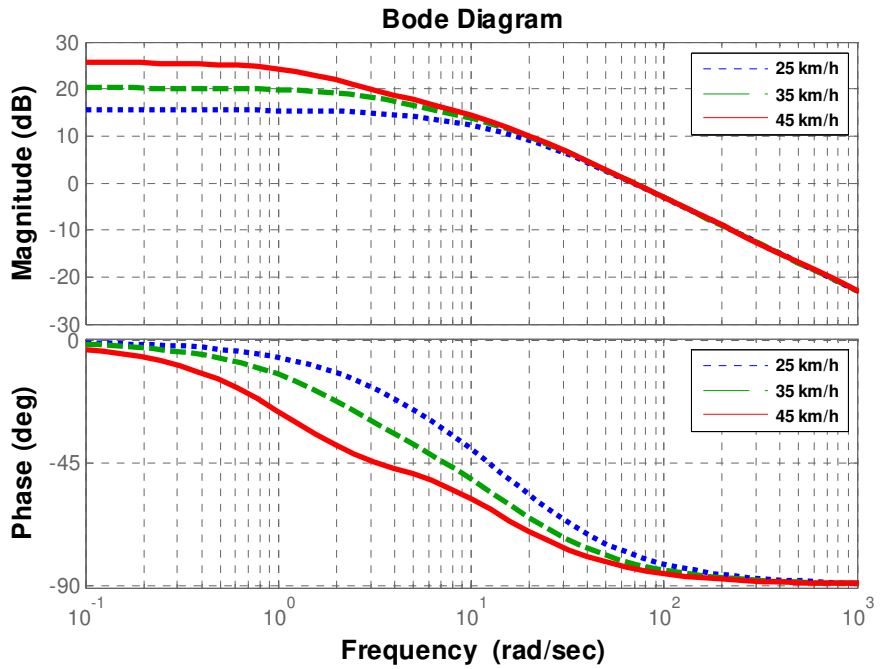

Fig.3. 6 Frequency response of γ at different vehicle speeds (steering input).

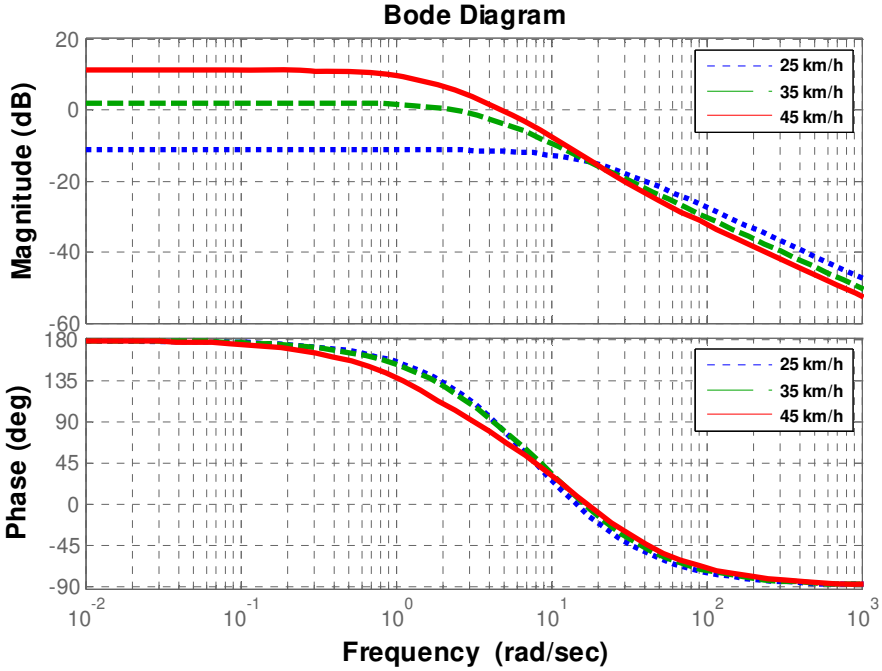

Fig.3. 7 Frequency response of β at different vehicle speeds (steering input).

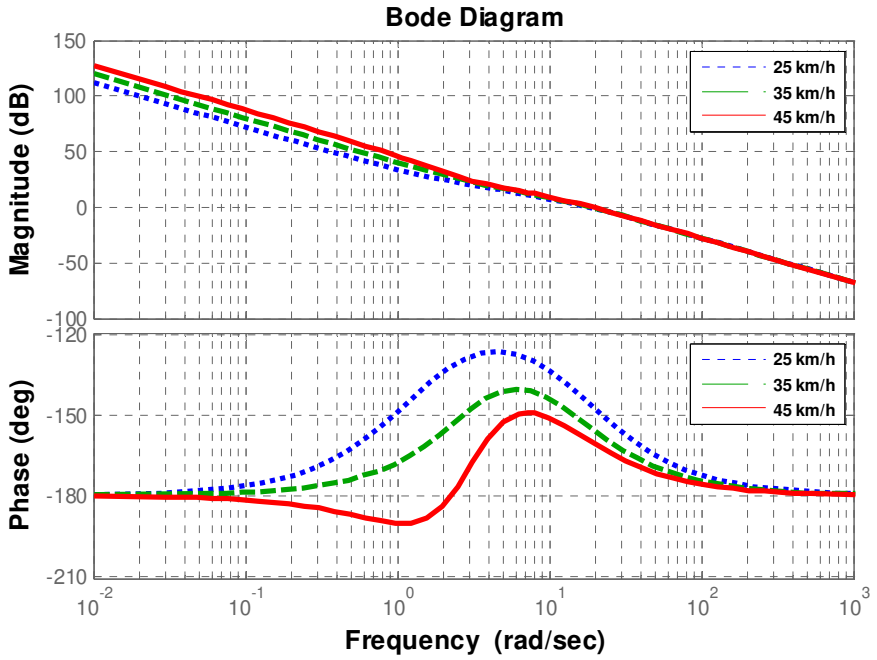

Fig.3. 8 Frequency response of y_l at different vehicle speeds (steering input).

From the model described in 2.27, the transfer functions from yaw rate (γ), body slip angle (β) and lateral offset at a preview point (y_l) to front steering angle can be obtain as below:

$$P_{\delta_f}^{\gamma}(s)=\frac{\gamma(s)}{\delta_f(s)}=G_{\delta_f}^{\gamma}(0)\cdot\frac{T_{\gamma\delta_f}\cdot s+1}{\frac{s^2}{\omega_n^2}+\frac{2\cdot\xi\cdot s}{\omega_n}+1} \tag{3.13}$$

$$P_{\delta_f}^{\beta}(s)=\frac{\beta(s)}{\delta_f(s)}=G_{\delta_f}^{\beta}(0)\cdot\frac{T_{\beta\delta_f}\cdot s+1}{\frac{s^2}{\omega_n^2}+\frac{2\cdot\xi\cdot s}{\omega_n}+1} \tag{3.14}$$

$$P_{\delta_f}^{y_l}(s)=\frac{y_l(s)}{\delta_f(s)}=\frac{V_x}{s}\cdot P_{\delta_f}^{\gamma}(s)+\frac{l_{pre}\cdot s+V_x}{s^2}\cdot P_{\delta_f}^{\beta}(s) \tag{3.15}$$

where

$$\omega_n=\frac{2\cdot l}{V_x}\cdot\sqrt{\frac{C_f\cdot C_r}{m\cdot I}\left(1+AV_x^2\right)} \tag{3.16}$$

$$\xi = \frac{m \cdot \left(l_f^2 \cdot C_f + l_r^2 \cdot C_r\right) + I \cdot \left(C_f + C_r\right)}{2 \cdot l \cdot \sqrt{m \cdot I \cdot C_f \cdot C_r \cdot \left(1 + AV_x^2\right)}} \tag{3.17}$$

$$A = -\frac{m}{2 \cdot l^2} \cdot \frac{l_f \cdot C_f - l_r \cdot C_r}{C_f \cdot C_r} \tag{3.18}$$

$$G_{\delta_f}^{\gamma}(0) = \frac{V_x}{l \cdot \left(1 + AV_x^2\right)}, \quad T_{\gamma\delta_f} = \frac{m \cdot l_f \cdot V_x}{2 \cdot l \cdot C_r} \tag{3.19}$$

$$G_{\delta_f}^{\beta}(0) = \frac{1 - \dfrac{m \cdot l_f \cdot V_x^2}{2 \cdot l \cdot l_r \cdot C_r}}{1 + AV_x^2} \cdot \frac{l_f}{l}, \quad T_{\beta\delta_f} = \frac{I \cdot V_x}{2 \cdot l \cdot l_r \cdot C_r} \cdot \frac{1}{1 - \dfrac{m \cdot l_f \cdot V_x^2}{2 \cdot l \cdot l_r \cdot C_r}} \tag{3.20}$$

Base on the vehicle parameters listed in the Appendix A, the bode plot of these three transfer functions with change to vehicle speed are shown from Fig. 3.6 to Fig. 3.8. It can be seen that vehicle motion becomes more sensitive with the increasing of speed.

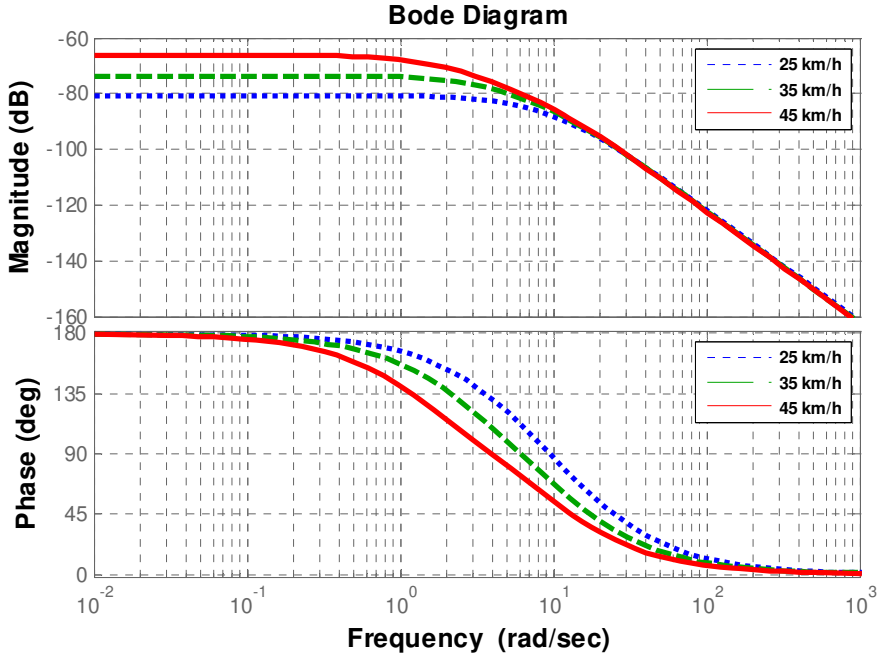

Fig.3. 9 Frequency response of β at different vehicle speeds (differential torque input).

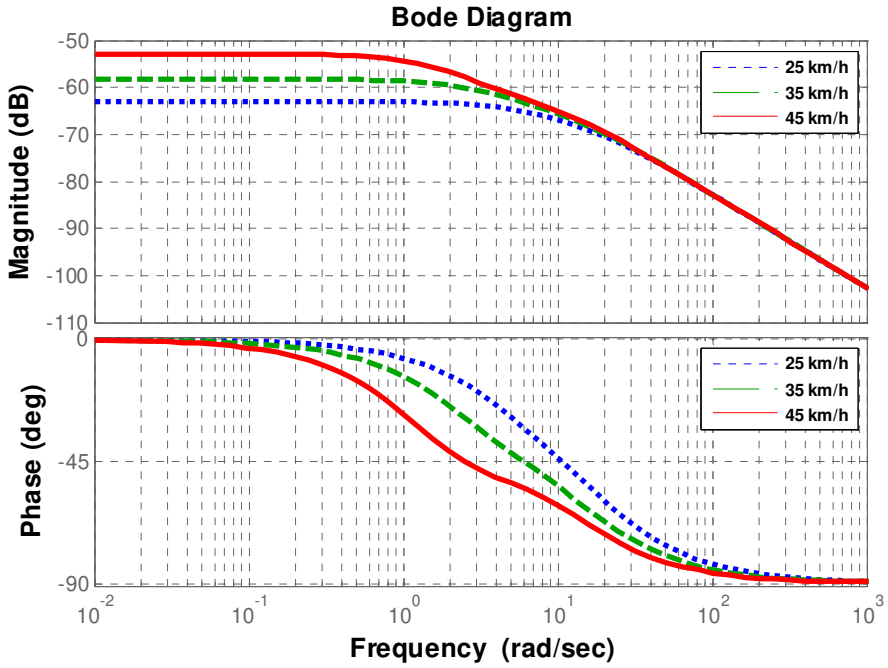

Fig.3. 10 Frequency response of γ at different vehicle speeds (differential torque input).

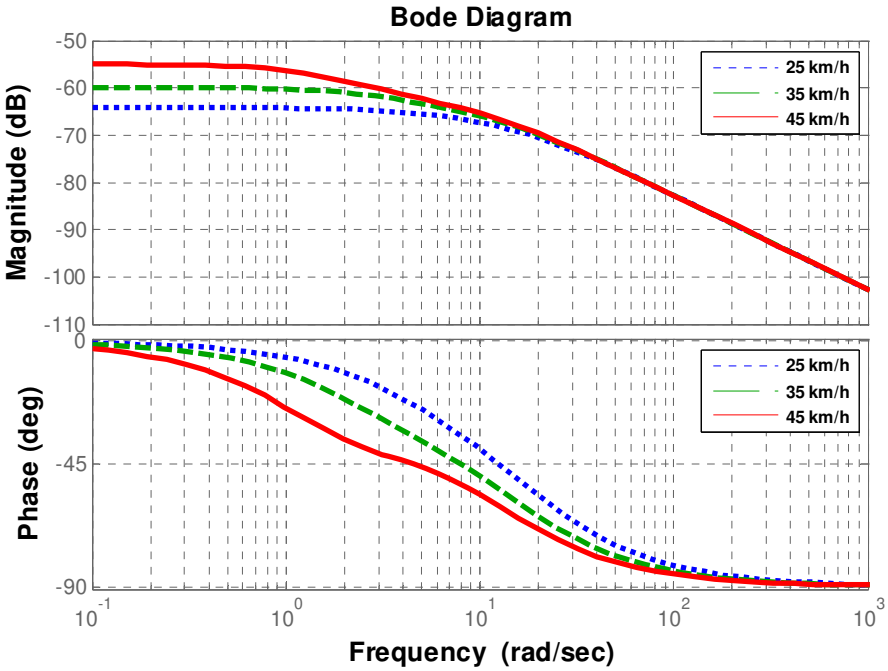

Fig.3. 11 Frequency response of y_l at different vehicle speeds (differential torque input).

3.3.2 Differential Torque Control

Traditionally realized by differential braking, direct yaw moment control (DYC) can be implemented more effectively using differential torque generated by the left and right IWMs [78]. This section analysis vehicle motion under different speed with yaw moment as control input.

Again, from the model described in 2.27, the transfer functions from yaw rate (γ), body slip angle (β) and lateral offset at a preview point (y_l) to differential torque can be obtain as below:

$$P_{N_z}^{\gamma}(s)=\frac{\gamma(s)}{N_z(s)}=G_{N_z}^{\gamma}(0)\cdot\frac{T_{\gamma N_z}\cdot s+1}{\frac{s^2}{\omega_n^2}+\frac{2\cdot\xi\cdot s}{\omega_n}+1} \tag{3.21}$$

$$P_{N_z}^{\beta}(s)=\frac{\beta(s)}{N_z(s)}=-G_{N_z}^{\beta}(0)\cdot\frac{1}{\frac{s^2}{\omega_n^2}+\frac{2\cdot\xi\cdot s}{\omega_n}+1} \tag{3.22}$$

$$P_{N_z}^{y_l}(s)=\frac{y_l(s)}{N_z(s)}=\frac{V_x}{s}\cdot P_{N_z}^{\gamma}(s)+\frac{l_{pre}\cdot s+V_x}{s^2}\cdot P_{N_z}^{\beta}(s) \tag{3.23}$$

where

$$G_{N_z}^{\gamma}(0)=\frac{V_x\cdot\left(C_f+C_r\right)}{2\cdot C_f\cdot C_r\cdot l^2\cdot\left(1+A\cdot V_x^2\right)},\quad T_{\gamma N_z}=\frac{m\cdot V_x}{2\cdot\left(C_f+C_r\right)} \tag{3.24}$$

$$G_{N_z}^{\beta}(0)=\frac{m\cdot V_x^2+2\cdot\left(l_f\cdot C_f-l_r\cdot C_r\right)}{4\cdot C_f\cdot C_r\cdot l^2\cdot\left(1+A\cdot V_x^2\right)} \tag{3.25}$$

Base on the vehicle parameters listed in the Appendix B, the bode plot of these three transfer functions with change to vehicle speed are shown from Fig. 3.8 to Fig. 3.10. Similar to the steering input, the vehicle motion becomes more sensitive to the yaw moment input with the increasing of speed. Also, as can be observed, except yaw rate, the other two states

are not so sensitive to the yaw moment control. However, as an additional control input to steering, it is important to investigate the control applications using differential torque.

3.4 Vehicle State Estimation Based on Kalman Filter

As mentioned in chapter 1, although many vehicle states can be easily obtained from onboard sensors, some of them cost too high to be measured directly. Therefore, state estimators become an essential part for the vehicle control system using only a limited number of sensors. For vehicle state estimation, two factors are crucial: models and estimation methodology. As the model was developed in the previous chapter, this section introduces estimation methods briefly.

The observer theory was first initiated by Luenberger for the state reconstruction of linear dynamical systems [79]. In 1960, Kalman introduced a state space approach in the time domain for multivariable linear causal systems. Unlike Luenberger observer which is based on deterministic environments, Kalman filter is based on the probability theory and applicable to processes that are linear stochastic [80].

Consider a linear time-invariant system in discrete form as given in equation 3.26, where w_k and v_k represent the process noise and measurement noise at step k, respectively. The two noises are assumed to be white, independent with each other, and with normal probability distributions [81].

$$\begin{aligned} x_{k+1} &= A \cdot x_k + B \cdot u_k + w_k, \\ y_k &= C \cdot x_k + v_k, \end{aligned} \tag{3.26}$$

The Kalman algorithm has two basic parts as given in equations 3.27 and 3.28, and its principle is illustrated in Fig. 3.11.

1) Time update

$$\begin{aligned} \hat{x}_k^- &= A \cdot \hat{x}_{k-1} + B \cdot u_{k-1} \\ P_k^- &= A \cdot P_{k-1} \cdot A^T + Q, \end{aligned} \tag{3.27}$$

2) Measurement update

$$
\begin{aligned}
K_k &= P_k^- \cdot C^T \cdot \left(C \cdot P_k^- \cdot C^T + R \right)^{-1} \\
\hat{x}_k &= \hat{x}_k^- + K_k \cdot \left(y_k - C \cdot \hat{x}_k^- \right) \\
P_k &= \left(I - K_k \cdot C \right) \cdot P_k^-
\end{aligned}
\tag{3.28}
$$

where the process noise covariance Q and measurement noise covariance R are given as

$$
Q = E[w_k w_k^T], \quad R = E[v_k v_k^T] \tag{3.29}
$$

3.5 Stability of Kalman Filter-based Control System

The stability of a control system is extremely important and must be addressed in the control system design. To check system stability, a number of criteria are available, for example, the controller can be designed into a transfer function, and the closed-loop poles can be checked by using methods such as root-locus and Bode plot. In case of observer-based control system, the influence of observer dynamics on the closed-loop system should also be considered. That is, observer and controller should be designed together to guarantee system stability.

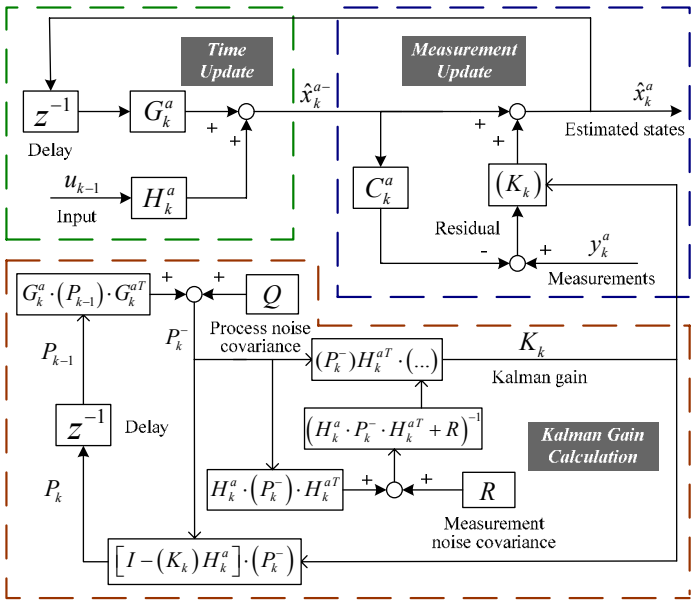

Fig. 3.11. Operating principle of the Kalman filter.

An intuitive design method is through the use of Kalman filter coupled with an LQR (Linear Quadratic Regulator) full state feedback gain. Such combination is often known as LQG (Linear Quadratic Gaussian) control [105]. To compensate steady state error, an integrator is often employed to function as another loop, which is known as LQI (Linear Quadratic Integral) control. That is, LQI control is the combination of LQG and integral control. An illustration of LQI is shown in Fig. 3.12.

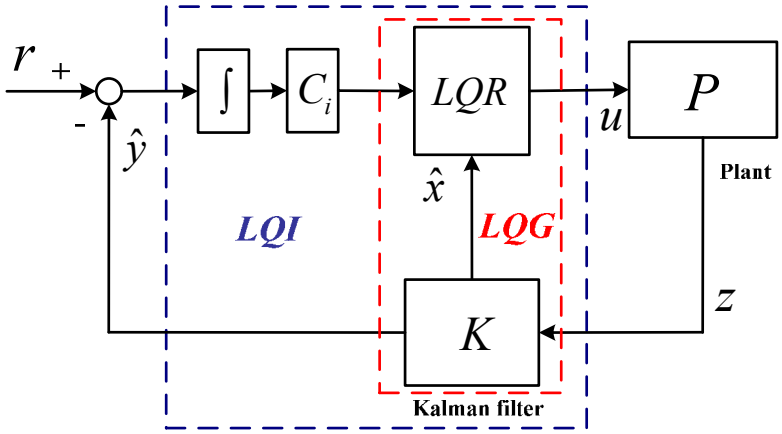

Fig. 3.12. Operating principle of the Kalman filter.

To facilitate discussion, the stability analysis below are conducted with continuous formulations. A continuous Kalman filter has the following dynamics

$$\dot{\hat{x}} = A \cdot \hat{x} + B \cdot u + K \cdot \left(y - C \cdot \hat{x} \right) \tag{3.29}$$

The eigenvalues of the feedback system in Fig. 3.12 are the union of the eigenvalues of the matrices

$$\begin{bmatrix} A - B \cdot K & -B \cdot C_i \\ C & 0 \end{bmatrix} \cup \left(A - K \cdot C \right) \tag{3.30}$$

Stability of the closed-loop system can be guaranteed if all the eigenvalues have strictly negative real parts. Notably, it enjoys a separation property, i.e., designs of state feedback and observer can be done independently, and so is the LQG control.

Another control method is PID control using the estimated variable as feedback signal, as shown in Fig. 3.13, where F_b is the PID controller, Λ is a indicator matrix which indicates which of the estimated states should be feedback to the F_b controller.

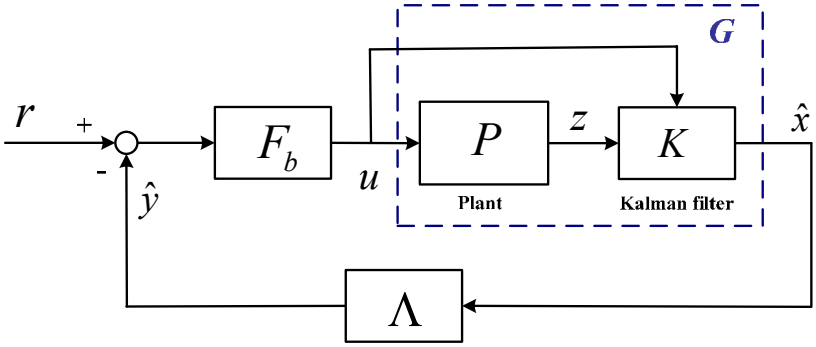

Fig. 3.13. Operating principle of the Kalman filter.

The state of the plant can be formulated as

$$\dot{x} = A \cdot x + Bu$$

$$\Rightarrow \quad x = \left(s \cdot I - A\right)^{-1} \cdot B \cdot u \tag{3.31}$$

And considering the Kalman filter equation 3.29, the below equation can be derived

$$\dot{\hat{x}} = A \cdot \hat{x} + B \cdot u + K \cdot C \cdot x - K \cdot C \cdot \hat{x}$$

$$\Rightarrow \left(s \cdot I - A + K \cdot C\right) \cdot \hat{x} = B \cdot u + K \cdot C \cdot x \tag{3.32}$$

Then, taking the equation 3.31 into 3.12 yields

$$\left(s \cdot I - A + K \cdot C\right)\hat{x} = \left[I + K \cdot C\left(s \cdot I - A\right)^{-1}\right] \cdot B \cdot u$$

$$\Rightarrow G = \frac{\hat{x}}{u} = \frac{\left[I + K \cdot C\left(s \cdot I - A\right)^{-1}\right] \cdot B}{s \cdot I - A + K \cdot C} \tag{3.33}$$

The closed-loop transfer function from feedback signal to reference can be formulated as equation 3.34.

$$\frac{\hat{y}}{r} = \frac{F_b \cdot (\Lambda \cdot G)}{1 + F_b \cdot (\Lambda \cdot G)} \tag{3.34}$$

Finally, we have the closed-loop transfer function as equation 3.35 by taking equation 3.33 into equation 3.24.

$$\frac{\hat{y}}{r} = \frac{F_b \cdot \left(\Lambda \cdot \dfrac{\left[I + K \cdot C (s \cdot I - A)^{-1} \right] \cdot B}{s \cdot I - A + K \cdot C} \right)}{1 + F_b \cdot \left(\Lambda \cdot \dfrac{\left[I + K \cdot C (s \cdot I - A)^{-1} \right] \cdot B}{s \cdot I - A + K \cdot C} \right)} \tag{3.35}$$

If the eigenvalues of the characteristic equation in equation 3.35 all have strictly negative real parts, that is, all lie in the open left-half complex plane, the system is stable.

3.6 Constrains of Observer-based Motion Control for Electric Vehicles

The aforementioned control and estimation methodologies are based on two assumptions: 1) all the sampling times of sensors are the same and therefore can be fused directly; 2) the

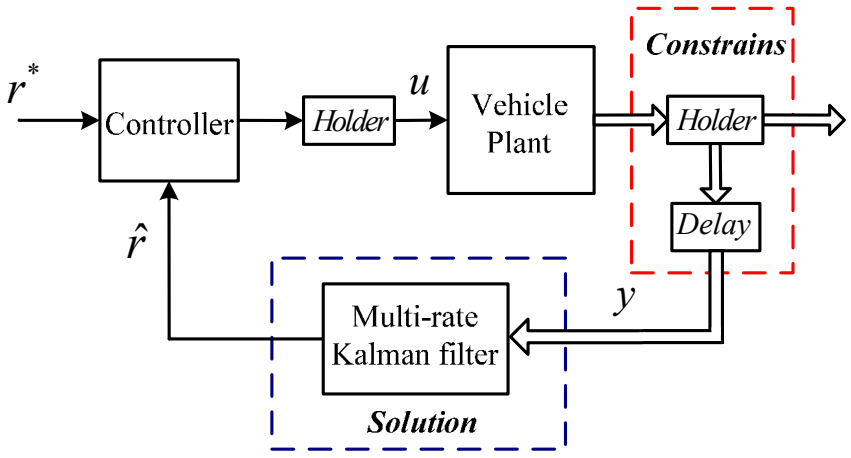

Fig. 3.12. Constrains of the observer-based method and solution.

sampling rate of input is the same with the feedback frequency. For vision-based EV control system as discussed in this dissertation, however, constraints exist in the visual measurements, i.e., the vision information is updated slower than the other onboard sensors, and is also slower than the system control input. The latter constrain is also known as N-delay input problem [1]. Moreover, the visual data are delayed due to image processing. The constrains are shown in Fig. 3.12.

In a multi-rate and delayed system, if normal estimator is employed for feedback, the signals in the feedback loop then become out-of-sequence and impulsive. Meanwhile, the control input determined by the estimations is therefore incorrect and non-smooth. In fact, the stability margin of the control system is deteriorated with such constrains [82]. For a control system, the optimal sampling frequency can be determined by its closed-loop bandwidth and system design requirements [111]. Suppose the system has a closed-loop bandwidth of f_c (Hz), and a general rule of thumb can be given to determine the range of the sampling period T as

$$\frac{1}{30 f_c} < T < \frac{1}{5 f_c} \tag{3.36}$$

In case of body slip angle control studied in this dissertation, the closed-loop bandwidth is about 9 Hz, and the sampling period range can then be determined by equation 3.3.6 as: 3 ms $< T <$21 ms. Furthermore, the closed-loop bandwidth of other applications such as yaw rate (γ) control is often higher than 30 Hz, and it often requires a sampling period of 1 ms. Therefore, it is desirable to boost the body slip angle control loop to 1 kHz for integrated control applications such as combined γ and β control.

One previous study focused on the multi-rate issue, and proposed a multi-rate observer for the calculation of input signal during two consecutive output sampling instances [83]. Unfortunately, it is open loop and cannot be applied to vehicle systems with high uncertainty and disturbances. This dissertation will design a multi-rate Kalman filter that can solve the multi-rate sensor fusion and the N-delay input problems.

3.7 Considerations on Performance Requirements

Vehicle control systems are investigated from many perspectives such as drivability, stability and economy. Among these directions, stability and drivability were given particular

attentions due to their importance to the drivers. Usually, stability is represented by body slip angle and drivability is indicated by yaw rate. In some cases, drivability alone cannot guarantee safety, and an integrated controller is therefore necessary to achieve both safety and drivability. In terms of control, two points need to be considered for a control system: robustness and reference following performance. Different applications have different evaluation criteria.

Considering the above performance requirements, in this dissertation, two applications on vision-based EV motion control are studied:

1) vision-based body slip angle control;

2) vision-based integrated lateral motion control.

The applications, performance representations and necessary control approaches are shown in Table 3.1.

Table 3. 1 Applications and Control Approaches

Application	**Performance Representation**	**Necessary Control Approach**
Body slip angle control (β)	Stability	Feedback
Integrated lateral motion control (γ, y_l)	Drivability	Feed-forward + Feedback

In addition to the controller, estimator is designed to provide information for the feedback loop. To increase control performance, a residual estimation-based multi-rate Kalman filter that can provide smooth estimate is desired.

3.8 Chapter Summary

This chapter first introduced two effective control approaches: 2DOF control and DOB methods. They will be applied to the applications studied in this dissertation. Since the most common actuators in EVs are AFS and IWMs, their effects on body slip angle, yaw rate and lateral offset at a previous point were then discussed. And then, Kalman filter was briefly introduced as a state estimation technique for vehicle applications. Then, the constrains of the observer-based control approach were explained. Finally, considering the performance requirements, two applications on vehicle stability and drivability were briefly introduced.

Chapter 4

Multi-rate Kalman Filter Design Considering Time Delay

This chapter focuses on developing estimation algorithms to solve the multi-rate and delay issues (the delay can be constant or random). First, a method for discretization of continuous model is introduced. Considering that measurements from different sources may have different sampling times and some of them are delayed, the two issues are then explained in details. And then, to deal with the constant or random measurement delay, two multi-rate Kalman filters with different approaches are designed. Moreover, their convergences of the proposed Kalman filters are analyzed.

4.1 Introduction

In many industrial applications such as vision-based EV control system, the sampling times of different sensors and actuators are not consistent, and some of the measured signals are delayed (constant or random) due to the processing time or/and transmission time. Therefore, Kalman filter design method considering multi-rate and delay issues are proposed in this chapter. Notably, constant delay is a special case of random delay, and the methods to solve random delay issue can be applied to state estimation with constant delay. On the other hand, solutions for constant delay such as state augmentation, although can be applicable to the random delay case, can be too complex to be implemented [30]. The state estimation methods discussed in this dissertation are under the framework of Kalman filter, and there are several points to consider:

1) System discretization. Models that are available in the form of continuous form need to be discretized for real implantation. In case of multi-rate system, more than one sampling time exist and the selection of discretization time should be considered.

2) Time update (prediction). After discretization, time update can be implemented based on the system model in the normal way. There is no difference among system components with different sampling rates.

3) Measurement update (correction). The predicted system states are kind of open-loop and need to be corrected using measurements. The system components with different sampling rates should be treated separately due to the inconsistent updates.

4.2 Discretizaion of Continuous Model

Most physical models are originally provided in the form of continuous-time differential equations or Laplace transfer functions, but computer implementations should be conducted in discrete-time manner [84]. In addition, many of the systems are time-varying, i.e., some parameters in the system model change from time to time. The two points need to be addressed in the system model for Kalman filter design.

Consider a continuous time-varying plant given by

$$\dot{x}(t) = A(t) \cdot x(t) + B(t) \cdot u(t) \tag{4.1}$$

$$y(t) = C(t) \cdot x(t) \tag{4.2}$$

And assume the corresponding discrete system is given as

$$x_{k+1} = G_k \cdot x_k + H_k \cdot u_k \tag{4.3}$$

$$y_k = C_k \cdot x_k \tag{4.4}$$

where the samples of state vector, measurement vector, system matrices are defined as

$$\begin{aligned} x_k &= x(k \cdot T), \quad y_k = y(k \cdot T) \\ A_k &= A(k \cdot T), \quad B_k = B(k \cdot T) \end{aligned} \tag{4.5}$$

and T is the sampling period.

To relate discrete-time formulations with continuous ones, it is desirable to define a discrete index k (also known as time step) that satisfying $t = k \cdot T$. The state, control input and output are then to be switched at each time $k \cdot T$, where k =0, 1, 2,….

By including a ZOH, the control part of the system (includes both control matrix B and control input u) can be held constant before entering the plant between control switchings. That is

$$B(t) \cdot u(t) = H_k \cdot u_k, \quad k \cdot T \le t < (k+1) \cdot T \tag{4.6}$$

The exact solution of equation 4.1 can be obtained as equation 4.7.

$$\mathrm{x}(t) = e^{\mathrm{A}(t_0)\cdot(t-t_0)}\mathrm{x}(t_0) + \int_{t_0}^{t} e^{\mathrm{A}(t_0)\cdot(t-\tau)}\mathrm{B}(\tau)\mathrm{u}(\tau)\,\mathrm{d}\tau \tag{4.7}$$

Consider t_0 and t as two neighboring sampling times which are defined as

$$t_0 = k \cdot T, \quad t = (k+1) \cdot T \tag{4.8}$$

Equation 4.7 can be recalculated as

$$\mathrm{x}\left((k+1)\cdot T\right) = e^{\mathrm{A}(k\cdot T)\cdot T}\mathrm{x}(k\cdot T) + \int_{k\cdot T}^{(k+1)\cdot T} e^{\mathrm{A}(k\cdot T)\cdot[(k+1)\cdot T-\tau]}\mathrm{B}(\tau)\mathrm{u}(\tau)\,\mathrm{d}\tau \tag{4.9}$$

Then, taking $\sigma = \tau - k \cdot T$ into equation 4.9 and combining it with equation 4.5, equation 4.10 can be obtained.

$$\mathrm{x}_{k+1} = e^{\mathrm{A}_k\cdot T}\mathrm{x}_k + \int_0^T e^{\mathrm{A}_k\cdot[T-\sigma]}\mathrm{B}(\tau)\cdot\mathrm{u}(\tau)\,\mathrm{d}\sigma \tag{4.10}$$

From time 0 to T, remember that $B(t) \cdot u(t)$ has a constant value of $B_k \cdot u_k$ due to the ZOH, they can be extracted from the integrand as

$$\mathrm{x}_{k+1} = e^{\mathrm{A}_k\cdot T}\mathrm{x}_k + \int_0^T e^{\mathrm{A}_k\cdot[T-\sigma]}\,\mathrm{d}\sigma\cdot\mathrm{B}_k\cdot\mathrm{u}_k \tag{4.11}$$

Changing $\tau = T - \sigma$ into equation 4.11 yields

$$\mathrm{x}_{k+1} = e^{\mathrm{A}_k\cdot T}\mathrm{x}_k + \int_0^T e^{\mathrm{A}_k\cdot\tau}\,\mathrm{d}\tau\cdot\mathrm{B}_k\cdot\mathrm{u}_k \tag{4.12}$$

Comparing equations 4.3 and 4.12, the disretized system matrices are given as equation 4.13.

$$G_k = e^{\mathrm{A}_k \cdot T}, \quad H_k = \int_0^T e^{\mathrm{A}_k \cdot \tau}\, \mathrm{d}\tau \cdot \mathrm{B}_k \tag{4.13}$$

Furthermore, equation 4.13 can be expanded as below

$$\begin{aligned} G_k &= I + A_k \cdot T + \frac{1}{2!} \cdot A_k^2 \cdot T^2 + \frac{1}{3!} \cdot A_k^3 \cdot T^3 + \ldots \\ H_k &= B_k \cdot T + \frac{1}{2!} \cdot A_k \cdot B_k \cdot T^2 + \frac{1}{3!} \cdot A_k^2 \cdot B_k \cdot T^3 + \ldots \end{aligned} \tag{4.14}$$

In case of small sampling period, G_k and H_k can be approximated by retaining only the first two terms and the first term, respectively. That is

$$\begin{aligned} G_k &\approx I + A_k \cdot T \\ H_k &\approx B_k \cdot T \end{aligned} \tag{4.15}$$

In addition, since the system measurement equation 4.2 is non-dynamical, matrix $C(t)$ can be assumed to be unchanged on discretization during the sampling period. That is

$$C_k = C(t), \quad k \cdot T \le t < (k+1) \cdot T \tag{4.16}$$

4.3 Problems Statement

With the discretization method above, a general discrete state space equation can be formulated as equation 4.17 by considering that the system model contains uncertainties and the sensor measurements are contaminated by noises.

$$\begin{aligned} x_{k+1} &= G_k \cdot x_k + H_k \cdot u_k + w_k \\ y_k &= C_k \cdot x_k + v_k \end{aligned} \tag{4.17}$$

where w_k and v_k represent process noise and measurement noise, respectively.

Two issues are considered here: multi-rate and delayed measurements. Furthermore, the delay can be constant or random depending on the delay periods.

4.3.1 Multi-rate Sampling

As mentioned in the introduction chapter, many industrial applications have to handle multi-rate and delayed measurements. For example, in the chemical process, there exist two sampling frequencies: the infrequently sampled measurements are known as primary measurement, and the frequently available variables are referred as secondary measurements [85]. The measurement equation can be described by equation 4.18.

$$\begin{bmatrix} y_k^{1st} \\ y_k^{2nd} \end{bmatrix} = \begin{bmatrix} C_k^{1st} & C_k^{1st\text{-}2nd} \\ C_k^{2nd\text{-}1st} & C_k^{2nd} \end{bmatrix} \cdot \begin{bmatrix} x_k^{1st} \\ x_k^{2nd} \end{bmatrix} + \begin{bmatrix} v_k^{1st} \\ v_k^{2nd} \end{bmatrix} \tag{4.18}$$

where the superscripts *1st* and *2nd* represent primary and secondary terms, respectively; the non-diagonal matrices are zeros if the primary and secondary measurements are not correlated, and it is the case that studied in this dissertation. Similarly, the measurement samplings in the field of mechatronics, although can be several different rates, are two in many cases [86], [87]. In fact, the system with more than two sampling frequencies can be handled by considering it as a combination of several dual-rates systems. Therefore, a system with two sampling rates is considered here.

Assume that the two different measurement times in the dual rate system are: the sampling period of secondary measurement (defined as T_s) which is shorter and the updating time of primary measurement (defined as T_l) which is much longer. Therefore, the selection of T_s and T_l for system discretization needs to be considered. If the system sampling time is set to T_l, data from the high-speed sensors have to be dropped during inter-sampling of the slow-speed device. This is a straightforward solution for the multi-rate issue but obviously deteriorates the estimation performance. An alternative method is to set the system sampling time to T_s. Then, all the information from the fast-rate sensors can be utilized. However, the inter-sample residuals of the slow-speed device must be addressed for Kalman filter implementation. The system measurements are given as

$$y_k = \begin{cases} \left[\left(y_k^{2nd} \right)^T \quad \left(y_k^{1st} \right)^T \right]^T, & if \quad k = i \cdot N, \\ \left[\left(y_k^{2nd} \right)^T \quad 0 \right]^T, & if \quad k \neq i \cdot N. \end{cases} \tag{4.19}$$

where $N=T_l/T_s$, which is known as multi-rate ratio or multiplicity.

4.3.2 Time-delay

Not only sampled infrequently, the primary measurements are also delayed in many situations [85]. Depending on the delayed periods, it can be categorized into random delay and constant delay cases.

Random time-delay:

The sampling sequence of a random delayed system is shown in Fig. 4.1. Unlike normal measurements, the information from the primary measurement is captured at step k-n_{d_i}, but is only available at step k due to reasons like process delay, where $n_{d\_i}=T_{d\_i}/T_s$ and T_{d_i} is the time delay of the primary measurement at time stamp i. n_{d_i} denotes the number of intervals between two successive primary measurements. For uneven delay, T_{d_i} varies from step to step. In this dissertation, it is assumed that the time delays are within one primary sampling period. Therefore, T_{d_i} can only be one value from the set $\{1, 2, \ldots, N\}$ at an arbitrary i.

The primary measurements equation can be formulated as equation 4.20.

$$y_k^{1st} = C_{k-n_{d\_i}}^{1st} \cdot x_{k-n_{d\_i}}^{1st} + v_{k-n_{d\_i}}^{1st} \tag{4.20}$$

The time interval between every two neighboring primary samples (i and i+1) is given as equation 4.21.

$$T_{i\_i+1} = T_l - T_{d\_i} + T_{d\_i+1} \tag{4.21}$$

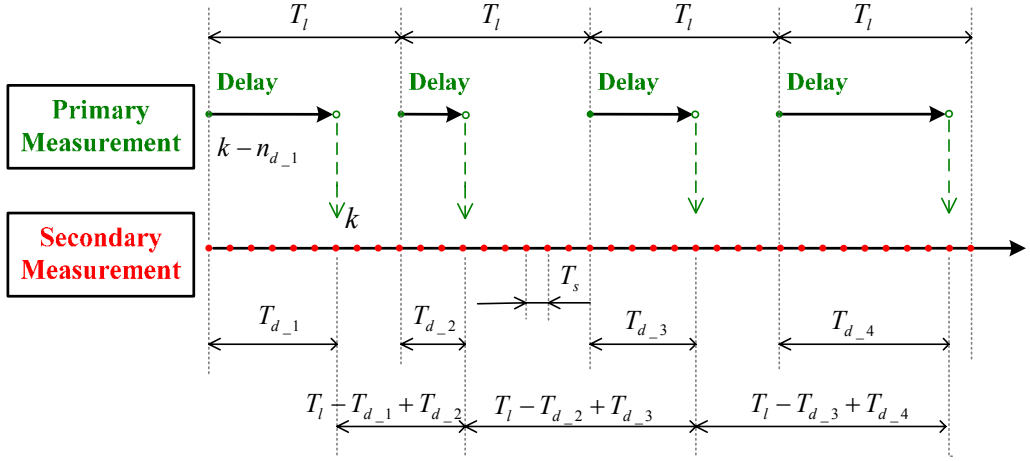

Fig.4. 1 System sampling sequence (primary measurement with random delay).

Constant time-delay:

Unlike the afore-discussed random delay, the measurement delay in this case does not change. For example, in the application of vision system, image processing time can be implemented to be nearly constant by modifying the image processing program (such as adding a delay).

In case of constant delay, the aforementioned T_{d_i} is constant for all the step i. That is

$$T_{d\_1} = T_{d\_2} = \ldots = T_{d\_i} = T_d = constant \tag{4.22}$$

and the time interval between every two neighboring primary samples is therefore T_l. The primary measurements equation can be formulated as equation 4.23.

$$y_k^{1st} = C_{k-n_d}^{1st} \cdot x_{k-n_d}^{1st} + v_{k-n_d}^{1st} \tag{4.23}$$

The sampling sequence of primary measurement with constant delay is shown in Fig. 4.2. Here, it is assumed that the time delay is within one sampling period of the camera. In fact, constant delay is a special case of random delay.

It should be noted that, although the above two situations assume the visual measurement delays are less than one sampling length of the camera, the multi-rate Kalman filter methodologies elaborated later in this chapter can also be applied for the cases if image processing takes more than one visual sampling period.

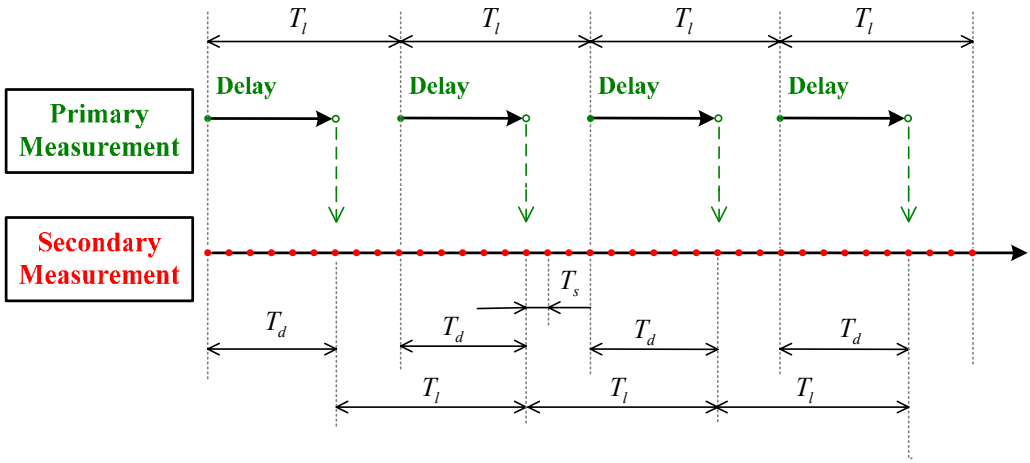

Fig.4. 2 System sampling sequence (primary measurement with constant delay).

4.4 Multi-rate Kalman filter Design Considering Constant Measurement Delay

The multi-rate and constant delay issues are solved one by one in this section: the constant delay problem is solved using state augmentation approach and, the multi-rate Kalman filter is then developed based on the augmented system.

4.4.1 Augmentation of Constant Measurement Delay

An intuitive solution to the problem of state estimation with constant measurement delay is the so-called state augmentation method [88]-[89]. Because the state-space formulation is retained, although has excessive computation load, this approach has been favored in both academic and industrial fields, which can be extended to solve the other problems such as the multi-rate issue discussed in this dissertation. Several state augmentation methods are available based on the required information to be augmented.

All delayed states augmentation (fixed-lag smoother):

A classical state augmentation algorithm is the fixed-lag smoothing approach which augments the current state with all the delayed states between measurement sampling time

$$x_k^a = \begin{bmatrix} x_k^T & x_{k-1}^T & \dots & x_{k-n_d}^T \end{bmatrix}^T, \quad y_k^a = \begin{bmatrix} \left(y_k^{2nd}\right)^T & \left(y_{k-n_d}^{1st}\right)^T \end{bmatrix}^T,$$

$$G_k^a = \begin{bmatrix} G_k & 0 & \cdots & 0 & 0 \\ I & 0 & \cdots & 0 & 0 \\ 0 & I & \cdots & 0 & 0 \\ \vdots & \ddots & \ddots & \ddots & \vdots \\ 0 & 0 & \dots & I & 0 \end{bmatrix}, H_k^a = \begin{bmatrix} H_k^T & 0 & \dots & 0 & 0 \end{bmatrix}^T, \qquad (4.24)$$

$$C_k^a = \begin{bmatrix} C_k^{2nd} & 0 & \cdots & 0 & 0 \\ 0 & 0 & \cdots & 0 & C_{k-n_d}^{1st} \end{bmatrix}.$$

and arriving time [90].

Remember that the delayed primary variables are measured at the instance k-n_d and arrive with a constant delay of n_d steps. The new system after fixed-lag augmentation is given as equation 4.24.

Due to the availability of secondary measurement at every short sampling instances, this method smoothes the past n_d states and, when the delayed primary measurement arrives, both primary and secondary measurements are used to smooth estimates. Obviously, this method is computational intensive for large time delay due to the large state expansion.

Measurement augmentation:

In many applications such as the one studied in this dissertation, the number of primary variables is less than the state dimension. Considering that not all the states are required to be estimated within the delay period, it is enough to augment the current state with only the primary measurements for the previous delayed n_d steps. The augmented system in this method is given as

$$x_k^a = \begin{bmatrix} x_k^T & \left(y_k^{1st}\right)^T & \cdots & \left(y_{k-n_d}^{1st}\right)^T \end{bmatrix}^T, \quad y_k^a = \begin{bmatrix} \left(y_k^{2nd}\right)^T & \left(y_{k-n_d}^{1st}\right)^T \end{bmatrix}^T,$$

$$G_k^a = \begin{bmatrix} G_k & 0 & \cdots & 0 & 0 \\ C_{k+1}^{1st} \cdot G_k & 0 & \cdots & 0 & 0 \\ 0 & I & \cdots & 0 & 0 \\ \vdots & \ddots & \ddots & \ddots & \vdots \\ 0 & 0 & \cdots & I & 0 \end{bmatrix}, H_k^a = \begin{bmatrix} H_k \\ C_{k+1}^{1st} \cdot H_k \\ 0 \\ \vdots \\ 0 \end{bmatrix}, \tag{4.25}$$

$$C_k^a = \begin{bmatrix} C_k^{2nd} & 0 & \cdots & 0 & 0 \\ 0 & 0 & \cdots & 0 & I \end{bmatrix}.$$

Being able to maintain the same amount of information, measurement augmentation method has smaller order than the state augmentation approach. However, its computational load is still heavy for large values of n_d which is the case in this dissertation.

Sample-state augmentation:

Compared with the aforementioned two augmentation approaches, another augmentation algorithm, proposed in [91] and named sample-state augmentation method in [35], is favorable in terms of calculation burden. The lagged measurement at step k represents the state n_d steps before, thus, only the information of the state at k-n_d need to be stored until the measurement arrival time. Instead of augmenting the state with all the previous states or all the previous primary measurements during delay period, it is sufficient to augment the state with the information at step k-n_d, when the primary measurement is sampled, i.e., the augmented state vector is

$$x_k^a = \begin{bmatrix} x_k^T & x_{k-n_d}^T \end{bmatrix}^T \tag{4.26}$$

The measurement vector is exactly the same with the previous two methods and, system matrices in this method are given as

$$G_k^a = \begin{bmatrix} G_k & 0 \\ 0 & I \end{bmatrix}, \quad H_k^a = \begin{bmatrix} H_k^T & 0 \end{bmatrix}^T,$$

$$C_k^a = \begin{bmatrix} C_k^{2nd} & 0 \\ 0 & C_{k-n_d}^{1st} \end{bmatrix}. \tag{4.27}$$

This state arrangement, at step k-n_d, has the state vector as expressed in equation 4.28.

$$x_k^a = \begin{bmatrix} x_{k-n_d}^T & x_{k-n_d}^T \end{bmatrix}^T \tag{4.28}$$

During the latency period of the primary measurement, the augmented states are only updated with the non-delayed measurement by using an indicator matrix which indicates which of the states must be updated and which should be neglected. That is, the indicator matrix is block diagonal with *1*s in the diagonals for states which should be updated and *0*s for states which are not to be updated [91]. After n_d steps, the primary measurement is optimally fused at step k.

This method, although has much less state order than the previous two augmentation approaches, has to double the original states. In this dissertation, the measurement vector is a subset of the state vector (except the non-measurable state), therefore, it is possible to modified the sample-state augmentation method that only primary measurement-related states are augmented for computation load reduction. It will be further explained in Chapter 5.

4.4.2 Multi-rate Kalman Filter Design Based on Inter-sample Residual Estimation

With the augmented state space equation, Kalman filter can be readily constructed. However, due to the sampling discrepancy among different sensors, the sampling time of the system need to be considered. A straightforward solution is to adapt the sampling rate of high-speed sensors to the slowest device with the sacrifice of estimator updating rate and loss of inter-sample information from high speed devices, i.e., transform the multi-rate system to a single-rate one. Another approach is the so-called multi-rate Kalman filter as studied in [22]-[24].

The multi-rate Kalman filter is aimed at utilizing more information from high-speed sensors and increasing the updating rate of the estimator for high-performance control. Furthermore, considering or neglecting the inter-sampling performances, two kinds of multi-rate Kalman filter can be designed as elaborated below.

Multi-rate Kalman filter without inter-sample residual estimation:

First, the system is discretized with the sampling time of the fastest device, i.e., secondary measurement time is set as the system discretization time. Then, the time update can be implemented in the normal way based on the system model as explained in the previous chapter. To distinguish different measurement sources, primary measurement-related prediction and secondary measurement-related prediction are separated as expressed in equation 4.29. As can be observed, they share the same form of time update.

$$\begin{aligned} \hat{x}_k^{1st-} &= A_{k-1}^{1st} \cdot \hat{x}_{k-1}^{1st} + B_{k-1}^{1st} \cdot u_{k-1} \\ \hat{x}_k^{2nd-} &= A_{k-1}^{2nd} \cdot \hat{x}_{k-1}^{2nd} + B_{k-1}^{2nd} \cdot u_{k-1} \end{aligned} \tag{4.29}$$

During the time intervals of $i \cdot T_l$, no primary information is available while the secondary signals can be obtained at every T_s time.

Therefore, the correction for secondary measurement can be updated normally as

$$\hat{x}_k^{2nd} = \hat{x}_k^{2nd-} + K_k^{2nd} \cdot \left(y_k^{2nd} - C_k \cdot \hat{x}_k^{2nd-} \right) \tag{4.30}$$

Meanwhile, during inter-samples, pseudo-corrections have to be implemented for the operation of the primary measurement update. An intuitive solution is to assume that the primary measurement is exactly the same as model-based prediction, and the primary measurement update therefore has the form of equation 4.31, which is equivalent to assume that, the primary measurement is the same with prediction, i.e., the inter-measurement residuals are set to zero. Using this method, corrections can still be made with information from high-speed sensors during the inter-sampling of the slow-rate device.

$$\hat{x}_k^{1st} = \begin{cases} \hat{x}_k^{1st-} & , \ if \quad k = i \cdot N, \\ \hat{x}_k^{1st-} + K_k^{1st} \cdot \left(y_k^{1st} - C_k \cdot \hat{x}_k^{1st-} \right), & if \quad k = i \cdot N. \end{cases} \tag{4.31}$$

By assuming that the measurements of the slow-rate sensors are the same as the model-based predictions during the inter-sampling periods, the above method realizes higher estimation accuracy and faster updating frequency than the single-rate one. The relevant applications can be found in satellite control [34] and construction monitoring system [16]. However, the assumption on measurements is not true in practice because of the presence of modeling errors. That is, inter-sampling residuals are not zero. In addition, the convergence of such method is questionable during inter-sampling periods, which will be discussed later in this chapter. Therefore, the inter-sample residuals must be computed for better estimation accuracy and convergence.

Multi-rate Kalman filter with inter-sample residual estimation:

As aforementioned, the above multi-rate Kalman filter cannot guarantee inter-sample performances of the estimate during measurement intervals. Therefore, a new method with inter-sampling residual estimation is proposed in this section as explained below.

The same as the multi-rate Kalman filter without inter-sample compensation, first, the sampling time of the secondary measurement is used to discretize the system and, the time update is expressed as given in equation 4.29. For correction of secondary prediction, equation 4.29 is also applicable.

During the time intervals of the primary measurement, in case of multi-rate Kalman filter with inter-sample residual estimation, the measurements are predicted even if they are not available and, the states estimation should have the form of equation 4.32.

$$\hat{x}_k = \hat{x}_k^- + K_k \cdot \left(\tilde{y}_k - C_k \cdot \hat{x}_k^- \right) \tag{4.32}$$

where

$$\tilde{y}_k = \begin{cases} \left[\left(y_k^{2nd} \right)^T, \left(y_k^{1st} \right)^T \right]^T, & if \quad k = i \cdot N, \\ \left[\left(y_k^{2nd} \right)^T, \left(\tilde{y}_k^{1st} \right)^T \right]^T, & if \quad k \neq i \cdot N. \end{cases}$$

In the above formulation, primary measurements during inter-samples need to be estimated. For Kalman filter design, measurements are utilized for residuals calculation, therefore, residuals will be considered instead of measurements in the following equation derivations. The basic idea of the inter-sample residual estimation is to utilize the residual of

the initial step that is available and propagate it to the following inter-measurement steps. After N steps, the residual is recalculated when new measurements come in.

The general definition of residual ε and estimation error e are shown in equations 4.33 and 4.34, respectively. The two equations play important roles in the inter-sample residual calculation.

$$\varepsilon = y - C \cdot \hat{x}^{-} \tag{4.33}$$

$$e = x - \hat{x} \tag{4.34}$$

To derive the pseudo-residual algorithm, process noise w_k and measurement noise v_k are assumed to be small and are hence ignored. This assumption is based on two considerations. First, the inter-sample residual compensation in this application is designed for visual information. As aforementioned, the vision model and the visual measurements are assumed to be accurate. Second, obtaining w_k and v_k in real time for algorithm implementation is difficult.

Based on the discrete system in equation 4.16, the algorithm for the inter-sample residual calculation can be generalized in four steps as follows:

1) When sensor measurements are available, the initial residual at step k is obtained as equation 4.35. The initial residual is available at each $i \cdot T_l$ step.

$$\varepsilon_k = y_k - C_k \cdot \hat{x}_k^{-} \tag{4.35}$$

2) Using equation 4.34 and considering that matrix C_k might not be invertible, the initial estimation error can be estimated by ε_k as

$$e_k = \left[\left(C_k^T \cdot C_k \right)^{-1} \cdot C_k^T - K_k \right] \cdot \varepsilon_k \tag{4.36}$$

3) From the definition of the estimation error in equation 4.34, the estimation dynamics at step $k+j$ can be propagated using equation 4.37, where $j \in [1, T_l / T_s)$.

$$
\begin{aligned}
e_{k+j} &= x_{k+j} - \hat{x}_{k+j} \\
&= x_{k+j} - \hat{x}^{-}_{k+j} - K_{k+j} \cdot (y_{k+j} - C_{k+j} \cdot \hat{x}^{-}_{k+j}) \\
&= (x_{k+j} - \hat{x}^{-}_{k+j}) - K_{k+j} \cdot (C_{k+j} \cdot x_{k+j} - C_{k+j} \cdot \hat{x}^{-}_{k+j}) \\
&= (I - K_{k+j} \cdot C_{k+j}) \cdot G_{k+j-1} \cdot e_{k+j-1}
\end{aligned} \tag{4.37}
$$

4) Finally, the pseudo-residual during the inter-sampling period is given by equation 4.38 and, it is updated using equation 4.37.

$$
\begin{aligned}
\tilde{\varepsilon}_{k+j} &= y_{k+j} - C_{k+j} \cdot \hat{x}^{-}_{k+j} \\
&= C \cdot x_{k+j} - C_{k+j} \cdot \hat{x}^{-}_{k+j} \\
&= C_{k+j-1} \cdot G_{k+j-1} \cdot e_{k+j-1}
\end{aligned} \tag{4.38}
$$

The above four steps are shown in Fig. 4.3. The first two steps are the initialization, and the estimation error is then self-propagated using equation 4.37. Finally, the inter-sample residuals are obtained using the estimated error dynamics. The estimation errors must be noted to be unknown in reality because some states are not available from the sensors. In

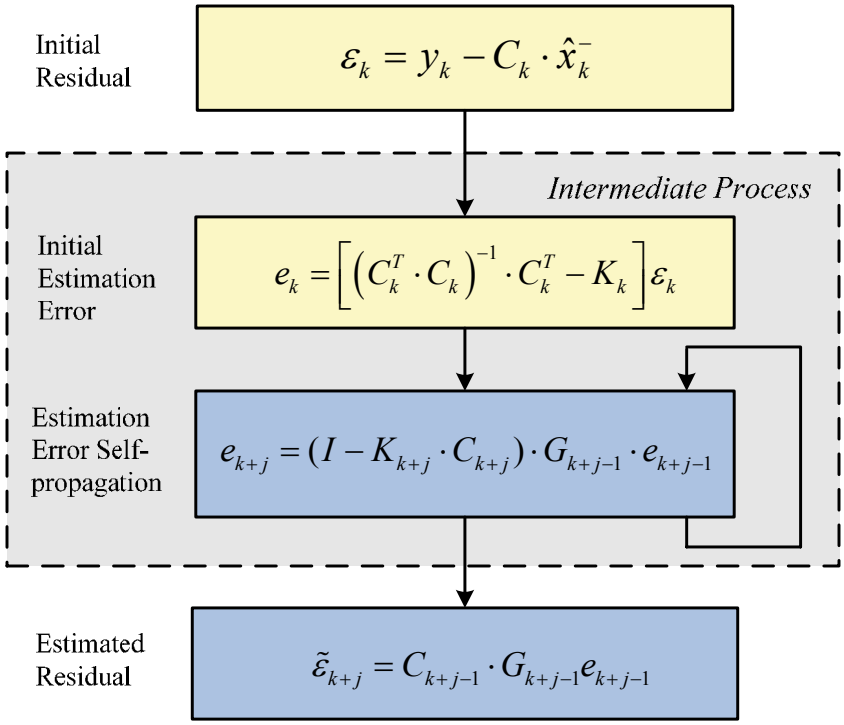

Fig.4. 3 Operating principle of the inter-sample residual estimation.

addition, the key factor for estimation correction is the residual. In this algorithm, the estimation errors function as intermediate quantities for the calculation of pseudo-residuals.

Equations 4.35-4.38 further yield a self-propagation equation for inter-sample residuals using the initial residual at step *k+j* as

$$\tilde{\varepsilon}_{k+j} = \prod_{m=1}^{j} Q_{k+m} \cdot \varepsilon_k \tag{4.39}$$

where

$$Q_{k+m} = C_{k+m} \cdot G_{k+m} \cdot \left(I - K_{k+m} \cdot C_{k+m}\right) \cdot C_{k+m}^T \cdot \left(C_{k+m} \cdot C_{k+m}^T\right)^{-1}$$

Notice that the above processes calculate the inter-sample residuals for all the states, and the secondary measurement-related states are not needed since they have true correction. The

below calculation is performed to extract the primary measurement-related states for measurement update.

$$\tilde{\varepsilon}_{k+j}^{1st} = C_{k+j}^{1st} \cdot \tilde{\varepsilon}_{k+j} \tag{4.40}$$

Finally, the primary measurement at any step k during sampling intervals can be given as the below equation for the operation of equation 4.32.

$$\tilde{y}_k^{1st} = C_k^{1st} \cdot \hat{x}_k^{-} + \tilde{\varepsilon}_k^{1st} \tag{4.41}$$

4.4.3 Convergence Analysis

In this section, the aforementioned two multi-rate Kalman filters are analyzed in terms of convergence performance in comparison with the idea case. The ideal case means that all the measurements are available at every short sampling time, i.e., the primary measurements are sampled at the frequency of secondary measurements.

1) Ideal case. Considering the discrete Kalman filter given in equations 4.3 and 4.4 , in the ideal case, measurements are available at every step, and the observation error at step $k+n$ is given as

$$\begin{aligned}
e_{k+n} &= x_{k+n} - \hat{x}_{k+n} \\
&= G_{k+n-1} \cdot x_{k+n-1} + H_{k+n-1} \cdot u_{k+n-1} + w_{k+n-1} - \overline{x}_{k+n} \\
&\quad - K_{k+n} \cdot \left(y_{k+n} - C_{k+n} \cdot \overline{x}_{k+n} \right) \\
&= \left(I - K_{k+n} \cdot C_{k+n} \right) \cdot G_{k+n-1} \cdot e_{k+n-1} - K_{k+n} \cdot w_{k+n} + \left(I - K_{k+n} \cdot C_{k+n} \right) \cdot w_{k+n-1} \\
&= \prod_{i=1}^{n} \left[(I - K_{k+i} \cdot C_{k+n}) \cdot G_{k+i-1} \right] \cdot e_k + \\
&\quad \sum_{p=0}^{n-1} \left\{ \prod_{i=p+1}^{n-1} \left[(I - K_{k+i+1} \cdot C_{k+i+1}) \cdot G_{k+i} \right] \cdot (I - K_{k+p+1} \cdot C_{k+p+1}) \cdot w_{k+p} \right\} \\
&\quad - \sum_{p=1}^{n} \left\{ \prod_{i=p+1}^{n} \left[(I - K_{k+i} \cdot C_{k+i}) \cdot G_{k+i-1} \right] \cdot K_{k+p} \cdot v_{k+p} \right\}
\end{aligned} \tag{4.42}$$

Obviously, well-designed Kalman gains perform n times to minimize the estimation error even if the system itself is unstable, and the subtraction of the measurement noise term v_{k+p} can further reduce the estimation error. That is, the estimation result can converge to true value gradually.

2) Multi-rate Kalman filter without inter-sample residual compensation. In the case where measurements during inter-samples are absent, the residuals are zero, and the observation error is derived as follows:

$$\begin{aligned} e_{k+n} &= x_{k+n} - \hat{x}_{k+n} \\ &= G_{k+n-1} \cdot x_{k+n-1} + H_{k+n-1} \cdot u_{k+n-1} + w_{k+n-1} - \overline{x}_{k+n} \\ &= G_{k+n-1} \cdot e_{k+n-1} + w_{k+n-1} \\ &= \prod_{i=0}^{n-1} \left(G_{k+i} \right) \cdot e_k + \sum_{p=0}^{n-1} \left[\prod_{i=p+1}^{n-1} \left(G_{k+i} \right) \cdot w_{k+p} \right] \end{aligned} \tag{4.43}$$

The error dynamic at step $k+n$ was found to be dependent only on the system matrix. That is, e_{k+n} is open loop. If the system is not stable, the estimation error cannot converge to the true value.

3) Multi-rate Kalman filter with inter-sample residual compensation. To improve the convergence performance, the observation error was derived using the algorithm given in Section IV as follows:

$$\begin{aligned} e_{k+n} &= x_{k+n} - \hat{x}_{k+n} \\ &= G_{k+n-1} \cdot x_{k+n-1} + H_{k+n-1} \cdot u_{k+n-1} + w_{k+n-1} - \overline{x}_{k+n} - K_{k+n} \cdot \tilde{\varepsilon}_{k+n} \\ &= G_{k+n-1} \cdot e_{k+n-1} + w_{k+n-1} - K_{k+n} \cdot \tilde{\varepsilon}_{k+n} \\ &= \prod_{i=0}^{n-1} \left(G_{k+i} \right) \cdot e_k + \sum_{p=0}^{n-1} \left[\prod_{i=p+1}^{n-1} \left(G_{k+i} \right) \cdot w_{k+p} \right] - \\ &\quad \sum_{p=1}^{n} \left[\prod_{i=p}^{n-1} \left(G_{k+i} \right) \cdot K_{k+p} \cdot \tilde{\varepsilon}_{k+p} \right] \end{aligned} \tag{4.44}$$

Compared with the multi-rate Kalman filter without residual compensation in 2), the estimation error at step $k+n$ was subtracted by the estimated residual, which can reduce estimation error. That is, this method showed better convergence performance than the multi-rate Kalman filter without residual compensation.

Meanwhile, the estimation error in this case can also be derived as

$$\begin{aligned} e_{k+n} &= x_{k+n} - \hat{x}_{k+n} \\ &= G_{k+n-1} \cdot e_{k+n-1} + w_{k+n-1} - K_{k+n} \cdot \tilde{\varepsilon}_{k+n} \\ &= G_{k+n-1} \cdot e_{k+n-1} + w_{k+n-1} - K_{k+n} \cdot C_{k+n-1} \cdot G_{k+n-1} \cdot e_{k+n-1} \\ &= \left(I - K_{k+n} \cdot C_{k+n}\right) \cdot G_{k+n-1} \cdot e_{k+n-1} + w_{k+n-1} \\ &= \prod_{i=1}^{n} \left[(I - K_{k+i} \cdot C_{k+i}) \cdot G_{k+i-1} \right] \cdot e_k + \\ &\quad \sum_{p=0}^{n-1} \left\{ \prod_{i=p+1}^{n-1} \left[(I - K_{k+i+1} \cdot C_{k+i+1}) \cdot G_{k+i} \right] \cdot (I - K_{k+p+1} \cdot C_{k+p+1}) \cdot w_{k+p} \right\} \end{aligned} \quad (4.45)$$

Compared with the ideal case in 1), the first two terms are the same. However, the measurement noise term is absent, which renders it worse than the ideal case.

In general, the multi-rate Kalman filter with residual compensation performs better than the one without compensation but behaves worse than the ideal case when measurements are available at every short sampling time.

4.5 Multi-rate Kalman filter Design Considering Uneven Measurement Delay

Unlike the constant delay, state augmentation method can be complex for state estimation with uneven delay [30]. Therefore, a measurement reconstruction method is developed to solve the random delay issue and, the inter-sample residual estimation is then performed based on the reconstructed measurement.

4.5.1 Measurement Reconstruction

As can be seen in Fig. 4.4, the out-of-sequence primary information is not straightforward for fusion with the secondary signals, and it is therefore desired to reconstruct it.

Consider that the primary data are sampled at $(i-1)\cdot T_l$, but are not available until time $(i-1)\cdot T_l + T_{d\_i}$, it is reasonable to assume that the samplings are taken at $(i-1)\cdot T_l + T_{d\_i}$ instead of $(i-1)\cdot T_l$. Thus, the delay is removed from the reconstructed sampling sequence. As the measurements at $(i-1)\cdot T_l + T_{d\_i}$ represent the information at $(i-1)\cdot T_l$, and corresponding modification of residual is necessary.

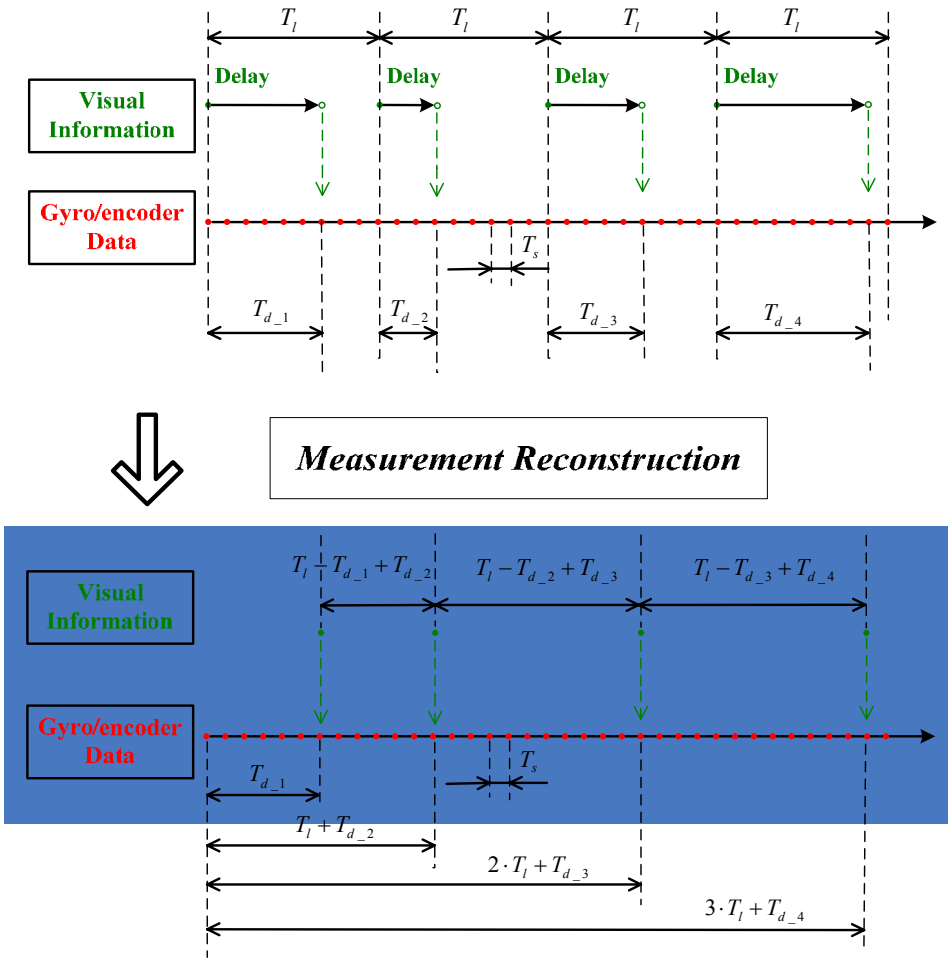

Fig.4. 4 Measurement reconstruction

After the above re-arrangement, the delays are removed from the primary measurements. However, the updates are still uneven and the sampling time is much longer than that of the secondary one. The problem is then transformed into designing a multi-rate Kalman filter for a discrete system with random multi-ratio. Two points need to be considered in this case: 1) residual modification at every $(i-1)\cdot T_l + T_{d\_i}$ time; 2) residuals estimation between every neighboring primary samples.

4.5.2 Inter-sample Residual Estimation

The solution for multi-rate measurement with random delay is also based on residual estimation technique. The overall algorithm can be summarized as: first consider the idea case when measurements are available at every T_s without delay, and derive the residual propagation equations. Then apply them to the multi-rate and delayed case.

Then, apply the residual calculation equation to the reconstructed measurements. The algorithm can be generalized in three situations as follows:

1) Initial n_{d_1} steps:

   At step k in [0, n_{d_1}), the residual ε_k is 0 due to the delay of measurement, i.e., the measurements are not available for initial residuals calculation.

2) Reconstructed residual at each (i-1)$\cdot n$ + n_{d_i} step:

   The measurement at each (i-1)$\cdot n$ + n_{d_i} step represents information at step (i-1)$\cdot n$, and the correct residual at that step is given as

$$\varepsilon_{(i-1)\cdot n} = y_{(i-1)\cdot n} - C \cdot x_{(i-1)\cdot n} \tag{4.46}$$

   Based on the propagation equation in equation 4.39, the residual at step (i-1)$\cdot n$ + n_{d_i} can be calculated as

$$\varepsilon_{(i-1)\cdot n+n_{d\_i}} = \prod_{m=1}^{n_{d\_i}} Q_{(i-1)\cdot n+m} \cdot \varepsilon_{(i-1)\cdot n} \tag{4.47}$$

   This can be interpreted as: prepare the correct residual propagation matrix, and then calculate the final residual when measurements are available.

3) Inter-sample residual:

The basic idea of the inter-sample residual estimation is to utilize the residual of the step 2 that is available and propagate it to the following inter-measurement steps. After $\left(n - n_{d\_(i-1)} + n_{d\_i}\right)$ steps (the delayed steps), the residual is recalculated when "new measurement" come in. However, it should be noticed that the so-called "new measurement" is not new because it is the delayed information.

Between every two neighboring sampling times of the camera, the residual ε_k can be expressed as

$$\varepsilon_k = \prod_{m=1}^{k-(i-1)\cdot n-n_{d\_i}} Q_{(i-1)\cdot n+n_{d\_i}+m} \cdot \varepsilon^{vis}_{(i-1)\cdot n+n_{d\_i}} \tag{4.48}$$

$$where \quad k \in \left((i-1)\cdot n+n_{d\_i},\ i\cdot n+n_{d\_(i+1)}\right)$$

Be noted that the residual in 4.48 includes the part for secondary residual, and the primary residual should be extracted from it using equation 4.40.

4.5.3 Convergence Analysis

The convergence of the proposed multi-rate Kalman filter with compensation for random delay is analyzed in this section. Considering that different periods have different convergence characteristics, three cases are considered as below

$1^{st}.\ \ k \in \left[0,\ \ n_{d\_1}\right);$

$2^{nd}.\ \ k \in \left(n_{d\_1},\ \ N + n_{d\_2}\right),$

$3^{rd}.\ \ k \in \left(\left(i-1\right)\cdot N + n_{d\_i},\ \ i\cdot N + n_{d\_(i+1)}\right),\ \ i \geq 2.$

1) In the first case, as the first sample is delayed, there is no signal feedback during this period; estimation error is therefore purely based on the model and initial error.

$$\begin{aligned} e_k &= x_k - \hat{x}_k \\ &= \prod_{i=0}^{k-1}\left(A_i\right)\cdot e_0 + \sum_{p=0}^{k-1}\left[\prod_{i=p+1}^{k-1}\left(A_i\right)\cdot w_p\right] \end{aligned} \tag{4.49}$$

It can be observed that the estimation error dynamics is open loop, i.e., the convergence during [0, n_{d_1}) cannot be guaranteed.

2) The residual at step n_{d_1} when the first measurement is available is calculated based on the below equation

$$\tilde{\varepsilon}_{n_{d\_1}} = \prod_{i=1}^{n_{d\_1}} Q_i \cdot \varepsilon_0 \tag{4.50}$$

where ε_0 is the initial residual.

Then, at any step during (n_{d_1}, N+n_{d_2}), the estimation error can be calculated as

$$\begin{aligned} e_{n_{d\_1}+k} &= x_{n_{d\_1}+k} - \hat{x}_{n_{d\_1}+k} \\ &= \prod_{i=0}^{k-1}\left(A_{n_{d\_1}+i}\right)\cdot e_{n_{d\_1}} + \sum_{p=0}^{k-1}\left[\prod_{i=p+1}^{n_{d\_1}-1}\left(A_{n_{d\_1}+i}\right)\cdot w_{n_{d\_1}+p}\right] \\ &\quad - \sum_{p=1}^{k}\left[\prod_{i=p}^{k-1}\left(A_{n_{d\_1}+i}\right)\cdot K_{n_{d\_1}+p}\cdot \tilde{\varepsilon}_{n_{d\_1}+p}\right] \end{aligned} \tag{4.51}$$

where

$$\begin{aligned} e_{n_{d\_1}} &= x_{n_{d\_1}} - \hat{x}_{n_{d\_1}} \\ &= \prod_{i=0}^{n_{d\_1}-1}\left(A_i\right)\cdot e_0 + \sum_{p=0}^{n_{d\_1}-1}\left[\prod_{i=p+1}^{n_{d\_1}-1}\left(A_i\right)\cdot w_p\right] \end{aligned}$$

It can be seen from equation 4.51 that in addition to the open loop dynamics, a term containing Kalman gain and estimated residual is added. The estimation error can then be minimized with suitable Kalman gains asymptotically.

Another interpretation of the error dynamics can be formulated as

$$\begin{aligned} e_{n_{d\_1}+k} &= x_{n_{d\_1}+k} - \hat{x}_{n_{d\_1}+k} \\ &= \prod_{i=1}^{k}\left[(I - K_{n_{d\_1}+i}\cdot C)\cdot A_{n_{d\_1}+i-1}\right]\cdot e_{n_{d\_1}} + \end{aligned}$$

$$\sum_{p=0}^{k-1}\left\{\prod_{i=p+1}^{k-1}\left[(I-K_{n_{d\_1}+i+1}\cdot C)\cdot A_{n_{d\_1}+i}\right]\cdot(I-K_{n_{d\_1}+p+1}\cdot C)\cdot w_{n_{d\_1}+p}\right\} \quad (4.52)$$

From the equation 4.52, it can be observed that the estimation error can be reduced along with the increasing of k, which can also prove the convergence of the proposed Kalman filter with residual estimation.

3) Then, the error dynamics hereafter at any step during $((i\text{-}1)\cdot N+n_{d\_i},\ i\cdot N+n_{d\_(i+1)})$, $i\geq 2$ share similar formulations. For simplicity, this section only considers the case when $i=2$. That is, at any step during $(N+n_{d\_2},\ 2\cdot N+n_{d\_3})$.

The residual at step n_{d_1} is calculated based on the below equation

$$\tilde{\varepsilon}_{n_{d\_2}}=\prod_{i=1}^{n_{d\_2}}Q_i\cdot\varepsilon_1 \quad (4.53)$$

Then, the estimation error can be calculated as

$$\begin{aligned}e_{N+n_{d\_2}+k}&=x_{N+n_{d\_2}+k}-\hat{x}_{N+n_{d\_2}+k}\\&=\prod_{i=0}^{k-1}\left(A_{N+n_{d\_2}+i}\right)\cdot e_{N+n_{d\_2}}+\sum_{p=0}^{k-1}\left[\prod_{i=p+1}^{N+n_{d\_2}-1}\left(A_{N+n_{d\_2}+i}\right)\cdot w_{N+n_{d\_2}+p}\right]\\&\quad-\sum_{p=1}^{k}\left[\prod_{i=p}^{k-1}\left(A_{N+n_{d\_2}+i}\right)\cdot K_{N+n_{d\_2}+p}\cdot\tilde{\varepsilon}_{N+n_{d\_2}+p}\right]\end{aligned} \quad (4.54)$$

where

$$\begin{aligned}e_{N+n_{d\_2}}&=x_{N+n_{d\_2}}-\hat{x}_{N+n_{d\_2}}\\&=\prod_{i=1}^{N+n_{d\_2}-n_{d\_1}}\left[(I-K_{n_{d\_1}+i}\cdot C)\cdot A_{n_{d\_1}+i-1}\right]\cdot e_{n_{d\_1}}+\\&\quad\sum_{p=0}^{N+n_{d\_2}-n_{d\_1}-1}\left\{\begin{array}{l}\prod_{i=p+1}^{N+n_{d\_2}-n_{d\_1}-1}\left[(I-K_{n_{d\_1}+i+1}\cdot C)\cdot A_{n_{d\_1}+i}\right]\cdot\\(I-K_{n_{d\_1}+p+1}\cdot C)\cdot w_{n_{d\_1}+p}\end{array}\right\}\end{aligned}$$

It can be seen from equation 4.54 that in addition to the open loop dynamics, a term containing Kalman gain and estimated residual is added. The estimation error can then be minimized with suitable Kalman gains asymptotically.

Or we can interpret the error dynamics as

$$\begin{aligned} e_{N+n_{d\_2}+k} &= x_{N+n_{d\_2}+k} - \hat{x}_{N+n_{d\_2}+k} \\ &= \prod_{i=1}^{k}\left[(I - K_{N+n_{d\_2}+i} \cdot C) \cdot A_{N+n_{d\_2}+i-1}\right] \cdot e_{N+n_{d\_2}} + \\ &\sum_{p=0}^{k-1}\left\{\begin{array}{l} \prod_{i=p+1}^{k-1}\left[(I - K_{N+n_{d\_2}+i+1} \cdot C) \cdot A_{N+n_{d\_2}+i}\right] \cdot \\ (I - K_{n_{d\_1}+p+1} \cdot C) \cdot w_{N+n_{d\_2}+p} \end{array}\right\} \end{aligned} \tag{4.55}$$

It can also be observed that the estimation error can be reduced along with the increasing of *k*.

4.6 Chapter Summary

This chapter mainly dealt with the theories related to multi-rate and delay issues. First, the discretization method for observer design was introduced. Then, considering the discrepancy between primary and secondary measurements, the multi-rate and delay (constant or random) issues were stated in detail. And then, multi-rate Kalman filter based on state augmentation was designed, and the convergence performance was analyzed. Finally, the multi-rate Kalman filter considering uneven delay was studied using measurement reconstruction method and inter-sample residual estimation algorithm and, the convergence performance was also analyzed and compared with the other methods. This chapter provides a general solution to state estimation with multi-rate and delay issues.

Chapter 5

Vision-based Multi-rate Estimation for Vehicle Body Slip Angle Control

In this chapter, a new method for vehicle body slip angle estimation is studied using the nontraditional sensor configuration and system model proposed in Chapter 2, which enables robust estimation against vehicle parameter uncertainties. Due to the sampling characteristics of the vision system, a multi-rate estimation method is employed. The proposed body slip angle estimation method is verified with simulations and experiments. And then, a 2DOF controller is designed with the estimated body slip angle as feedback. It is demonstrated that, the open loop stability margin of the system with the multi-rate feedback can be improved compared with the with single-rate feedback case.

5.1 Introduction

Body slip angle, also known as sideslip angle, is considered as one of the key enablers for vehicle motion control systems [54]. However, off-the-shelf products for body slip angle measurement such as noncontact optical sensor and GPS-based apparatus are very expensive for practical applications [39]. Therefore, cost-effective methods for vehicle body slip angle estimation have been studied extensively during the last few decades [52]-[54]. Based on the models used, past research can be generally divided into two categories: kinematic model-based and dynamic model-based methods. In [54], the body slip angle was calculated based on its kinematic relationship with the yaw rate, longitudinal acceleration, and so on; however, this method involves integration of sensor signals and, therefore, requires high-precision sensors. Given that the kinematic model does not include time-varying parameters such as tire cornering stiffness, the driving condition change has little influence on the estimation accuracy. However, this method is heavily affected by sensor noise and drift [39]. The second method is based on vehicle dynamics with either linear or nonlinear bicycle model. In [52], linear bicycle model-based observers were constructed and verified with experimental data. To provide more design freedom and avoid unobservable situations, lateral acceleration

was utilized as an additional measurement in [55], but uncertainties (cornering stiffness) are also brought into the system observation equation. Although the linear observer is easy to use, the parameters of the linear models are fixed; thus, not all driving conditions can be addressed. Considering the nonlinear characteristics of tires, nonlinear model-based methodologies provide better estimation accuracy under different driving conditions compared with the linear one. For example, in [58], a nonlinear vehicle model was considered as a bounded Jacobian system for more accurate results under different running situations. However, such nonlinear estimators are very complex and theoretically immature [39], [39].

Meanwhile, look-ahead cameras have increasingly become popular in vehicles. Most related studies and products are designed for lane departure warning, lane keeping, or collision avoidance [61]. Nevertheless, investigating other applications using the onboard vision system is desirable. Based on the simple linear model that combines the vehicle and vision models proposed in Chapter 2, a body slip angle estimation method is investigated, and the visual model is independent of the uncertain parameters of the vehicle, such as cornering stiffness. Moreover, as stated before, vehicle position measurement from the vision system is very accurate. Therefore, incorporating visual information can increase the estimator's design freedom without introducing uncertainties into it. However, two issues arise with this method. The first one is visual measurement delay caused by image processing (in this chapter, it is assumed that the delay is constant), and it is generally too long to be neglected. Furthermore, as the sampling time of the normal camera is much longer than that of the other onboard sensors, fusing these signals presents a multi-rate issue.

5.2 Sensor Configurations for Body Slip Angle Estimation

As aforementioned, body slip angle needs to be estimated due to the high cost of direct measurement. Actually, more than one sensor configuration can be utilized for such application. In this section, before explaining the proposed multi-rate Kalman filter for body slip angle estimation, some typical sensor configurations are reviewed in terms of observability and model uncertainty.

To facilitate the discussion, all the models that to be presented are given in the state space form as below

$$\dot{x} = A \cdot x + B \cdot u \tag{5.1}$$

$$y = C \cdot x + D \cdot u \tag{5.2}$$

5.2.1 Traditional Sensor Configuration 1: Gyro Sensor

The most widely used method, although has different kinds of transformations, is based on the dynamic model given below, and yaw rate is the only signal required for observer construction.

$$A = \begin{bmatrix} -\dfrac{2\cdot\left(C_f + C_r\right)}{mV_x} & -1 - \dfrac{2\cdot\left(C_f l_f - C_r l_r\right)}{mV_x{}^2} \\ \dfrac{2\cdot\left(C_r \cdot l_r - C_f \cdot l_f\right)}{I_z} & -\dfrac{2\cdot\left(C_f l_f^2 + C_r l_r^2\right)}{I_z \cdot V_x} \end{bmatrix},$$

$$B = \begin{bmatrix} \dfrac{2\cdot C_f}{m\cdot V_x} & 0 \\ \dfrac{C_f \cdot l_f}{I_z} & \dfrac{1}{I_z} \end{bmatrix}, \quad C = \begin{bmatrix} 0 & 1 \end{bmatrix}, \quad x = \begin{bmatrix} \beta & \gamma \end{bmatrix}^T, \quad u = \begin{bmatrix} \delta_f & N_z \end{bmatrix}^T. \tag{5.3}$$

Although this method is very simple, it is unobservable in case of neutral steering ($C_f \cdot l_f - C_r \cdot l_r = 0$) which can be seen from the observability matrix below, i.e., observability matrix rank is less than the system order. Moreover, the performance of this method is deteriorated by model uncertainties such as C_f and C_r which are time-varying in different driving conditions.

$$rank\left(\begin{bmatrix} C \\ CA \end{bmatrix}\right) = rank\left(\begin{bmatrix} 0 & 1 \\ \dfrac{2\cdot\left(C_r \cdot l_r - C_f \cdot l_f\right)}{I_z} & -\dfrac{2\cdot\left(C_f l_f^2 + C_r l_r^2\right)}{I_z \cdot V_x} \end{bmatrix}\right) = 1 \tag{5.4}$$

5.2.2 Traditional Sensor Configuration 2: Gyro and Lateral Acceleration Sensors

Aimed at building an always observable model and increasing the design freedom of the estimator, some studies include lateral acceleration a_y as a additional measurement. The measurement matrices in equation 5.2 then become

$$C = \begin{bmatrix} 0 & 1 \\ -\dfrac{2\cdot\left(C_f + C_r\right)}{m} & -\dfrac{2\cdot\left(C_f l_f - C_r l_r\right)}{mV_x} \end{bmatrix},\quad D = \begin{bmatrix} 0 & 0 \\ \dfrac{2\cdot C_f}{m} & 0 \end{bmatrix}. \tag{5.5}$$

As can be seen in equation 5.6, the rank of the observability matrix in case of $C_f \cdot l_f = C_r \cdot l_r$ is equal to two by only the first two rows, i.e., this model is observable even when the vehicle is in neutral steering.

$$rank\left(\begin{bmatrix} C \\ CA \end{bmatrix}\right) = rank\left(\begin{bmatrix} 0 & 1 \\ -\dfrac{2\cdot\left(C_f + C_r\right)}{m} & -\dfrac{2\cdot\left(C_f l_f - C_r l_r\right)}{mV_x} \\ \vdots & \vdots \end{bmatrix}\right) \geq 2 \tag{5.6}$$

Unfortunately, this method brings uncertainties (C_f and C_r) into the measurement matrices C and D in addition to the original uncertainties contained in the matrix A, which may decreases estimation accuracy in different driving conditions.

5.2.3 Proposed Sensor Configuration: Gyro Sensor and Vision System

The proposed model in Chapter 2 combines traditional vehicle bicycle model and a vision model, and the system matrices are given in equation 2.27. Again, the observability matrix is formulated in equation 5.7.

$$rank\left(\begin{bmatrix} C \\ C\cdot A \\ C\cdot A^2 \\ C\cdot A^3 \end{bmatrix}\right) = rank\left(\begin{bmatrix} 0 & 1 & 0 & 0 \\ 0 & 0 & 1 & 0 \\ 0 & 0 & 0 & 1 \\ -\dfrac{2(C_f l_f - C_r l_r)}{I} & -\dfrac{2(C_f l_f^2 + C_r l_r^2)}{IV_x} & 0 & 0 \\ 0 & 1 & 0 & 0 \\ V_x & l_{pre} & V_x & 0 \\ \vdots & \vdots & \vdots & \vdots \end{bmatrix}\right) \geq 4 \quad (5.7)$$

Only by checking the first six rows, even if the vehicle is in neutral steering condition, the rank of the observability matrix is equal to four, which means that this model is observable. In addition, as can be seen from matrices A and C, no uncertainties are introduced by this method. For example, parameters such as l_{pre} can be calibrated beforehand, and the vehicle velocity can be calculated from wheel speed [93]-[94]. Therefore, it enables robust estimation against changes in vehicle parameters. The merits of this model can be summarized as: 1) observable even in neutral steering situation; 2) no new uncertainties included; 3) increased design freedom for the observer.

On the other hand, the issues brought by this model such as multi-rate and measurement delay have to be solved for estimator implantation. For time delay, image processing time is considered as constant in this chapter, and the random delay theory will be applied to integrated vehicle lateral control system in the next chapter. For the multi-rate problem, a straightforward solution is to down-sample fast-rate sensors to adapt slower device and then construct a normal single-rate Kalman filter. In this application, gyroscope and encoders can be sampled every 33 ms to fit the sampling period of the camera. However, if the single-rate estimator is employed, the sampling rates between the state feedback and the control input of the IWMs cannot match, which brings limitation to the controller design. Thus, the multi-rate Kalman filter based on state augmentation that proposed in Chapter 4 is employed to solve the multi-rate and constant delay issues.

5.3 Multi-rate Kalman Filter Design with Constant Delay Compensation for Vehicle Body Slip Angle Estimation

To conduct estimation in real time, system discretization is indispensability. Based on the equation 4.14, the continuous system given in equation 2.27 can be approximately discretized using the sampling time T_s as below, where T_s is set to 1 ms as it is the fastest sampling time in the system. It should be noted that if T_l is selected as the dicretization time, the estimator then becomes a single-rate one. The single-rate estimator will be compared with the multi-rate one later in the simulation and experimental verification section.

$$x_k = \begin{bmatrix} \beta_k & \gamma_k & \psi_k & y_{l_k} \end{bmatrix}^T,\ u = \begin{bmatrix} \delta_{f_k} & N_{z_k} \end{bmatrix}^T,\ y_k = \begin{bmatrix} \gamma_k & \psi_k & y_{l_k} \end{bmatrix}^T,$$

$$G_k = \begin{bmatrix} \left(-\frac{2(C_f + C_r)}{mV_x}\right)\cdot T_s + 1 & \left(-1 - \frac{2(C_f l_f - C_r l_r)}{mV_x{}^2}\right)\cdot T_s & 0 & 0 \\ \left(-\frac{2(C_f l_f - C_r l_r)}{I}\right)\cdot T_s & \left(-\frac{2(C_f l_f^2 + C_r l_r^2)}{I\cdot V_x}\right)\cdot T_s + 1 & 0 & 0 \\ 0 & T_s & 1 & 0 \\ V_x \cdot T_s & l_{pre}\cdot T_s & V_x \cdot T_s & 1 \end{bmatrix}, \quad (5.8)$$

$$H_k = \begin{bmatrix} \frac{2C_f}{mV_x}\cdot T_s & \frac{2C_f l_f}{I}\cdot T_s & 0 & 0 \\ 0 & \frac{1}{I}\cdot T_s & 0 & 0 \end{bmatrix}^T,\ C_k = C = \begin{bmatrix} 0 & 1 & 0 & 0 \\ 0 & 0 & 1 & 0 \\ 0 & 0 & 0 & 1 \end{bmatrix}.$$

Remember that the estimation approach proposed in Chapter 4 involves two steps for multi-rate and constant delay issues: state augmentation and inter-sample residuals estimation. Based on the system in equation 5.8, using the two steps, a Kalman filter is designed for body slip angle estimation.

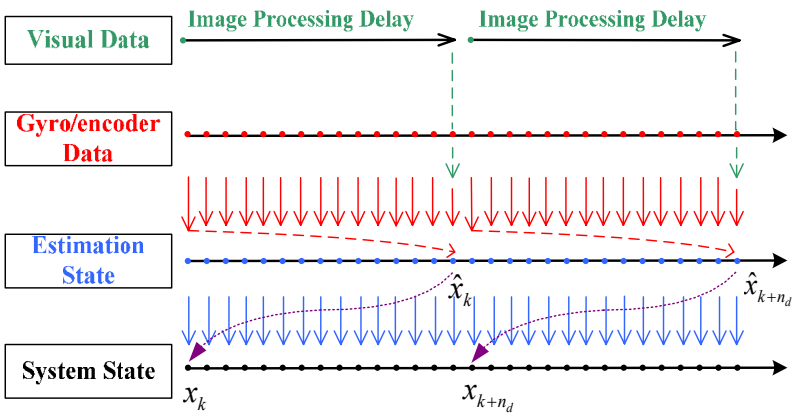

Fig.5. 1 System sampling sequence (multi-rate and constant delay)

5.3.1 Augmentation of Delayed Visual Measurements

Several augmentation methods to handle delayed measurements are introduced in the previous chapter. In consideration of calculation burden, it is desirable to augment the current state with the sampled measurements n_d steps before. That is

$$x_k^a = \begin{bmatrix} \beta_k & \gamma_k & \psi_k & y_{l_k} & \psi_{k-n_d} & y_{l_{k-n_d}} \end{bmatrix}^T \tag{5.9}$$

or in a compact form as given in equation 5.10.

$$x_k^a = \begin{bmatrix} x_k^T & \left(y_{k-n_d}^{vis}\right)^T \end{bmatrix}^T = \begin{bmatrix} x_k^T & \left(x_{k-n_d}^{vis}\right)^T \end{bmatrix}^T \tag{5.10}$$

The system matrices are then become

$$G_k^a = \begin{bmatrix} G_k & O_{4\times 2} \\ O_{2\times 2} & O_{2\times 2} \quad I_{2\times 2} \end{bmatrix}, \quad H_k^a = \begin{bmatrix} H_k^T & O_{2\times 2} \end{bmatrix}^T,$$

$$C_k^a = C = \begin{bmatrix} 0 & 1 & 0 & 0 & 0 & 0 \\ 0 & 0 & 0 & 0 & 1 & 0 \\ 0 & 0 & 0 & 0 & 0 & 1 \end{bmatrix}. \tag{5.11}$$

Unfortunately, the above system is not observable as can be easily checked from its observability matrix. Then, a trick is performed to assume that the visual information between step k and k-n_d are the same. The system matrices are then changed to

$$G_k^a = \begin{bmatrix} G_k & O_{4\times 2} \\ O_{2\times 2} & I_{2\times 2} \quad O_{2\times 2} \end{bmatrix}, \quad H_k^a = \begin{bmatrix} H_k^T & O_{2\times 2} \end{bmatrix}^T,$$

$$C_k^a = C = \begin{bmatrix} 0 & 1 & 0 & 0 & 0 & 0 \\ 0 & 0 & 0 & 0 & 1 & 0 \\ 0 & 0 & 0 & 0 & 0 & 1 \end{bmatrix}. \tag{5.12}$$

and the system becomes observable. Given the time delay is constant, the errors introduced by this assumption are approximately non-changeable and, can therefore be compensated by tuning of process noise covariance Q.

During the latency period of the visual measurement, the augmented states are only updated with the yaw rate signal (the inter-sample updates will be considered in the residual estimation part), and the visual states are optimally fused at step k after n_d steps.

5.3.2 Design of Multi-rate Kalman Filter

The multi-rate Kalman filter is designed based on the proposed inter-sample residual technique given in Chapter 4. It is aimed at utilizing the yaw rate signal every 1 ms and increasing the updating rate of the estimator to 1 kHz which match with the frequency of the control input for enhanced control performance. Just like normal Kalman filters, the design of multi-rate one consists of three parts: time update (prediction), measurement updates (correction) and Kalman gain design.

1) Time update

   The time update of the multi-rate Kalman filter can be implemented in the same way as the single-rate one. That is, the vehicle model-related states and vision model-related states can be updated together using the system model as shown in equation 5.13.

$$\hat{x}_k^{a-} = G_{k-1}^a \cdot \hat{x}_{k-1}^a + H_{k-1}^a \cdot u_{k-1} \tag{5.13}$$

2) Measurement update

The camera's sampling period is T_l. During the time intervals of $i \cdot T_l$, no information from the vision system is available. Therefore, pseudo-corrections have to be implemented for the operation of the measurement update. Conventional multi-rate Kalman filter assumes that the measurements from the vision system are exactly the same as those of the model-based predictions, i.e., the inter-measurement residuals from the vision system are zero. However, as shown mathematically in the previous chapter, the convergence of this method cannot be guaranteed. The multi-rate Kalman filter with inter-sample estimation is thus employed. The estimation equation is given as

$$\hat{x}_k^a = \hat{x}_k^{a-} + K_k \cdot \left(\tilde{y}_k^a - C_k^a \cdot \hat{x}_k^{a-} \right) \tag{5.14}$$

where

$$\tilde{y}_k^a = \begin{cases} \left[\gamma_k ,\ \psi_{k-n_d} ,\ y_{lk-n_d} \right]^T , & if \quad k = i \cdot n_d , \\ \left[\gamma_k ,\ \bar{\psi}_{k-n_d} ,\ \bar{y}_{lk-n_d} \right]^T , & if \quad k \neq i \cdot n_d . \end{cases}$$

and the inter-sample visual pseudo-measurements can be calculated using equations 4.38 and 4.39.

3) Kalman gain design

The performance of Kalman filters relies on the adjustment of the Kalman gain, which is determined by Q and R. In this application, both Q and R are composed of vehicle model-related and vision model-related parts. As shown in equation 5.15, they are designed in diagonal forms to release the calculation burden. That is, the individual noise elements are assumed to be noncross related [93].

$$Q = \begin{bmatrix} Q^{veh} & 0 \\ 0 & Q^{vis} \end{bmatrix}, \quad R = \begin{bmatrix} R^{veh} & 0 \\ 0 & R^{vis} \end{bmatrix}. \tag{5.15}$$

The Kalman gain is calculated based on the degree by which the model and the measurements are weighted. Q represents the confidence placed on the observer model. If Q is set to be large, the Kalman gain becomes large accordingly, and the estimates therefore rely more on the measurements. R determines how much information from the measurements can be trusted, and the Kalman filter will follow the measurements more if R is smaller. Given that the system in this research is based on the combined model, the Q and R elements related to the different models need to be considered independently. For example, given that the vehicle model contains more uncertainties than the vision model, the elements of Q^{veh} are set to be relatively larger than those of Q^{vis}. The elements of R can be determined by offline analysis of the sensor signals [92]-[93].

5.4 Body Slip Angle Controller Design with Multi-rate Feedback

The experimental vehicle employed in this study is small and light, but its body slip angle response is in the same level as the high-speed region of normal vehicles [94]. Therefore, implementing a control system that can manipulate the body slip angle to the desired value for handling and stability improvement is necessary. For traditional vehicles, active steering or differential braking is often employed as an actuator for lateral motion manipulation [95]-[97]. In the case of EVs with IWMs, the differential torque can be generated quickly and precisely by the left and right wheels, which can be effectively utilized for vehicle motion control. In this section, to achieve the goal of reference following, a 2DOF controller is designed with body slip angle feedback from a single-rate or multi-rate Kalman filter.

The controller structure is shown in Fig. 5.1. Notably, sampling restrictions exist for both control inputs and outputs. That is, the control inputs are restricted by zero-order holders based on the update rate of the Kalman filter. Specifically, if single-rate Kalman filter is employed, the sampling frequency of the control input has to be down-sampled accordingly to match with the updating rate of the feedback.

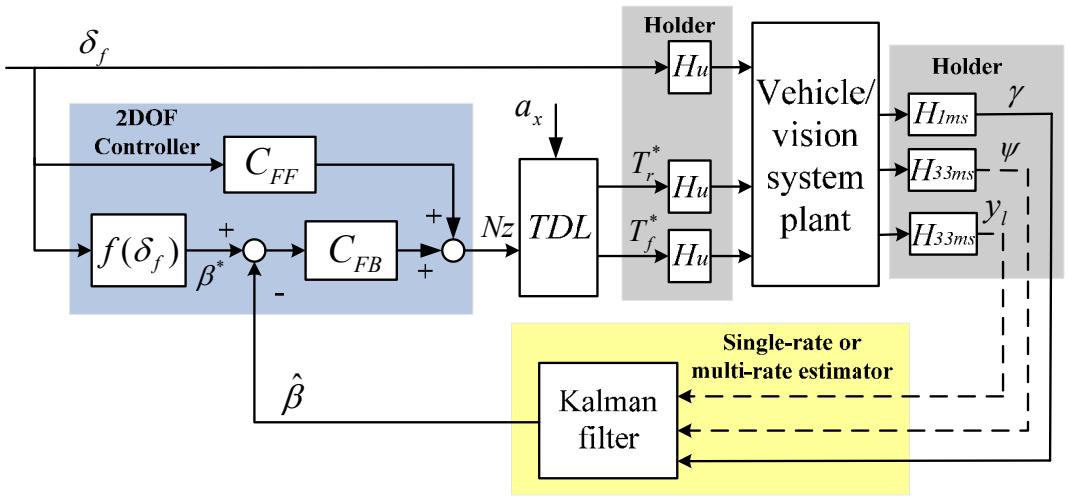

Fig.5. 2 Controller structure with body slip angle estimator.

5.4.1 Desired Body Slip Angle

Desired body slip angle can be defined in several ways in consideration of different purposes. Based on the vehicle dynamic equation 2.19, some studies calculate the reference body slip angle by assuming that a steady state response is desired [97], The desired body slip angle then becomes a function of the vehicle speed and the driver's steering input. Meanwhile, a desirable limit can be found on the body slip angle, and it changes under different road conditions [97]. Considering that drivers find it hard to recognize road conditions accurately, many vehicle stability control systems address the body slip angle control issue by preventing it from becoming too large [95]. Moreover, many traffic accidents occur because of excessive body slip angle [97]. For simplicity, this study assumes the desired slip angle to be zero.

5.4.2 Design of 2DOF Controller

As an effective method, the 2DOF controller is employed for reference tracking. This method consists of two parts: feed-forward and feedback controllers. The feed-forward controller is aimed at regulating the body slip angle to track the desired value. In this study, the feed-forward controller is designed to compensate for the steering-generated β, which can be calculated as equation 5.16 using the DC gains of the transfer functions from the body slip angle to the steering angle and yaw moment.

$$C_{FF} = \frac{G_{\delta_f}^{\beta}(0)}{G_{N_z}^{\beta}(0)} \cdot \delta_f$$
$$= \frac{4l_r l C_f C_r - 2l_f C_f m V_x^2}{m V_x^2 + 2\left(l_f C_f - l_r C_r\right)} \cdot \delta_f \tag{5.16}$$

To compensate for the modeling error and the error during transient operation, the feedback controller is indispensible. For information feedback, the body slip angle is estimated with either the single-rate or multi-rate Kalman filter. The estimated β is utilized as a feedback signal, and a proportional–integral controller is then designed based on the pole placement. Together, the feed-forward and feedback controllers generate the yaw moment for reference tracking.

On the one hand, the control period can be every 1 ms. On the other hand, the single-rate Kalman filter generates output every 33 ms, and the multi-rate Kalman filter is updated every 1 ms. Based on the parameters of the experimental vehicle given in the Appendix A and the open-loop stability analysis, the gain margins of the single-rate and multi-rate systems are given in Table 5.1. As shown in Table 5.1, the gain margin is increased by the multi-rate feedback. Therefore, the multi-rate controller can provide smoother control input than the single-rate one.

Table 5. 1 Stability Margin Comparison

	Single-rate	Multi-rate
Closed-loop pole (Hz)	-2	-2
Gain Margin (dB)	5.92	22.8
Crossover Freq.(Hz)	15.15	477.46

5.4.3 Torque Distribution Law (TDL)

After obtaining the desired yaw moment N_z, TDL must be considered. As aforementioned, the rear two wheels are utilized as actuators, and they can generate positive/negative torques easily. Therefore, a simple TDL can be defined as

$$T_r^* = \frac{m \cdot r \cdot a_x}{2} - \frac{r \cdot N_z}{d_r}$$
$$T_l^* = \frac{m \cdot r \cdot a_x}{2} + \frac{r \cdot N_z}{d_r} \tag{5.17}$$

where a_x is the vehicle's longitudinal acceleration rate and N_z is the yaw moment to be distributed. It means that, on one hand, the IWMs generate forward torques for vehicle driving; on the other hand, the left and right wheels generate torques in different direction for body slip angle control. It should be noted here that, if integrated with other controllers, the TDL may need to be modified as wheel torques are the main source to manipulate vehicle motion.

5.5 Simulations and Experiments

In this section, simulations and experiments are performed to verify the proposed body slip angle estimator and controller.

5.5.1 Body Slip Angle Estimation

Simulations:

The performance of the proposed multi-rate Kalman filter was compared with the other methods based on the vehicle specifications given in the Appendix A. The vehicle was assumed to run at a speed of 25 km/h, and a sinusoidal steering input was given. For comparison, traditional bicycle model-based Kalman filter, combined model-based single-rate Kalman filter, combined model-based multi-rate Kalman filter without inter-sample residual estimation and combined model-based multi-rate Kalman filter withinter-sample residual estimation are studied in the simulations. First of all, a simulation is conducted by assuming that the vehicle model and Kalman filter model are the same. As can be observed from Fig. 5.3, all of the methods match with true value very well. However, this assumption is not true due to the change of tire cornering stiffness.

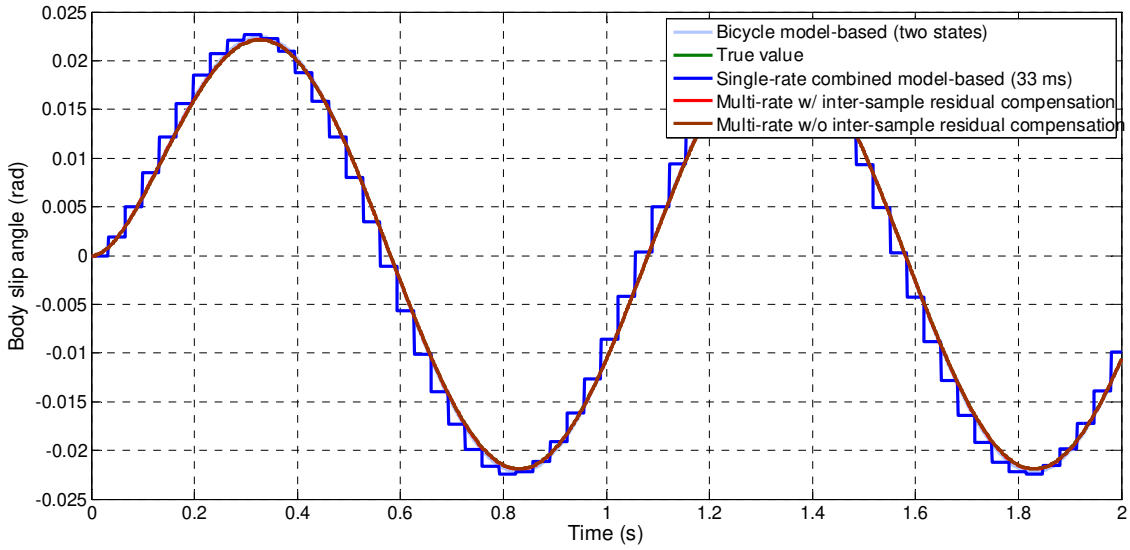

Fig.5. 3 Simulation comparison of the body slip angle estimation based on different estimation methods (without model discrepancy).

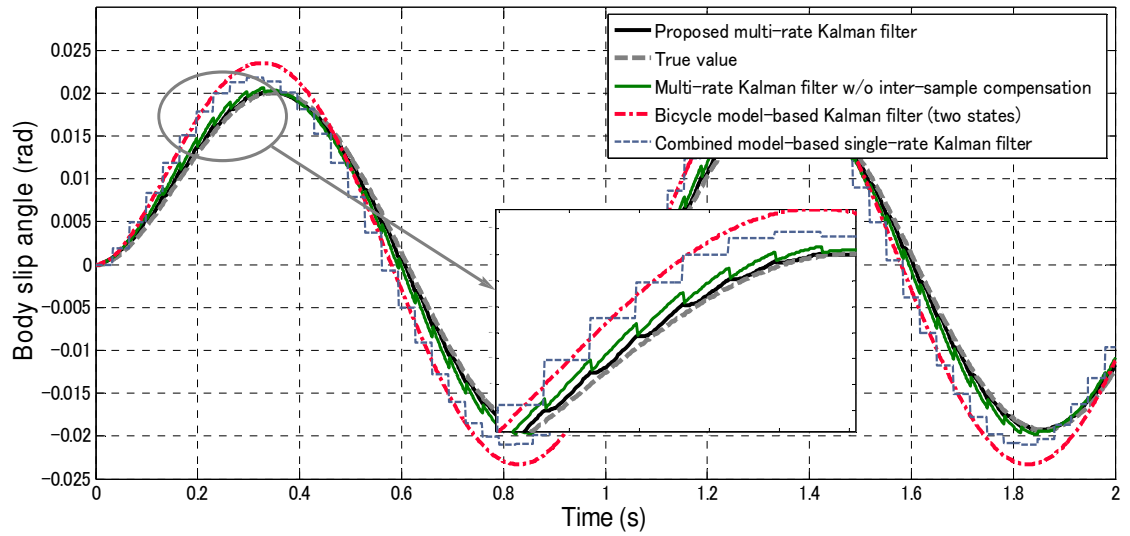

Fig.5. 4 Simulation comparison of the body slip angle estimation based on different estimation methods (with model discrepancy).

To demonstrate clearly the effectiveness of the proposed method, the vehicle model and the Kalman filter model were made different from each other: the real C_f and C_r were set as 1.2 times larger than the estimator ones. A performance comparison among the bicycle model-based Kalman filter, combined model-based single-rate Kalman filter, combined model-based multi-rate Kalman filter without inter-sample residual estimation, and the proposed method is shown in Fig. 5.4. The bicycle model-based method cannot track the true value because of model discrepancy. The combined model-based single-rate estimator performed better because of the addition of visual information but was affected by slow update rate. The combined model-based multi-rate estimator without inter-sample compensation exhibited better performance than the previous two methods; however, theoretically speaking, it cannot converge to the true value as discussed in section 4. Meanwhile, the proposed multi-rate Kalman filter with inter-sample compensation provided the best estimation result compared with the other methods. It should be noted that, for fair comparison, the corresponding elements of Q and R were set to be the same for all the methods.

Experiments:

Field tests were conducted with our experimental vehicle for realistic verification of the proposed estimator. A sinusoidal steering input was provided by the driver, and the vehicle speed varied from 0 km/h to 30 km/h during the operation. Similar to the simulation settings, the Cf and Cr of the Kalman filter were made different from those of the real vehicle. In fact, the Kalman filter model was fixed in the experiment and could not be exactly the same with the vehicle.

The proposed multi-rate observer was compared with the other methods (Fig. 9). The bicycle model-based estimation result cannot track the true value very well because of model discrepancy. The combined model-based single-rate estimator was only updated at a rate of 30 Hz and was not able to utilize all the information from the fast-rate sensors. Hence, the estimation result was not satisfactory. In Fig. 9, the multi-rate Kalman filter without inter-sample compensation tracks the sensor measurement very well except for some vibrations at transient conditions. The proposed multi-rate estimator, which was compensated by inter-sample residuals, performed smoother and more accurately than the other methods.

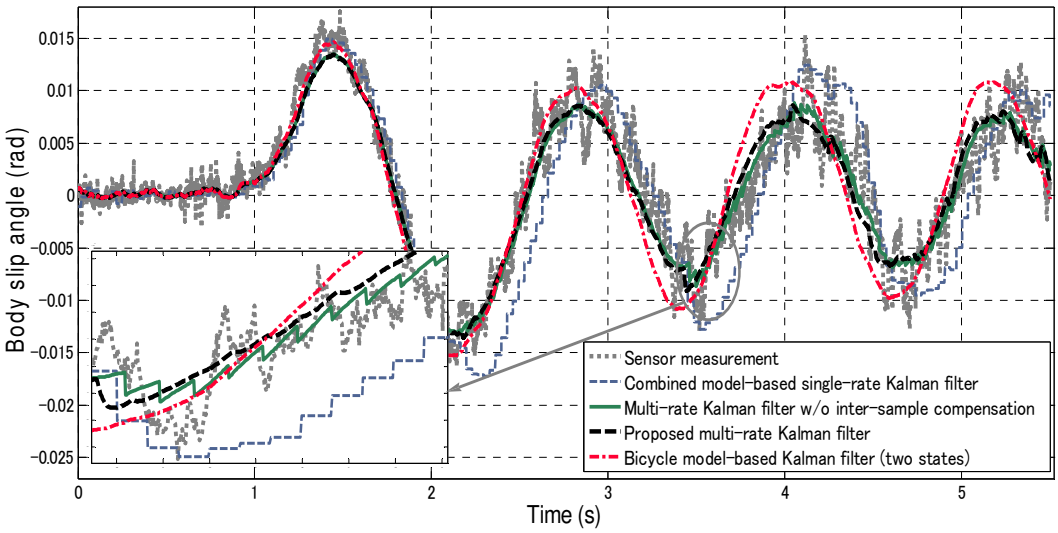

Fig.5. 5 Estimation method comparisons based on experimental data.

5.5.2 Body Slip Angle Control

Simulations:

Based on the aforementioned analysis, only the single-rate Kalman filter and the multi-rate Kalman filter with inter-sample residual compensation can converge, and both are more robust against vehicle parameter uncertainties than the bicycle model-based method. The two methods were compared in the simulation with regard to the effect on control performance based on the proposed 2DOF controller. In the simulation, the vehicle was tested with a single-lane change maneuver at a speed of 25 km/h. For fair comparison, the gain margins of the two control system were set to be the same.

As shown in Fig. 5.6 (a), the performance of the single-rate Kalman filter-based controller is worse than that of the multi-rate Kalman filter-based controller. In fact, the feedback gain in the case of the single-rate Kalman filter cannot be set large enough for reference tracking because of its low open-loop stability margin. In addition, the feedback gain in the case of the multi-rate estimator can be designed to track the reference. That is, the system stability margin is increased using the multi-rate Kalman filter as feedback. Fig. 5.6 (b) shows the control input comparison of the two methods.

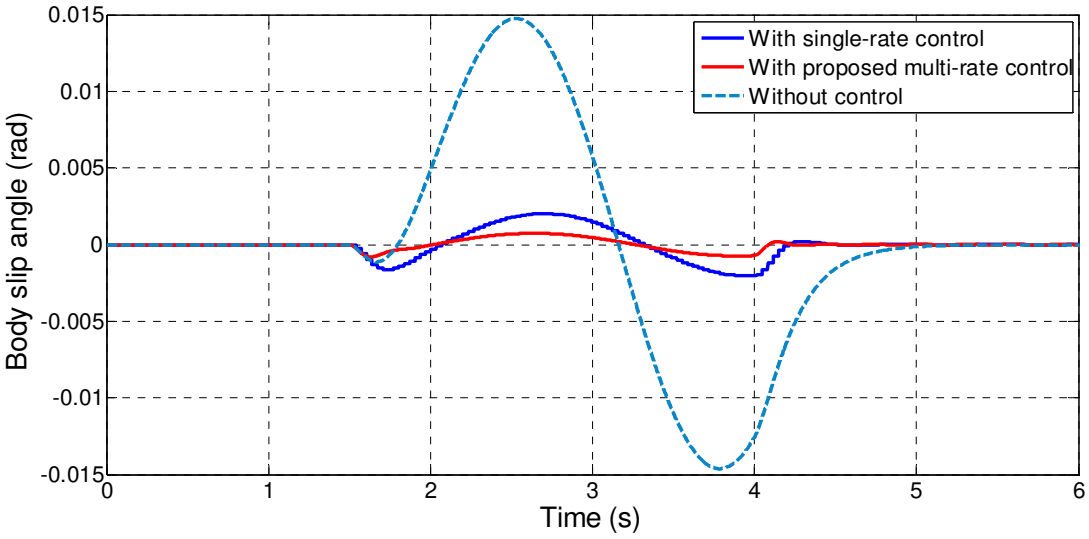

(a)

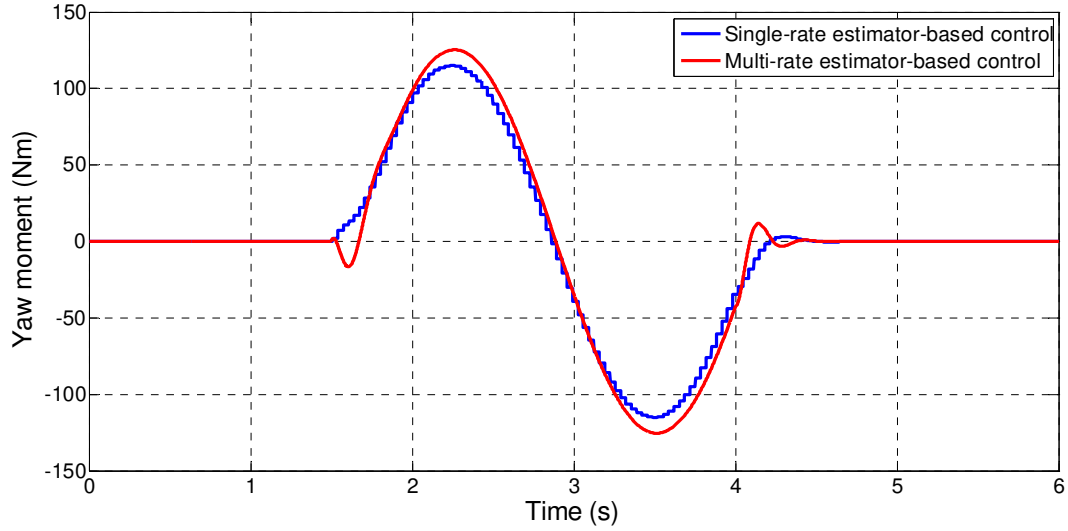

(b)

Fig.5. 6 Simulation comparison of the controller performance based on single-rate and multi-rate Kalman filters. (a) Body slip angle control comparison among the setup without control, single-rate estimator-based control, and proposed multi-rate control. (b) Yaw moment control input comparison between single-rate and multi-rate controllers.

Experiments:

Subsequently, the body slip angle controllers using either the single-rate or the proposed multi-rate Kalman filter were implemented and compared in the experiments. For fair comparison, front-steering motor was employed to generate a single-lane change steering input with the same pattern. That is, the steering inputs were the same across all the experiments. The steering input is shown in Fig. 5.7 (a).

IWMs were used to generate differential torque to minimize the body slip angle. Based on the system sampling rate, both single-rate and multi-rate controllers were studied. As shown in Fig. 5.7 (b), the amplitude of the body slip angle without control can reach almost 0.03 rad. With the single-rate controller, the body slip angle can be minimized, as illustrated by the blue dotted line. However, the feedback performance of such method deteriorated because of the low stability margin. Meanwhile, the body slip angle can be suppressed even further using the proposed multi-rate controller, as represented by the red line in Fig. 5.7 (b). The control input of the two cases, which is the yaw moments generated by the differential torque of the left and right wheels, are shown in Fig. 5.7 (c).

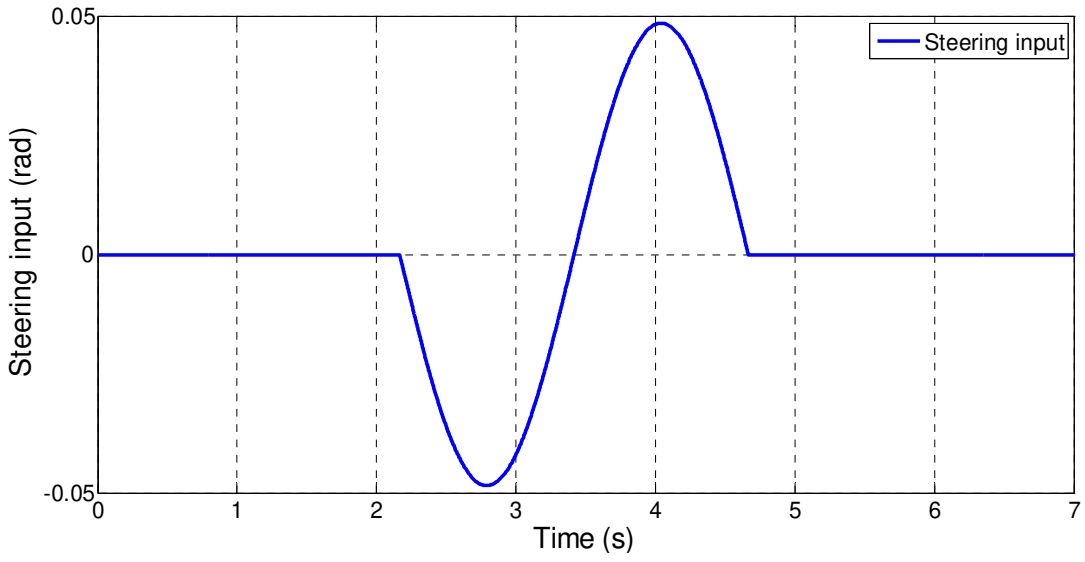

(a)

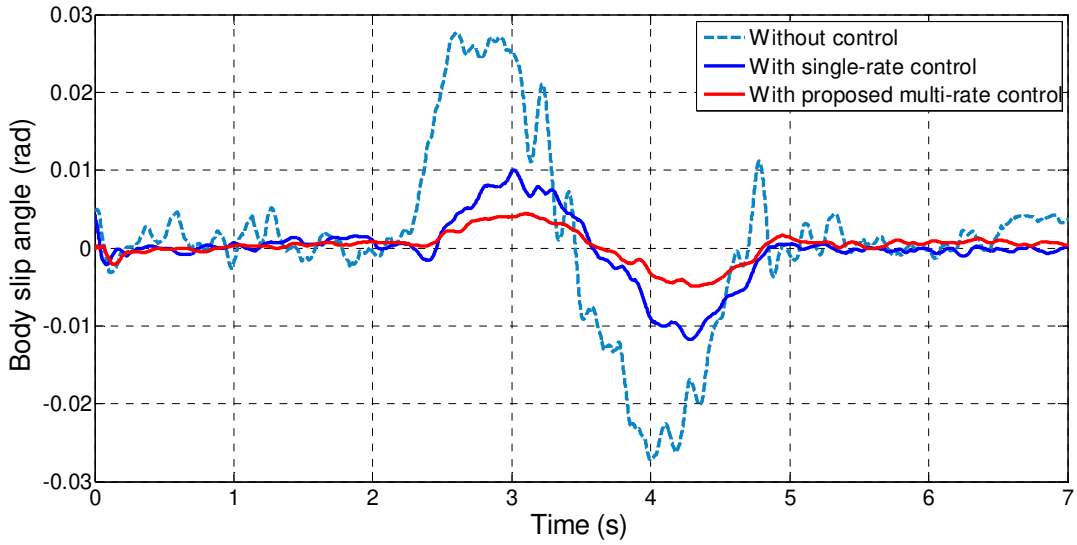

(b)

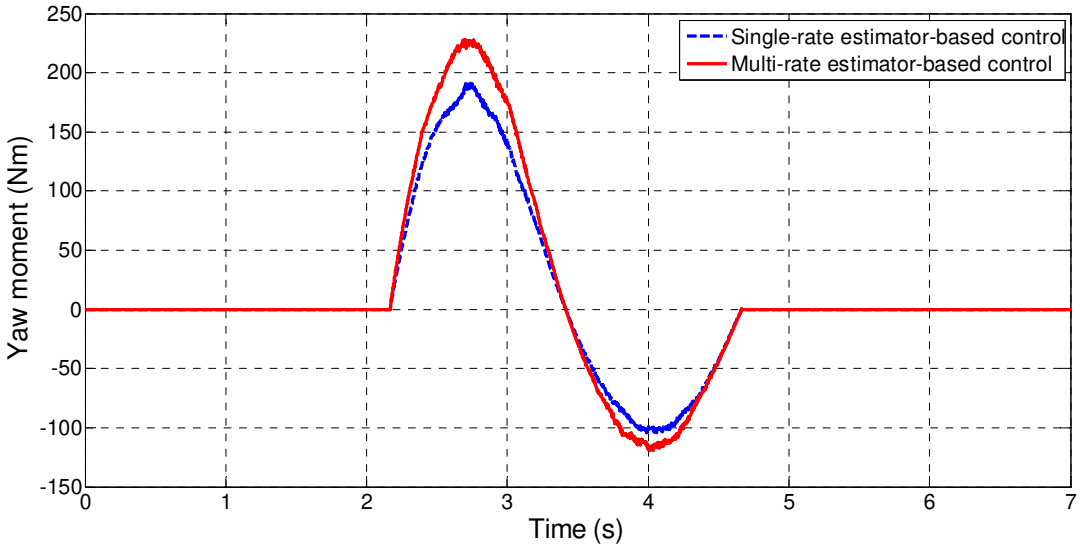

(c)

Fig.5. 7 Experimental comparison of the controller performance. (a) Steering input by EPS. (b) Body slip angle control comparison among the setup without control, single-rate estimator-based control, and the proposed multi-rate control. (c) Yaw moment control input comparison between the single-rate and multi-rate controllers.

5.6 Chapter Summary

In this chapter, a linear vehicle bicycle model was augmented with a simple visual model. As the visual model contains few uncertain parameters and increases observer's design freedom, the combined model-based estimator provided more accurate estimation result compared with the traditional bicycle model-based one. However, two issues are raised by the combined vehicle and vision models: 1) image processing introduces delay into the visual measurements and 2) the sampling time of a normal camera is much longer than that of other onboard sensors. For electric vehicles, the control period of motors is much shorter than the sampling time of a normal camera. Considering the above-mentioned delay and multi-rate problems, a multi-rate Kalman filter with inter-sample compensation was designed. Then, a 2DOF controller was designed using the estimated body slip angle as feedback for reference tracking. With the proposed multi-rate estimator, the controller achieved better tracking performance than the single-rate method. The effectiveness of the proposed estimator and controller was demonstrated by both simulations and experiments.

Chapter 6

Vision-based Multi-rate Estimation for Integrated Vehicle Lateral Control

In this chapter, an integrated vehicle lateral control method is studied to improve vehicle lateral safety and stability. The system model employed is the same the one used in Chapter 5 which is described in Chapter 2. This control system utilizes front steering to control vehicle position and differential torque between left and right wheels to control yaw motion; yaw rate and vehicle position information are feedback signals. However, as a two-input-two-output system, the two feedback loops have different frequencies which present difficulty for controller design. Moreover, due to image processing, uneven visual information delay should be considered in this application. The two problems are solved using the multi-rate Kalman filter proposed in Chapter 4 that reconstructs measurements and inter-sample residuals. First of all, the research background is introduced to explain the necessity of implementing integrated vehicle lateral control system, and the issues for fusing yaw rate and visual information are explained. Then, multi-rate Kalman filter with residual reconstruction is developed to estimate vehicle lateral position. Finally, an integrated vehicle lateral controller is designed with the information from a gyro sensor and the multi-rate Kalman filter as feedback.

6.1 Introduction

For vehicle stability control systems, online information of vehicle states such as yaw rate are considered as key enablers. In [77], a yaw moment control algorithm was developed using differential torque of IWMs for vehicle yaw motion stabilization. Another research tried to control both yaw rate and body slip angle at the same time using IWMs [39]. Some research utilize front wheel steering for body slip angle control and yaw moment for yaw rate control [97]. In fact, differential torque is an effective input to control yaw rate as can be seen from the bode plot of γ/N_z as shown in Fig. 3.10. Yaw rate can be easily obtained from a gyroscope sensor which is widely used for a variety of control applications.

Meanwhile, automatic steering methods for lane keeping have been extensively investigated by automotive companies and research institutions. Joel C. McCall *et al.* surveyed some previous research, proposed their own methods for lane detection and evaluated the methods with systematic criteria [61]. Another research was conducted by M. Bertozzi *et al.* [99], they used stereo vision system to detect lane and obstacles on the road. In addition to the literatures in academic field, many patents were generated on lane detection and lane following systems. Timothy W. Kaufmann *et al.* proposed methods to detect vehicle offset to the lane and to control the steering wheel accordingly for lane keeping [100]; Toru Saito *et al.* invented a similar device for lane keeping assistance [101]. While lane keeping strategies of these proposed methods differ somewhat, most of them use look-ahead onboard vision system for lane detection and location, i.e., the vehicle position information can be obtained from onboard vision system in real time.

Most of the previous studies focused on independent yaw motion control or vehicle position control; however, they have limitations if independently controlled. For example, even if yaw rate is controlled to be zero, the vehicle may deviate from the desired path; on the other hand, the vehicle may spin (yaw rate is too large) even the vehicle is kept within the lane. In [102], they derived some equations to relate yaw rate and vehicle lateral position, and employed steering for control the two states. In this Chapter, an integrated lateral controller addressing yaw motion and vehicle position at the same time is investigated.

Unfortunately, yaw rate and vehicle position are acquired from different devices and thus have different sampling rates. This brings trouble to the controller design. For traditional vehicles, this can be solved easily by adjusting the fast sampling times to adapt to the vision system. However, for the application of EVs, the sampling time of motors is in millisecond-level which requires faster feedback information compared with traditional vehicles using internal combustion engines and hydraulic actuators. The sampling rate of normal cameras is not fast enough for EV-related motion control applications. In addition, image processing time is not constant in practice (because of different incoming images and processing loads). In this study, the information from vision system is considered to be random delayed. For measurement delay, a widely employed approach is to augment the states with delayed measurements. However, in case of uneven and large time delay as the system investigated in this study, expansion of system state space equation is difficult to be practically implemented. In this paper, the uneven delay issue is solved with a residual reconstruction approach. Moreover, sampling mismatch between vision system and other onboard sensors is addressed in the Kalman filter design.

6.2 Infrequent and Random Delayed Visual Information

The integrated vehicle lateral controller has two loops: front steering is used to control vehicle position and differential torque is utilized to control yaw motion. For controller design with more than one loop, a unified sampling time is necessary. However, as stated before, visual information and yaw rate signal have different updating frequencies. As the secondary measurement, the updating time of yaw rate is short (T_s), and the sampling period of the primary device, the camera, is much longer (T_l). In addition, measurements from the vision system are random delayed due to image processing time needed. Therefore, the visual output equation becomes

$$y_k^{vis} = C \cdot x_{k-n_{d\_i}}^{vis} + v_{k-n_{d\_i}}^{vis}, \quad if \quad k = (i-1) \cdot N + n_{d\_i} \tag{6.1}$$

From equation 6.1, it can be known that the information from the vision system at step k represents the measurement at step k-n_{d_i}. Notably, n_{d_i} is not constant due to the varying of image processing time. In this research, T_{d_i} is managed to be less than one sampling period of the camera, therefore, n_{d_i} can only be one value from the set {1, 2, …, 33} at an arbitrary visual stamp i. In case of constant and small time delay, augmentation of state vector can be effectively employed. However, state augmentation approach is calculation intensive and complex for the random delay with large multi-ratio which is the case discussed in this dissertation.

The vehicle model-related and vision model-related measurement can be expressed together as given in equation 6.2. Visual information is not always available at every time step. Therefore, the inter-sample residuals of the visual information must be addressed for Kalman filter design.

$$y_k = \begin{cases} \left[\left(y_k^{veh} \right)^T \quad \left(y_k^{vis} \right)^T \right]^T & if \quad k = (i-1) \cdot N + n_{d\_i}, \\ \left[\left(y_k^{veh} \right)^T \quad 0 \right]^T & if \quad k \neq (i-1) \cdot N + n_{d\_i}. \end{cases} \tag{6.2}$$

6.3 Multi-rate Kalman Filter Design with Uneven Delay Compensation for Integrated Vehicle Lateral States Estimation

The multi-rate Kalman filter design involves two steps: measurement reconstruction, and inter-sample residual estimation. The time sequences before and after reconstruction are shown in Fig. 6.1.

6.3.1 Measurement Reconstruction

As can be seen in Fig. 6.1 (a), the out-of-sequence visual information is not straightforward for fusion with other sensor signals, and it is therefore desired to reconstruct the visual signals. Consider that the image data are sampled at $(i-1)\cdot T_l$, but are not available until time $(i-1)\cdot T_l + T_{d\_i}$, it is reasonable to assume that the samplings are taken at $(i-1)\cdot T_l + T_{d\_i}$ instead of $(i-1)\cdot T_l$. Thus, the delay is removed from the reconstructed sampling sequence. As the measurements at $(i-1)\cdot T_l + T_{d\_i}$ represent the information at $(i-1)\cdot T_l$, and corresponding modification of residual is necessary.

After the above re-arrangement, the delays are removed from the measurements. However, the visual updates are still uneven and the sampling time is much longer than that

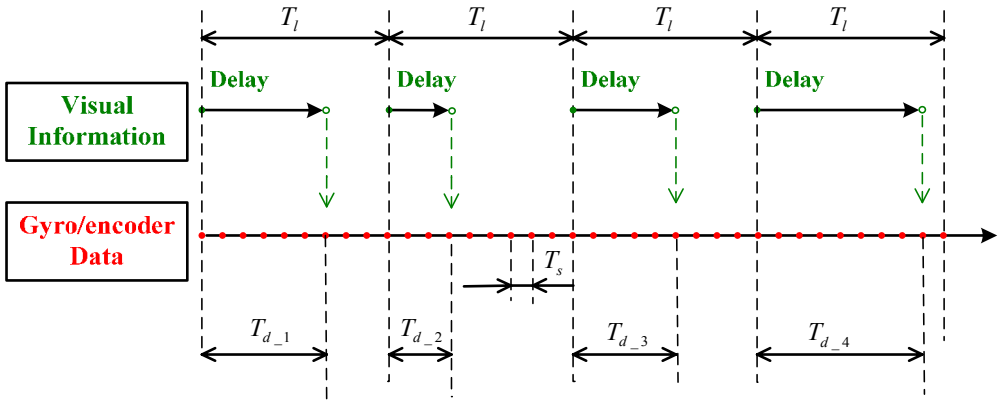

(a)

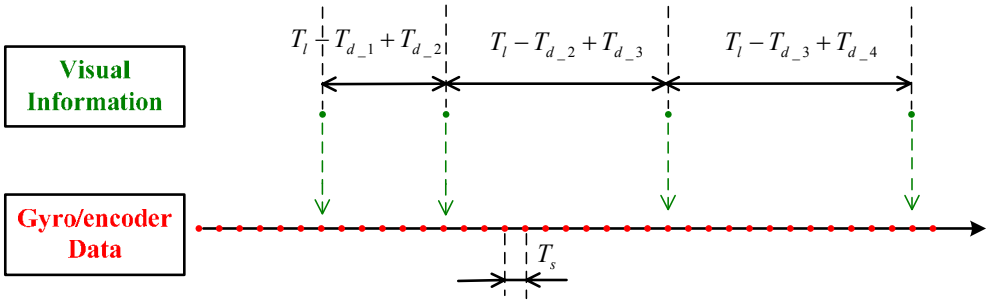

(b)

Fig.6. 1 Measurement sequence. (a) Normal sampling sequence. (b) After measurement reconstruction.

of the yaw rate. The problem of this study is therefore transformed into designing a multi-rate Kalman filter for a discrete system with random multi-ratio. Two points need to be considered in this case: 1) residual modification at every $(i-1)\cdot T_l + T_{d\_i}$ time; 2) residuals estimation between every neighboring visual samples.

6.3.2 Design of Multi-rate Kalman Filter

Based on the reconstructed measurement, the multi-rate Kalman filter is designed using the inter-sample residual technique given in Chapter 4. It is aimed at utilizing the yaw rate signal every 1 ms (instead of 33 ms in case of single-rate Kalman filter) and increasing the updating rate of the estimator to 1 kHz which can match with the frequency of the control input for enhanced control performance. Different from the augmented model utilized in Chapter 5, the model employed here is the original one given in equation 5.8. Like normal Kalman filters, the design of multi-rate Kalman filter has three parts: time update (prediction), measurement updates (correction), and Kalman gain design.

1) Time update

For the time update, there is no difference between multi-rate Kalman filter and single-rate one, i.e., the vehicle model-related states and vision model-related states can be updated together using the system model as given in equation 6.3.

$$\hat{x}_k^- = G_{k-1} \cdot \hat{x}_{k-1} + H_{k-1} \cdot u_{k-1} \tag{6.3}$$

2) Measurement update

The measurement updates can be explained in terms of residual, and have to consider three situations as explained in Chapter 4. The first one is the period before the first sample comes, where there are no measurement updates. The second situation is residual reconstruction at every visual information arrival time. This is because of the arrived visual information actually reflects previous state, and they have to be modified to represent the current one. The last situation is residual estimation between every neighboring visual samples. The sampling period of the vision system is $T_l - T_{d\_i} + T_{d\_i+1}$, which changes from time to time depending on the delay time of image processing. During the updating intervals, no information from the vision system is available. Therefore, pseudo-corrections have to be implemented for the operation of the measurement update. The multi-rate Kalman filter with measurement reconstruction and inter-sample estimation given in Chapter 4 is employed. The estimation equation is given as

$$\hat{x}_k = \hat{x}_k^- + K_k \cdot \tilde{\varepsilon}_k \tag{6.4}$$

where

$$\tilde{\varepsilon}_k = \begin{cases} \left[\varepsilon_k^{veh},\ 0 \right]^T, & if \quad k \in \left[0,\ n_{d\_1} \right), \\ \left[\varepsilon_k^{veh},\ \tilde{\varepsilon}_k^{vis} \right]^T, & if \quad k \geq n_{d\_1}. \end{cases}$$

and the visual pseudo-residuals at step k ($k \geq n_{d\_i}$) can be calculated using equations 4.47 and 4.48.

3) Kalman gain design

The performance of Kalman filters relies on the adjustment of Q and R. Here, both Q and R are composed of vehicle model-related and vision model-related parts. As shown in equation 6.5, they are designed in diagonal forms to release the calculation burden. That is, the individual noise elements are assumed to be noncross related [93].

$$Q = \begin{bmatrix} Q^{veh} & 0 \\ 0 & Q^{vis} \end{bmatrix}, \quad R = \begin{bmatrix} R^{veh} & 0 \\ 0 & R^{vis} \end{bmatrix}. \tag{6.5}$$

The Kalman gain is calculated based on the degree by which the model and the measurements are weighted. Q represents the confidence placed on the observer model. If Q is set to be large, the Kalman gain becomes large accordingly, and the estimates therefore rely more on the measurements. R determines how much information from the measurements can be trusted, and the Kalman filter will follow the measurements more if R is smaller. Given that the system in this research is based on the combined model, the Q and R elements related to the different models need to be considered independently. For example, given that the vehicle model contains more uncertainties than the vision model, the elements of Q^{veh} are set to be relatively larger than those of Q^{vis}. The elements of R can be determined by offline analysis of the sensor signals.

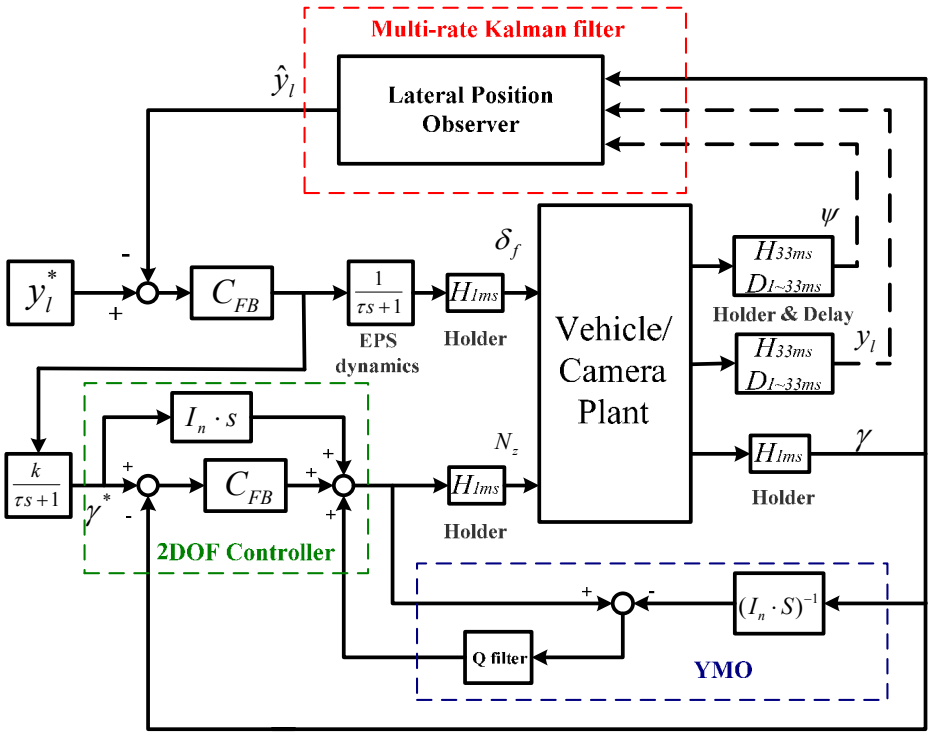

Fig.6. 2 Integrated lateral controller for EVs

6.4 Integrated Vehicle Lateral Controller with Multi-rate Feedback

As aforementioned, independent yaw control or lane keeping control has limitations. Therefore, controlling yaw motion and vehicle lateral position at the same time is desirable. As shown in Fig. 4, two controllers are incorporated in the system. The upper controller is designed for vehicle lateral position manipulation, i.e., if the vehicle is deviated from the desired path, the controller generates a steering control command for path correction. The lower controller is implemented for yaw motion stabilization based on the well-known two-degree-of-freedom controller and yaw moment observer (YMO) [78]. The steering input for vehicle position control generates a desired yaw rate (it is simplified as a first order transfer function in this simulation), and the differential torque of EVs can correct yaw motion in case of undesired vehicle movement.

Obviously, there are two feedback loops: yaw rate feedback and lateral position feedback loops. Due to the sampling restriction of vision system, the two loops have different sampling rates. That is, yaw rate has higher sampling frequency than the visual information; moreover, the vision signals are contaminated by time-varying delays. Thus, the multi-rate Kalman filter considering random delay proposed in the previous section is employed to generate the lateral position signal at the same updating rate as yaw rate. Then, the sampling time of the overall system can be unified.

6.4.1 Vehicle Lateral Position Controller

The vehicle lateral position controller aims at controlling vehicle lateral position to a predefined value using front steering system. It involves two parts: the lateral position estimator and position controller. In fact, this kind of controller has been studied thoroughly in the literatures such as [95]. For example, a feedback controller can be easily designed based on the transfer function from lateral distance to front steering angle which is given in equation 3.15. The yaw moment also has effect on vehicle position, however, the DC gain of the transfer function from y_l to N_z is so small that yaw moment is not a effective way for vehicle position control.

The problem of conventional method is, the sampling rate of the whole system has to be decreased for controller design due to the restriction of visual feedback. In this research, the

slow updating rate of visual signals is solved using a multi-rate Kalman filter and, the controller can then be design in a normal way without down-sample the sampling time of the whole system.

6.4.2 Yaw Motion Controller

Yaw motion control for EVs is a mature technique studied by many researchers. Among them, YMO is a novel direct yaw-moment control approach based on disturbance observer which compensates immeasurable terms as lumped disturbances.

The basic idea of YMO is to reconstruct equation 2.17 as

$$I_n \cdot \frac{d\gamma}{dt} = N_z - N_t - N_d \tag{6.6}$$

where N_d is the disturbance yaw moment, N_t is the moment generated by tires. By using the moment N_z as control input and yaw rate as measurement, the disturbance observer can be designed as the lower part in Fig. 6.2. This method can compensate the lumped disturbance and nominalize the system as

$$\gamma(s) \approx \frac{1}{I_n \cdot s} N_{in}(s) \tag{6.7}$$

Using this method, all the un-modelled dynamics as well as disturbances can be compensated by additional yaw moment control input. The feed forward controller of yaw motion control is therefore designed as inverse of the transfer function from yaw rate to yaw moment input as given below

$$C_{FF} = I_n \cdot s \tag{6.8}$$

6.5 Simulations and Experiments

Yaw rate can be easily and frequently obtained from a gyro sensor, therefore, in this section, simulations and experiments are only performed to verify the proposed vehicle position estimator. The controller performance is verified by simulations.

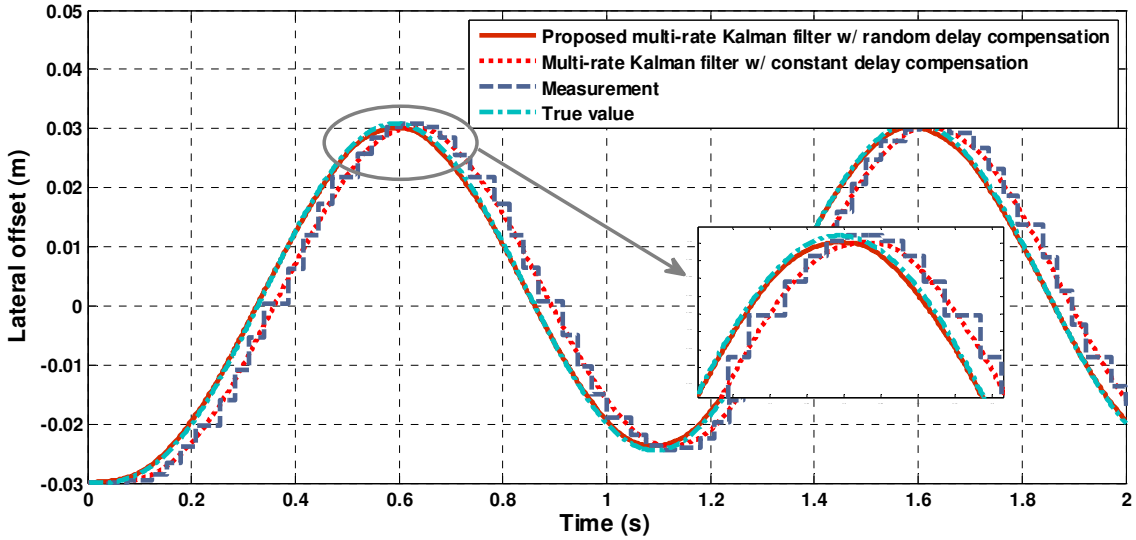

Fig.6. 3 Estimation comparison in simulation.

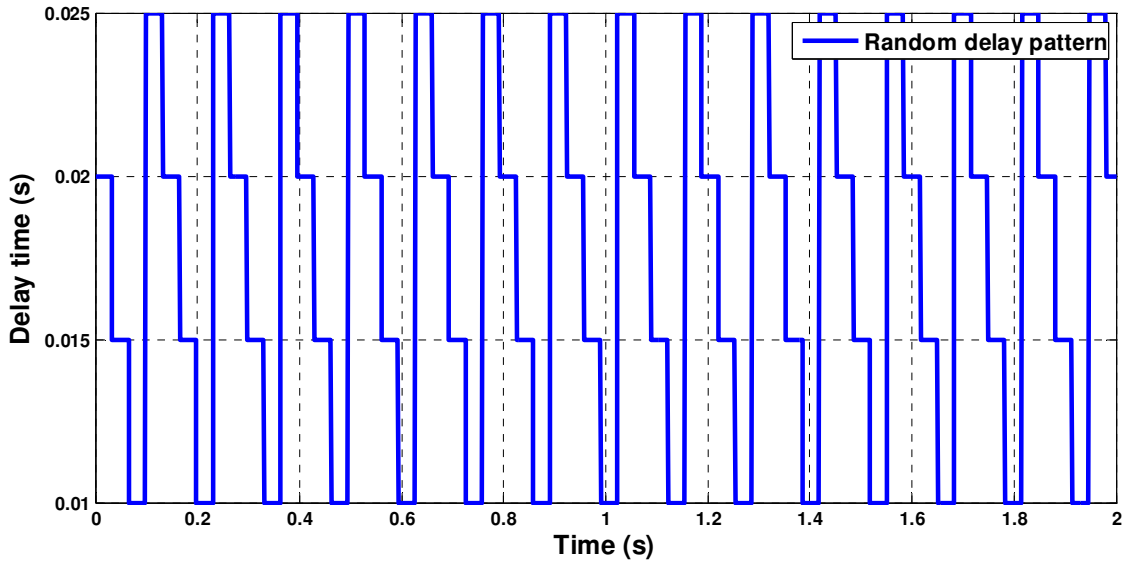

Fig.6. 4 Random delay pattern (0.02s, 0.015s, 0.01s, 0.025s) in simulation.

6.5.1 Vehicle Lateral Position Estimation

Simulation:

The performance of the proposed multi-rate Kalman filter with random delay compensation was demonstrated in simulation. The vehicle was assumed to run at a speed of 30 km/h, and a sinusoidal steering input was given. To simulate real condition, the vehicle model and the Kalman filter model were made different from each other: the cornering stiffness were set as 1.2 times larger than the estimator ones. Moreover, a random delay pattern was generated as shown in Fig. 6.4, where a pattern in the form of {20 ms, 15 ms, 10 ms, 25 ms} is repeated. As can be seen in Fig. 6.3, the vehicle lateral offset measurement was random delayed by the random delay pattern. That is, it could not match with true value. With the proposed multi-rate estimator with random delay and inter-sample compensations, even in the condition of vehicle model mismatch, the estimation can match with the true value very well.

Experiment:

The same as simulation, the proposed Kalman filter exhibits better performance than the multi-rate Kalman filter with a constant delay compensation in experiments, where a sine steering was applied. It can also smooth the visual sampling as can be seen in Fig. 6.5. The image processing delay pattern is shown in Fig. 6.6.

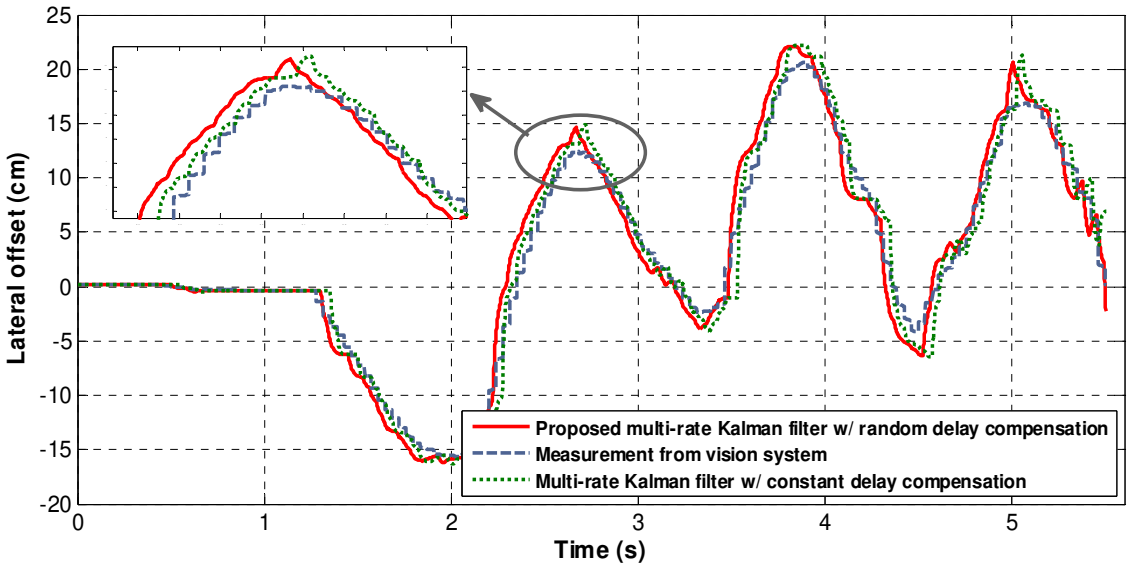

Fig.6. 5 Estimation comparison based on experimental data.

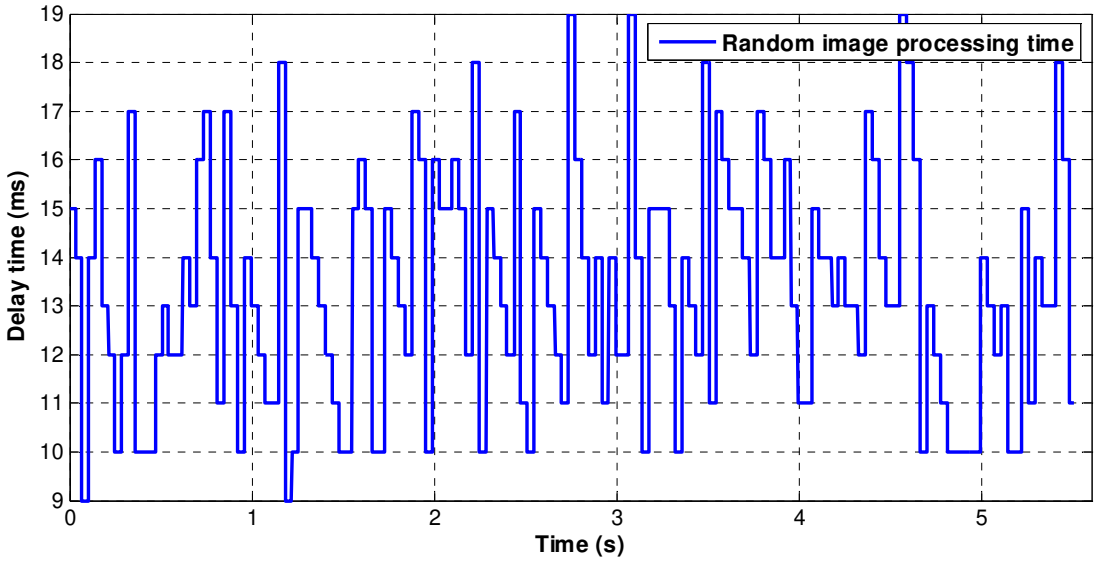

Fig.6. 6 Random image processing time in one experiment.

6.5.2 Integrated Vehicle Lateral Control

Simulation:

After obtaining the lateral offset, it can be feedback at the same frequency as yaw rate. As described in section 5, the front steering is employed for vehicle position control, and the rear differential torque is utilized for yaw moment stabilization. The vehicle is assumed to run at the speed of 30 km/h. An initial position error is set to be 0.15m, and the desired one is set to 0.1 m.

Therefore, the steering system generates an input for reference tracking. Meanwhile, the differential torque is calculated by the 2DOF and YMO for yaw moment control. The simulation results are shown from Fig. 6.7 to Fig 6.10.

Fig. 6.7 shows the steering input comparison between vehicle position control only case and integrated vehicle lateral control case. The feedback gain is set to be the same, and the two values are therefore very close to each other. Fig. 6.8 is the yaw moment control input comparison. In case of position control only, yaw moment is zero, i.e., no control is applied. Fig. 6.9 is the vehicle position control result. As can be observed, both of the two methods can manipulate the vehicle position. The yaw rates comparison are given in Fig. 6.10. The yaw rate in case of position control is much larger than the integrated controller.

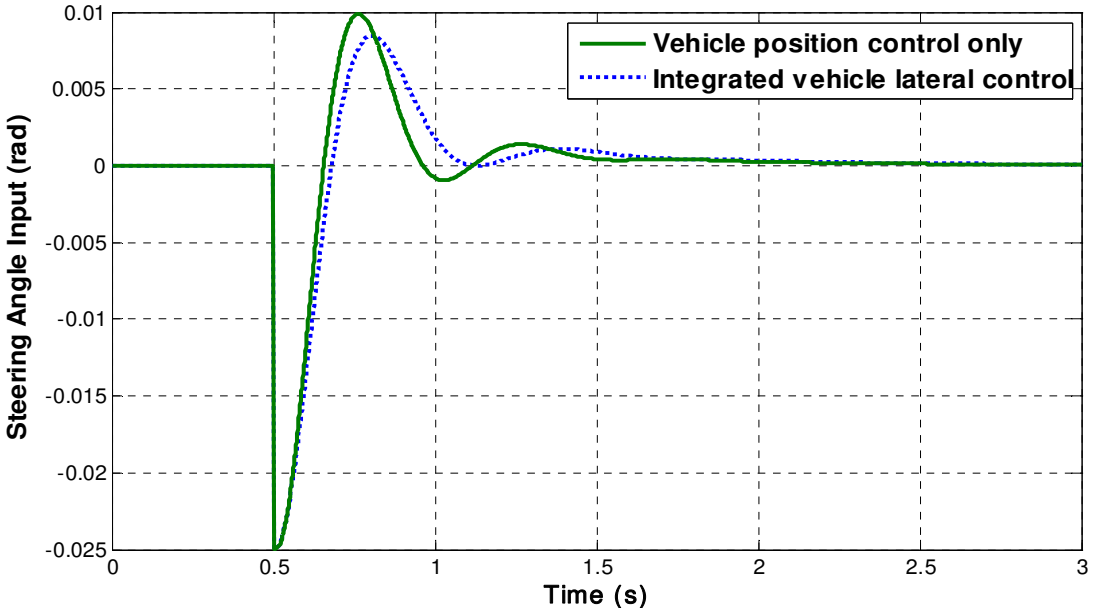

Fig.6. 7 Steering angle input comparison.

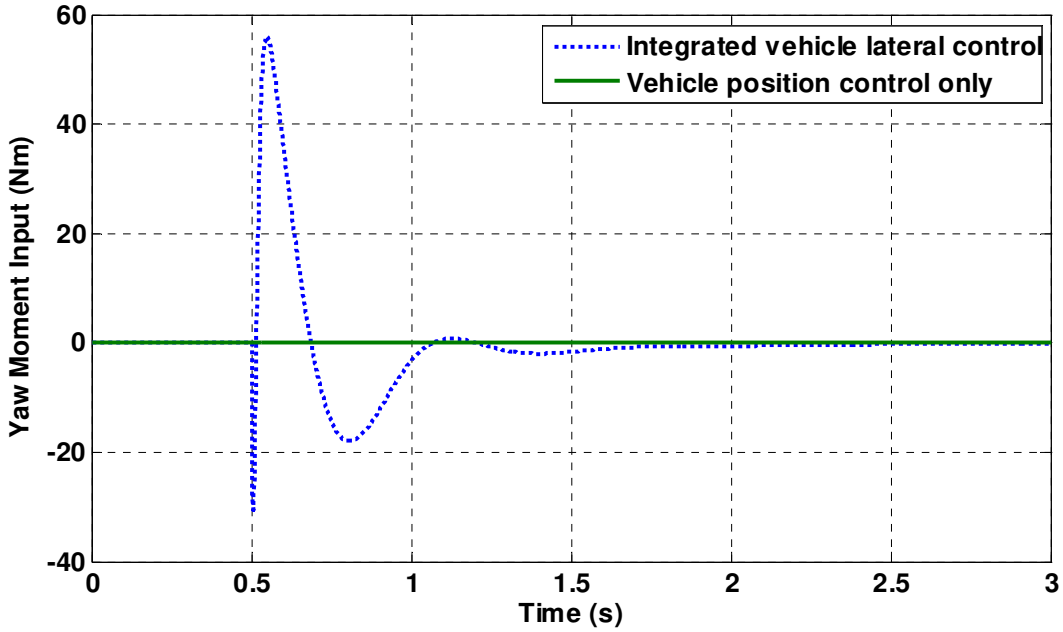

Fig.6. 8 Yaw moment input for yaw rate control.

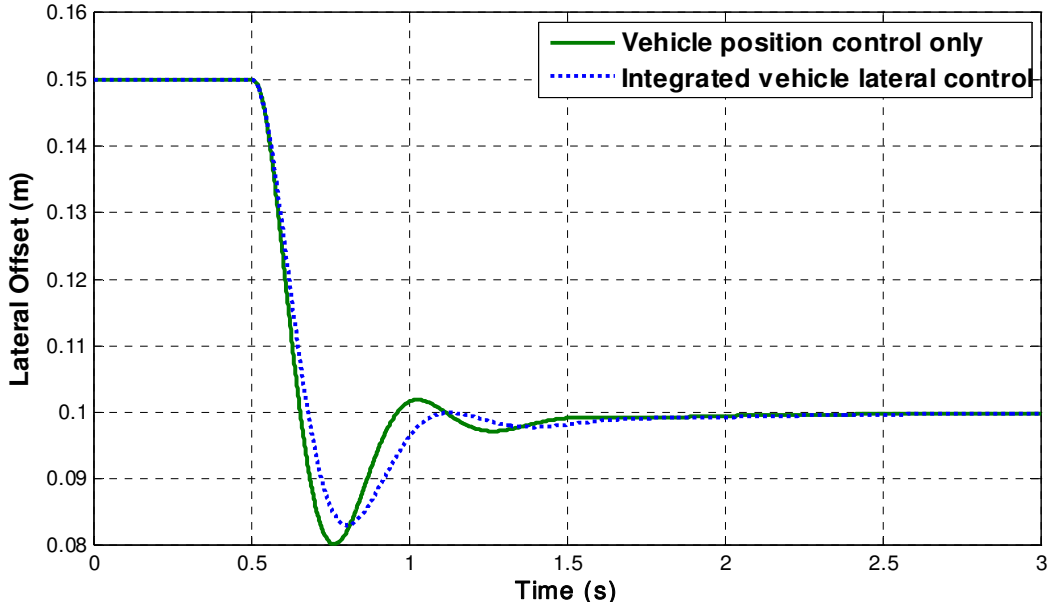

Fig.6. 9 Steering angle input for vehicle position control.

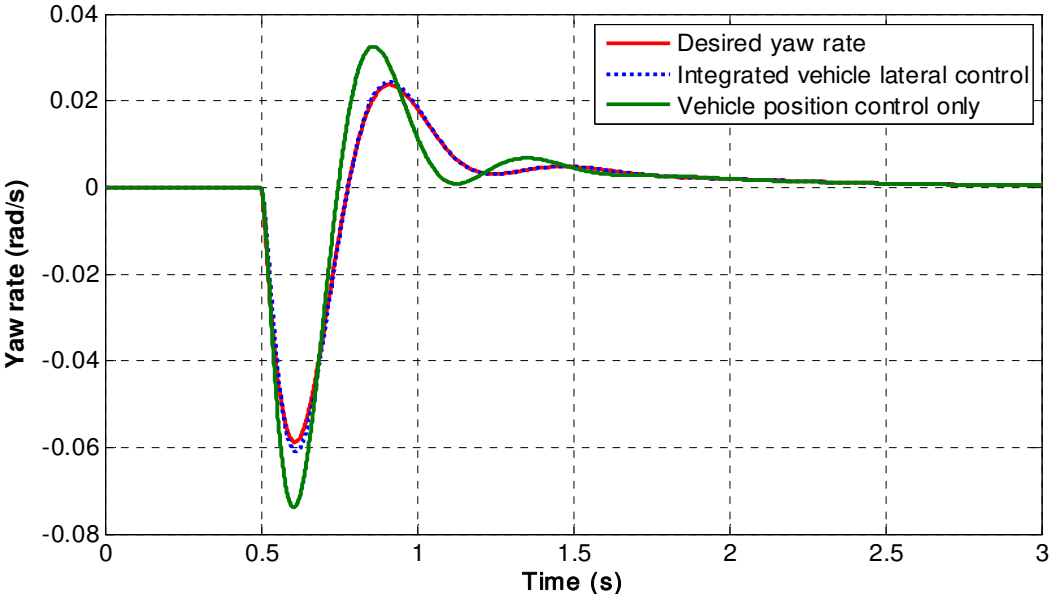

Fig.6. 10 Steering angle input for vehicle position control.

6.6 Chapter Summary

In this chapter, considering the importance of vehicle lateral control, an integrated control system that addressing both vehicle motion and position is proposed. However, the feedback signals of vehicle position and motion have different rates. How to unify the sampling rates of the two feedback loops becomes a problem. Employing the multi-rate Kalman filter in Chapter 4, an estimator that can update vehicle position more frequently is designed, and the updating rate can match with the rate of control input. This chapter can be summarized as: first of all, a combined vehicle and vision model was derived. Then, the multi-rate and uneven time-delay issues were explained and formulated. Aimed at solving the uneven and multi-rate sampling issues, multi-rate Kalman filter is designed. Finally, simulation and experiment results were demonstrated to show the effectiveness of the proposed Kalman filter, and simulations were conducted to verify the integrated control system.

Chapter 7

Conclusions and Future Works

7.1 Conclusions

In this dissertation, new estimation methodologies considering multi-rate and time delay issues were developed based on the inter-sample residual estimation technique, and were then applied to vision-based state estimation and control systems for electric vehicles. What should be highlighted are, the proposed multi-rate Kalman filter address inter-sampling performances during intermittent periods of sensor measurements, and therefore can smooth estimation performance. In addition, it can serve as a general solution for state estimation with multi-rate and delayed measurements. That it, this method is not only applicable for vision-based system, but can also be applied to chemical process monitoring and control, GPS-based estimation and control, etc.

Moreover, this dissertation raised an interesting topic for EV motion control that, besides the advantages that are inherently available, what kind of unique challenges are brought by EVs and what are the countermeasures for control performance improvement. For example, the control periods of conventional vehicles are tens of milliseconds or hundreds of milliseconds, and no problem exist if the feedback information is slow as long as the input and output match with each other. However, in case of EVs, the sampling frequency of the actuators (IWMs) is high and a consistent feedback rate is desirable in consideration of control performance. In this dissertation, the above problems were solved using a multi-rate Kalman filter with inter-sampling compensation. On the other hand, from the viewpoint of vehicle safety and stability control, some vehicle states need to be estimated instead of direct measurement, and non-traditional sensor configurations can be a solution for robust estimation against model uncertainties. For example, a body slip angle estimation methodology that is robust against vehicle parameter varying was proposed using a new type of sensor configuration.

7.1.1 Multi-rate Estimation Considering Measurement Delay

The proposed multi-rate Kalman filter is aimed at enhancing inter-sampling performances of the estimation. Based on different delay periods, this dissertation investigated two situations: multi-rate measurements with constant delay and multi-rate measurements with random delay. Both of the two issues were solved based on the inter-sample residual estimation technique.

For the multi-rate and constant delay issue, the system was first augmented using the delayed measurements, and a Kalman filter was then built based on the augmented system. To smooth sampling intervals of the primary measurements, an inter-sampling residual estimation method was developed. Demonstrated by the convergence analysis, the Kalman filter with inter-sample residual compensation was better than the without case in terms of convergence performance and, was naturally better than the single-rate Kalman filter.

Considering that state augmentation can be complex for random delay case, a measurement (residual) reconstruction method was employed to deal with the delay issue. After reconstruction, the constant sampling with random delay issue was transformed to a random sampling without delay one. Again, with inter-sample residual estimation approach, the “blank” steps were compensated and smoothed. Convergence analyses were also conducted to verify the proposed method.

7.1.2 Vision-based Multi-rate Estimation and Control for EVs

Onboard vision systems are becoming more and more popular in nowadays vehicles and this dissertation investigated two estimation and control applications using onboard camera based on the afore-proposed multi-rate Kalman filter.

Robust estimation of vehicle states such as body slip angle is a challenging issue for vehicle motion control systems. Considering the unobservability and model uncertainty issues, a non-traditional sensor configuration that combines gyro sensor and onboard vision system was explored for robust estimation of body slip angle. As gyro signal and visual information have different sampling characteristics, the multi-rate Kalman filter with delayed information augmentation was employed for better estimation performance. The estimated body slip angle was then utilized by a 2DOF controller for stability control. The proposed estimator and controller were verified by both simulations and experiments.

Yaw motion control and vehicle position control have been independently investigated for

decades. However, this is not enough in some situations. For example, even if the yaw rate is controlled to be zero, the vehicle may deviate from the desired path; on the other hand, the vehicle may spin even the vehicle is kept within the lane. Therefore, this dissertation proposed an integrated lateral control system that manipulates vehicle yaw motion and position together for EVs. Considering the fast control input characteristics of EVs, a multi-rate Kalman filter with measurement reconstruction method was employed to provide vehicle position information with adequate updating frequency. The estimator was tested by both simulations and experiments, and the effectiveness of the controller was verified by simulations.

7.2 Future Works

This dissertation addressed both theories and applications, i.e., new multi-rate estimation methods and new vision-based applications for EVs were investigated. However, there remain some open issues for future improvements.

→ Theory aspect:

For measurement updates of a Kalman filter, two important factors have to be considered, i.e., Kalman gain and residual. This dissertation solved the inter-sample residual issue, but simplified the problem by keeping a constant Kalman gain during inter-sampling periods of the visual measurements. The future work can be: find characteristics for visual measurements, i.e., design the noise covariance of the visual measurements in a better way. Also, online tuning of process noise is a challenging but interesting topic.

→ Application aspect:

Experimental verification of the integrated vehicle lateral control system should be conducted. Also, fault detection and isolation methods for visual information can be studied in case of the malfunction of the vision system. On the other hand, vision system provides additional information on vehicle states that can be utilized for the fault detection of other onboard sensors and actuators.

Appendix A

Experimental Electrical Vehicle Introduction

The experimental vehicle used in this research is a single-seat EV with IWMs, as shown in Fig. A.1. The prototype is produced by Toyota Auto Body Co., Ltd., and it was modified for studies related to capacitor and motion control [103] by our laboratory. The vehicle's specification is given in Table A.1.

The vehicle structure and sensor configurations are shown in Fig. A.2. In this vehicle, 28 electric double-layer capacitor (EDLC) modules with a total voltage of 210 V were installed, and they were directly connected to an inverter to drive the two IWMs attached in the rear wheels. The maximum speed of this vehicle can reach up to 45 km/h. For the steering system, a Maxon DC motor was installed to drive the front-steering shaft, and it can operate with steer-by-wire function. A PC104 embedded computer with real-time Linux system was employed for vehicle control, and the control program was configured to run at the speed of one millisecond per cycle. Based on the measured and estimated vehicle state information, the controller calculates the desired torques in real time and gives the commands to the inverter for torque generation. For vehicle state measurement and estimation, several sensors were installed. An accelerometer/gyro-integrated sensor was installed in the vehicle's CoG to

Fig.A. 1 Experimental vehicle COMS

provide longitudinal acceleration and yaw rate information. A steering angle sensor was attached to the steering shaft to detect the steering angle and direction. Wheel speed encoders were installed in the front wheels (nondriven wheels) to acquire the vehicle velocity. To evaluate the estimation results, S-400, a noncontact optical sensor produced by Corrsys-Datron was installed for online body slip angle acquisition. The onboard vision system includes a Grasshopper camera produced by Point Grey and a laptop computer for image processing. The camera was installed at the top of the vehicle with a tilt angle of 8° and a preview distance of 5.135 m, and the frame rate of the camera was set to 30 fps. The images captured by the camera were grabbed by a CARDBUS frame grabber in the laptop and then processed by the image processing program in real time. The image processing software was

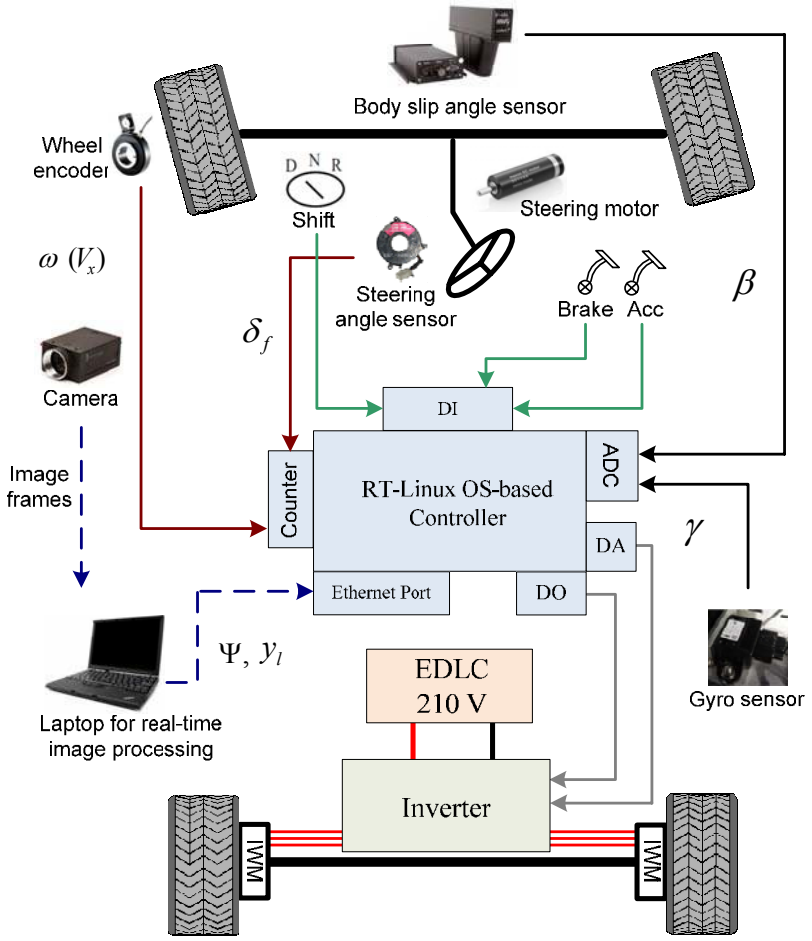

Fig.A. 2 Structure of the experimental vehicle

implemented in C++ with OpenCV and Point Grey Research's libraries, and the image processing time was designed to be constant (30 ms) for the benefit of data post-processing. The final outputs from the vision system are ψ and y_l, which were sent to the vehicle controller based on socket programming using UDP protocol.

Table A. 1 Vehicle Parameters

ITEM	Description
Vehicle Parameters	
Total mass (m)	380 kg
Distance from CoG to front axle (lf)	0.8 m
Distance from CoG to rear axle (lr)	0.6 m
Tread at rear axle (dr)	0.82 m
Wheel radius (r)	0.22 m
Front tire cornering stiffness (Cf)	6,000 N/rad
Rear tire cornering stiffness (Cr)	6,000 N/rad
Yaw moment of inertial (Iz)	136.08 N·m/(rad/s^2)
Maximum torque of IWM	100 N·m
Sensor Configurations	
Gyro/acceleration integrated Sensor	Nissan EWTS53BC
Steering angle sensor	Nissan 47945-AS500
Wheel encoder	Aisin AW
Acceleration pedal sensor	Toyota Auto Body
Brake on/off sensor	Toyota Auto Body
Body slip angle sensor	CORRSYS-DATRON S-400
Onboard camera	Point Grey GRAS-03K2M
Control System	
Inverter	Myway (PWM Vector Control)
Sampling time	0.001 s
Operation system	Real-time Linux
Control computer	PC104 board, A/D board, D/A board, Counter board

Appendix B

Image Processing Techniques for Lane Detection

To feedback vehicle position information in real time, vision system (hardware) and image program (software) are indispensable. The vision system setup is illustrated in Fig. B.1. The images are first captured by the camera, and are then sent to the laptop for image processing. Finally, the processed signals are sent to vehicle controller.

For the image program, it basically has two parts: transform image plane to road plane and lane detection/extraction.

Mapping from image plane to road plane:

Camera can map 3-dimensional world onto its 2-dimensional image view, however, this kind of mapping lose important information such as depth and that is why many researches use stereo camera instead of single one. For the application of road information capturing, since common road can be simplified as planar, i.e., the coordinate in vertical direction is zero, a monocular camera is fairly enough to correlate pixels of the image with real road. In case of roads with slope, grade estimation methods can be employed to compensate the influence of road shape [111], [112].

Fig. B.2 shows the geometric relationships among pinhole camera, image plane and road plane. To find the mapping matrix from image coordinate to road coordinate, one typical method is to calibrate the camera model C which is composed of both intrinsic and extrinsic

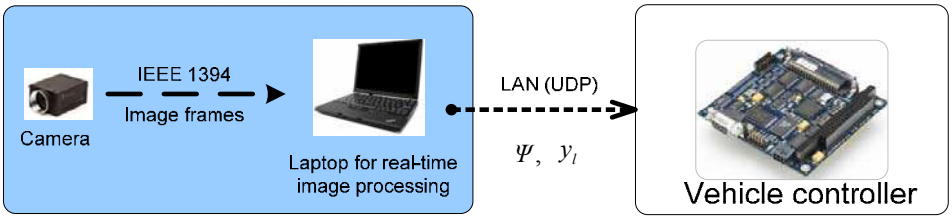

Fig.B. 1 Structure of the experimental vehicle

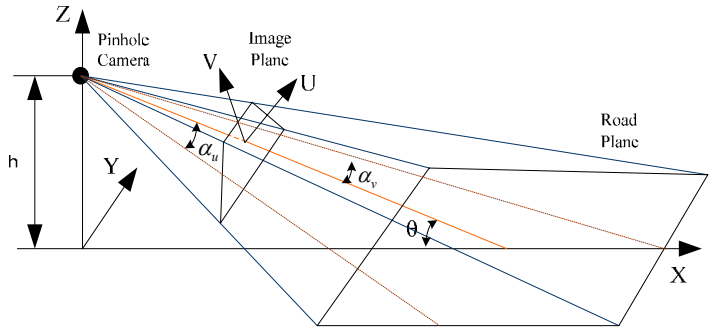

Fig.B. 2 Geometric relationship among camera, image plane and road

parameters, this model can be expressed as equation B.1, where K is the intrinsic parameter matrix, R and V are the rotational matrix and translating vector, respectively.

$$C = K[R \mid V] \tag{B.1}$$

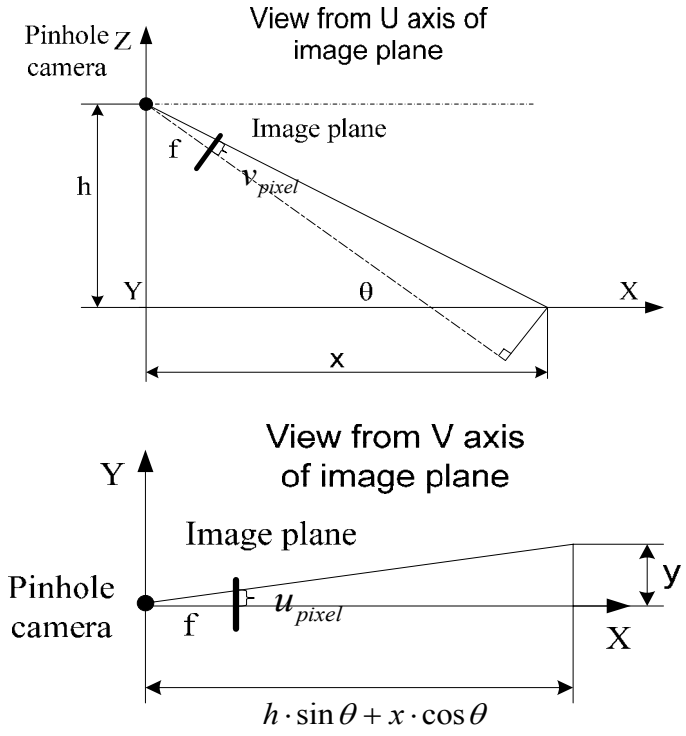

Fig.B. 3 View from different of image plane axes

The above method needs complex calibration, and another more straightforward method to get road coordinates from image pixel positions is to derive functions based on geometric relationships as shown in Fig. B.1 [104]. For better demonstration, Fig. B.2 is reconstructed as Fig. B.3 from *U* and *V* axes of the image plane.

It is desirable to analyze one arbitrary pixel in the image plane and its projection on road plane. In Fig. B.3, h is the height of camera, f is focal length, θ is camera inclination angle, α_v and α_u are angle of view in vertical and horizontal axis of image planes respectively, (u_{pixel}, v_{pixel}) is a arbitrary pixel coordinate in the image plane. Assume the resolution of image is m by n, the following functions mapping road coordinate to pixel coordinate can be derived.

$$\begin{aligned} u_{pixel} &= \frac{m-1}{2} \cdot (1 + \frac{h - x \cdot \tan\theta}{h \cdot \tan\theta + x} \cdot \cot\alpha_v) + 1 \\ v_{pixel} &= \frac{n-1}{2} \cdot (1 - \frac{y}{h \cdot \sin\theta + x \cdot \cos\theta} \cdot \cot\alpha_u) + 1 \end{aligned} \tag{B.2}$$

From the two equations, given any pixel in the image plane, the corresponding road coordinate can be calculated. After pixel remapping, a new 2-D array of pixels is generated, and the resulting image represents a bird view of the road region in front of the camera/vehicle. From the above equations, it can be known that, the row of pixel coordinate only has relationship with x coordinate of road plane, while the column of pixel coordinate correlate with both x and y coordinate of road plane.

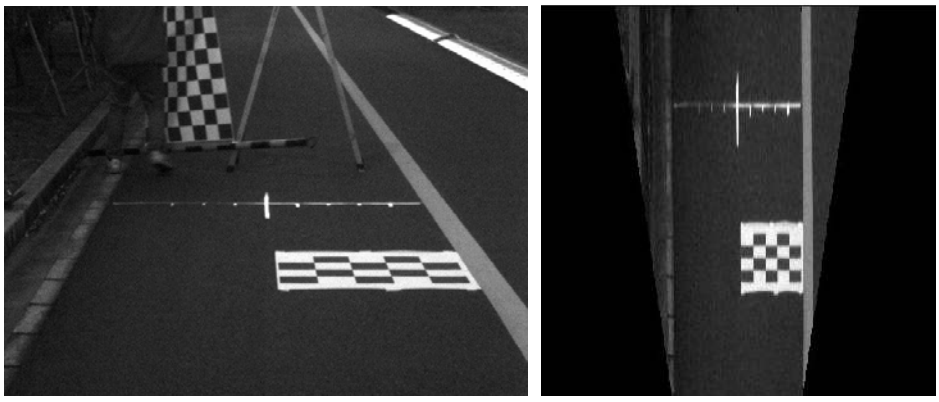

Fig.B. 4 Original and mapped view of the road.

Lane detection and extraction:

In most applications, the key road feature that needs to be sensed is lane. Thanks to the strong brightness contract between road and lane, the two can be distinguished with suitable algorithm. Since images contain noise more or less, it is desirable to smooth the image before applying lane finding algorithm. Two typical smoothing algorithms are Wiener filter and Median filter. Wiener filter performs as a low pass filter in the area where there are no edges, and it can remove blurs due to linear motion or unfocussed optics which is common for the images captured by on-board cameras; Median filter is an effective nonlinear filter that can suppress isolated noise without blurring sharp edges, specifically, the filter replaces a pixel by the median of all pixels in the neighborhood. Another effective method for image smoothing is Gaussian filter. The Gaussian filter gives more weight to the current pixel position and then tapers the weights as distance increases according to the Gaussian formula. By weighting a pixels contribution to the final pixel value, this filter can better preserve edges than the Median filter which specifies equal weights to all pixels within the filter window. The 2-D Gaussian filter written in Cartesian coordinates x and y, with Gaussian standard deviation of σ and centered on zero has the form of equation B.3.

$$G(x, y) = \frac{1}{2 \cdot \pi \cdot \sigma^2} e^{\frac{-(x^2+y^2)}{2 \cdot \sigma^2}} \tag{B.3}$$

After pre-processing, the lane detection algorithm can be implemented. The most common used feature extraction methods are Sobel and Laplacian. Sobel operator performs a 2-D spatial gradient measurement on an image, it uses a pair of 3x3 convolution masks, one estimating the gradient in the x-direction while the other estimating the gradient in the y-direction; the mask slide over the image, manipulating a square of pixels at a time; unlike the Sobel method which approximates the gradient, Laplacian operator is a convoluted mask to approximate the second derivative, and checks for zero crossings, i.e., when the resulting value goes from negative to positive or vice versa, the regions of rapid intensity change can be highlighted; Laplacian is therefore often used for edge detection. The Laplacian $L(x,y)$ of an image with pixel intensity values $I(x,y)$ is given by

$$L(x, y) = \frac{\partial^2 I}{\partial x^2} + \frac{\partial^2 I}{\partial y^2} \tag{B.4}$$

The above mentioned methods is a two step process. Alternatively, Laplacian of Gaussian (LoG) method can perform the same function in a one step manner as equation B.5.

$$\begin{aligned} LoG(x,y) &= LoG_{xx}(x,y) + LoG_{yy}(x,y) \\ &= -\frac{1}{\pi \cdot \sigma^4} \cdot \left(1 - \frac{x^2+y^2}{\pi \cdot \sigma^2}\right) \cdot e^{\frac{-(x^2+y^2)}{2 \cdot \sigma^2}} \end{aligned} \tag{B.5}$$

LoG will give zero to the uniform region of the image; wherever a change occurs, the LoG will give a positive response on the darker side and a negative response on the lighter side, and hence the lane can be extracted.

Although the white lane can be extracted from the image using the methods above, the position of white pixels is still unknown; since most of the applications need exact lane position, it is desirable to locate the lane quantitatively, for example, get gradient and intercept of the lane in the image plane. In this study, RANdom SAmple Consensus (RANSAC) algorithm is adopted to generate the solution. This is a re-sampling technique that gives solutions by using the minimum number data required for model estimation. RANSAC randomly selects smallest data set and solve for the model parameters; then find how many data items in total fit the model with the calculated parameters within a user given tolerance; if the fitting ratio is big enough, accept fit and exit with success, otherwise proceed to prune outliers. The image process examples are shown in Fig. B.5.

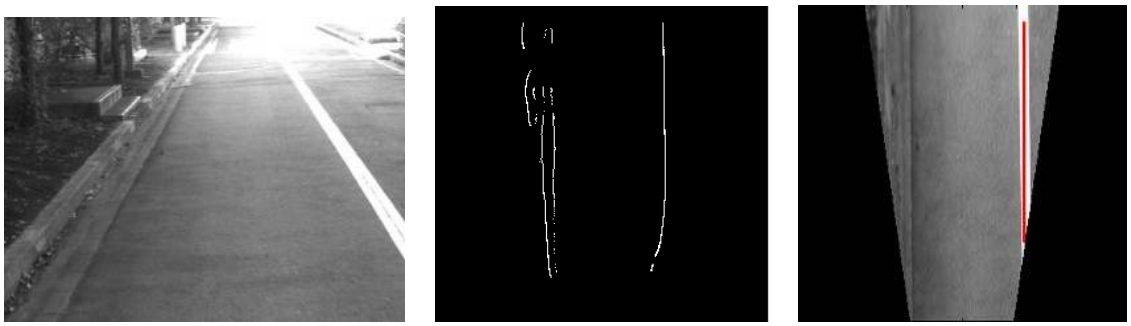

Fig.B. 5 Image processing results (from left to right: original image, Binarized image, Lane fitting result).

Bibliography

[1] H. Fujimoto, “General framework of multirate sampling control and application to motion control systems,” Ph.D Dissertation, The University of Tokyo, 2000.

[2] Glasson, Douglas P, “Development and application of multirate digital control,” Control Systems Magazine, pp. 2-8, 1983.

[3] Hara, T.; Tomizuka, M., "Multi-rate controller for hard disk drive with redesign of state estimator," American Control Conference, 1998. Proceedings of the 1998, vol.5, no., pp.3033-3037 vol.5, 21-26 Jun 1998.

[4] T. Hara and M. Tomizuka, “Performance enhancement of nulti-rate controller for hard disk drives,” IEEE Transactions on Magnetics, March 1999, pp. 898-903.

[5] Phillips, A.M., Tomizuka, M., "Multirate estimation and control under time-varying data sampling with applications to information storage devices," American Control Conference, 1995. Proceedings of the, vol.6, no., pp.4151-4155, vol.6, Jun, 1995.

[6] S. Wu and M. Tomizuka, “Multi-rate Digital Control with Interlacing and Its Application to Hard Disk Drives,” Proceedings of the 2003 American Control Conference, Denver, June 4-6, pp. 43474352, 2003.

[7] Y. Gu and M. Tomizuka, “Multi-Rate Feedforward Tracking Control for Plants with Nonminimum Phase Discrete Time Models,” Transactions of the ASME, Journal of Dynamic Systems, Measurement and Control, Vol. 123, pp. 556-560, 2001.

[8] Tomizuka, M., “Multi-rate control for motion control applications,” The 8th IEEE International Workshop on Advanced Motion Control, pp. 21- 29, March 2004.

[9] Hiroshi Fujimoto, Yoichi Hori, Takashi Yamaguchi, and Shinsuke Nakagawa, “Proposal of Perfect Tracking and Perfect Disturbance Rejection Control by Multirate Sampling and Applications to Hard Disk Drive Control”, in Proc. 38th IEEE Conference on Decision and Control (CDC99), pp. 5277 – 5282, Phoenix, 1999.

[10] Hiroshi Fujimoto, Yoichi Hori, and Atsuo Kawamura, “High Performance Perfect Tracking Control Based on Multirate Feedforward / Feedback Controllers with Generalized Sampling Periods”, in Proc. 1999 IFAC World Congress, vol. C, pp. 61 –66, Beijing, 1999.

[11] H. Fujimoto, Y. Hori and A. Kawamura, Perfect Tracking Control Based on Multirate Feedforward Control with Generalized Sampling Periods, IEEE Trans. on Industrial Electronics, Vo1.48, No.3, pp.636-644, 2001.

[12] A. Al-Mamun, T. Suthasun, S. M. Sri-Jayantha, and T. H. Lee, “Multirate controller for dual actuated servomechanism in hard disk drive,” Control Intell. Syst., pp. 32-43, January 2007.

[13] Hiroshi Fujimoto, "Short-Span Seeking Control of Hard Disk Drives with Multirate Vibration Suppression PTC", *IEEJ Transactions on Electrical and Electronic Engineering*, vol. 4, No. 2, pp. 184--191, 2009.

[14] Sato, T.; Hattori, Y.; Araki, N.; Konishi, Y.; , "Design of a hard disk drive control system in a multirate system for improvement in the steady-state intersample response," Advanced Control of Industrial Processes (ADCONIP), 2011 International Symposium on , vol., no., pp.120-123, 23-26 May 2011

[15] D-J. Lee and M. Tomizuka, “Multirate optimal state estimation with sensor fusion,” Proceedings of the 2003 American Control Conference, Denver, June 4-6, pp. 2887-2892, 2003.

[16] Andrew Smyth, Meiliang Wu, “Multi-rate Kalman filtering for the data fusion of displacement and acceleration response measurements in dynamic system monitoring,” Mechanical Systems and Signal Processing, Volume 21, Issue 2, February 2007, Pages 706-723.

[17] Koseki, T.; Patterson, G.; Suzuki, T., "Visual state feedback digital control of a linear synchronous motor using generic video-camera signal," Electrical Machines and Systems, 2008. ICEMS 2008. International Conference on, vol., no., pp.1095-1100, 17-20 Oct. 2008.

[18] Ravindra D. Gudi, Sirish L. Shah, Murray R. Gray, "Adaptive multirate state and parameter estimation strategies with application to a bioreactor", AIChE Journal Volume 41, Issue 11, pages 2451–2464, November 1995.

[19] Fujimoto, H.; Hori, Y., "Visual servoing based on multirate sampling control-application of perfect disturbance rejection control," Robotics and Automation, 2001. Proceedings 2001 ICRA. IEEE International Conference on , vol.1, no., pp. 711- 716 vol.1, 2001.

[20] Fujimoto, H.; Hori, Y., "Visual servoing based on intersample disturbance rejection by multirate sampling control-time delay compensation and experimental verification," Decision and Control, 2001. Proceedings of the 40th IEEE Conference on , vol.1, no., pp.334-339 vol.1, 2001.

[21] Fujimoto, H.; Hori, Y., "High speed robust visual servoing based on intersample estimation and multirate control," Advanced Motion Control, 2002. 7th International Workshop on, vol., no., pp. 104- 109, 2002.

[22] David McNeil Mayhew, “Multi-rate Sensor Fusion for GPS Navigation Using Kalman Filtering,” Master Thesis, Virginia Polytechnic Institute and State University, 1999.

[23] B. M. Nguyen, “Research on sideslip angle estimation using GPS and multi-rate Kalman filter for electric vehicle stability control,” Master Thesis, The University of Tokyo, 2012.

[24] Sakata, Koichi, “Multirate Control Techniques for Fast and Precise Positioning and Applications to High-Precision Stages,” PhD Dissertation, Yokohama National University, 2011.

[25] Takayuki Shiraishi and Hiroshi Fujimoto, “Positioning Control for Piezo Scanner using Multirate Perfect Inverse Model Based Iterative Learning Control,” in Proc. Proc. IEEE/ASME International Conference on Advanced Intelligent Mechatronics, Montreal, pp.993-998, 2010.

[26] A. Gelb, Applied Optimal Estimation, The Analytical Sciences Corporation, 1974.

[27] Bak, M., Larsen, T.D., Norgaard, M., Andersen, N.A., Poulsen, N.K., Ravn, O., “Location estimation using delayed measurements,” Advanced Motion Control, 5th International Workshop on, pp.180-185, 1998.

[28] R. Amirthalingam, S.W. Sung, J.H. Lee, Two-step procedure for data-based modeling for inferential control applications, AIChE J. 46 (2000) 1974–1988.

[29] Gavrilets, V. “Autonomous Aerobatic Maneuvering of Miniature Helicopters: Modeling and Control,” Ph.D Dissertation, Massachusetts Institute of Technology, 2003.

[30] T.D. Larsen, N.A. Andersen, O. Ravn, N.K. Poulsen, “Incorporation of time delayed measurements in a discrete-time Kalman filter,” in Proceedings of the 37th IEEE Conference on Decision & Control, Tampa, FL, USA, pp. 3972–3977, 1998.

[31] H.L. Alexander, “State estimation for distributed systems with sensing delay,” SPIE: Data Structures and Target Classification 1470, pp. 104–111, 1991.

[32] R. van der Merwe, “Sigma-point Kalman filters for probabilistic inference in dynamic state-space models,” Ph.D. Dissertation, OGI School of Science & Engineering- Oregon Health & Science University, 2004.

[33] Natori, K., Tsuji, T., Ohnishi, K., Hace, A.; Jezernik, K., “Time-Delay Compensation by Communication Disturbance Observer for Bilateral Teleoperation Under Time-Varying

Delay," Industrial Electronics, IEEE Transactions on, vol.57, no.3, pp.1050-1062, March 2010.

[34] Bhanderi, D., "Attitude Estimator for Rømer," M.Sc. Thesis, Aalborg University, June, 2001.

[35] Ajit Gopalakrishnan, Niket S. Kaisare, Shankar Narasimhan, "Incorporating delayed and infrequent measurements in Extended Kalman Filter based nonlinear state estimation," Journal of Process Control, Volume 21, Issue 1, January 2011, Pages 119-129.

[36] Bavdekar, V. A., Prakash, J., Patwardhan, S. C., & Shah, S. L. "Moving window ensemble Kalman filter for delayed and multi-rate measurements," In Proceedings of 18th IFAC world congress, Milano, Italy, August, 2011.

[37] Cariou, C., Lenain, R., Thuilot, B., Martinet, P., "Motion planner and lateral-longitudinal controllers for autonomous maneuvers of a farm vehicle in headland," Intelligent Robots and Systems, 2009. IROS 2009. IEEE/RSJ International Conference on , vol., no., pp.5782-5787, 10-15 Oct. 2009

[38] Yoichi Hori, "Future Vehicle driven by Electricity and Control-Research on Four Wheel Motored-UOT Electric March II," IEEE Trans. on Ind. Electron., vol.51, no.5, Oct.2004.

[39] C. Geng, L. Mostefai, M. Denai and Y. Hori, "Direct Yaw-Moment Control of an In-Wheel-Motored Electric Vehicle Based on Body Slip Angle Fuzzy Observer", IEEE Trans. Ind. Electron., vol. 56, no. 5, pp.1411-1419, May 2009.

[40] H. Yoichi, "Motion control of electric vehicles and prospects of supercapacitors," IEEJ Trans Elec Electron Eng, vol.4, no.2, 2009.

[41] N. Matsumoto, H. Kuraoka, M. Ohba, "An experimental study on vehicle lateral and yaw motion control," IECON '91., vol., no., pp.113-118 vol.1, 28, Nov. 1991.

[42] Egami, S., Fujimoto, H., "Range extension control system for electric vehicles based on front and rear driving force distribution considering load transfer," IECON 2011, vol., no., pp.3852-3857, 7-10 Nov. 2011.

[43] Fujimoto, H., Sumiya, H., "Advanced safety range extension control system for electric vehicle with front- and rear-active steering and left- and right-force distribution," Advanced Intelligent Mechatronics (AIM), 2012 IEEE/ASME International Conference on, pp.532-537, July 2012.

[44] R. Wang and J. Wang, "Fault-Tolerant Control for Electric Ground Vehicles With Independently-Actuated In-Wheel Motors," J. Dyn. Sys., Meas., Control 134, 2012.

[45] Daniel Wanner, etc., “Fault-Tolerant Control of Electric Vehicles with In-Wheel Motors through Tyre-Force Allocation,” The 11th International Symposium on Advanced Vehicle Control, 2012.

[46] Kang, J., kyongsu, Y., and Heo, H., “Control Allocation based Optimal Torque Vectoring for 4WD Electric Vehicle,” SAE Technical Paper 2012-01-0246, 2012.

[47] Lu Xiong, Zhuoping Yu, “Control allocation of vehicle dynamics control for a 4 in-wheel-motored EV,” Power Electronics and Intelligent Transportation System (PEITS), 2009 2nd International Conference on, pp.307-311, Dec. 2009.

[48] Yan Chen, Junmin Wang, “Energy-efficient control allocation with applications on planar motion control of electric ground vehicles,” American Control Conference (ACC), 2011, pp.2719-2724, June 2011.

[49] A. Viehweider, Y. Hori, “Electric Vehicle Lateral Dynamics Control based on Instantaneous Cornering Stiffness Estimation and an Efficient Allocation Scheme,” Proc. of MATHMOD 7th International Conference, Vienna, Austria, pp. 1-6, 2012.

[50] Li Feiqiang, Wang Jun, Liu Zhaodu, "On the vehicle stability control for electric vehicle based on control allocation," Vehicle Power and Propulsion Conference, 2008. VPPC '08. IEEE , pp.1-6, Sept. 2008.

[51] R. Daily, and D. M. Bevly, “The Use of GPS for Vehicle Stability Control Systems,” IEEE Trans. Ind. Electron., vol. 51, no. 2, pp.270-277, Apr. 2004.

[52] Y. Fukada, “Slip-Angle Estimation for Vehicle Stability Control”, Vehicle System Dynamics, vol. 32, no.4, pp.375-388, 1999.

[53] D. M. Bevly, J. Ryu, J.C. Gerdes, “Integrating INS Sensors With GPS Measurements for Continuous Estimation of Vehicle Sideslip, Roll, and Tire Cornering Stiffness,” IEEE Trans. Intell. Transp. Syst., vol.7, no.4, pp.483-493, Dec. 2006.

[54] A. T. van Zanten, “Bosch ESP systems: 5 Years of experience,” Proc. SAE Automotive Dynamics and Stability Conf., Troy, MI, May 2000, 2000-01-1633.

[55] Y. Aoki, T. Uchida, Y. Hori “Experimental Demonstration of Body Slip Angle Control based on a Novel Linear Observer for Electric Vehicle,” IECON 2005, 31st Annual Conference of IEEE, pp.6-10, Nov. 2005.

[56] F. Cheli, E. Sabbion, M. Pesce, S. Melzi, “A Methodology for Vehicle Sideslip Angle Identification: Comparison with Experimental Data,” Vehicle System Dynamics, vol. 45, no. 6, pp. 549-563, Jun. 2007.

[57] Christoph Arndt, Johannes Karidas, and Rainer Busch, “Design and Validation of a Vehicle State Estimator,” Proc. of AVEC’04, pp.41-45, 2004.

[58] G. Phanomchoeng, R. Rajamani, and D. Piyabongkarn, “Nonlinear Observer for Bounded Jacobian Systems, With Applications to Automotive Slip Angle Estimation,” IEEE Trans. Autom. Control, vol.56, no.5, pp.1163-1170, May 2011.

[59] C. Geng, L. Mostefai, Y. Hori, “Body slip angle observer for electric vehicle stability control based on empirical tire model with fuzzy logic approach,” IECON 2008, 34th Annual Conference of IEEE, pp.108-113, Nov. 2008.

[60] J. Yoon, W. Cho, B. Koo, and K. Yi, “Unified Chassis Control for Rollover Prevention and Lateral Stability,” IEEE Trans. Veh. Technol., vol. 58, no. 2, pp.596-609, Feb. 2009.

[61] J. C. McCall, and M. M. Trivedi, “Video Based Lane Estimation and Tracking for Driver Assistance: Survey, System, and Evaluation,” IEEE Trans. Intell. Transp. Syst., vol.7, no.1, pp.20-37, 2006.

[62] V. Cerone, M. Milanese, and D. Regruto, “Combined Automatic Lane-Keeping and Driver's Steering Through a 2-DOF Control Strategy,” IEEE Trans. Control Syst. Technol., vol. 17, no. 1, pp.135-142, Jan. 2009.

[63] V. Cerone, M. Milanese, D. Regruto, “Experimental results on combined automatic lane keeping and driver's steering,” American Control Conference, 2007, pp.3126-3131, Jul. 2007.

[64] S. Ibaraki, S. Suryanarayanan, and Masayoshi Tomizuka, “Design of Luenberger State Observers Using Fixed-structure H/sub infinity/Optimization and Its Application to Fault Detection in Lane-keeping Control of Automated Vehicles,” IEEE/ASME Trans. Mechatron., vol. 10, no. 1, pp.34-42, 2005.

[65] Rucco, A., Notarstefano, G., Hauser, J., “Dynamics exploration of a single-track rigid car model with load transfer,” Decision and Control (CDC), 2010 49th IEEE Conference on , vol., no., pp.4934-4939, 15-17 Dec. 2010.

[66] Kai-Ten Feng, Han-Shue Tan, Tomizuka, M., “Automatic steering control of vehicle lateral motion with the effect of roll dynamics,” American Control Conference, 1998. Proceedings of the 1998, pp.2248-2252 vol.4, Jun 1998.

[67] Padhy, P.K., Sasaki, T., Nakamura, S., Hashimoto, H., “Modeling and position control of mobile robot,” Advanced Motion Control, 2010 11th IEEE International Workshop on, pp.100-105, 21-24 March 2010.

[68] Kosecka, J., Blasi, R., Taylor, C.J., Malik, J., “Vision-based lateral control of vehicles,” Intelligent Transportation System, 1997. ITSC '97., IEEE Conference on, pp.900-905, 9-12 Nov 1997.

[69] Binh Minh Nguyen, etc., “GPS Based Estimation of Vehicle Sideslip Angle Using Multi-rate Kalman Filter With Prediction of Course Angle Measurement Residual,” FISITA , Nov. 2012.

[70] Anderson, R., Bevly, D.M., “Estimation of tire cornering stiffness using GPS to improve model based estimation of vehicle states,” Intelligent Vehicles Symposium, 2005. Proceedings. IEEE, pp. 801- 806, June 2005.

[71] Katsuhiko Ogata, Modern Control Engineering, Prentice Hall, 2002.

[72] K. Kawashima, T. Uchida, Y. Hori, “Rolling Stability Control of In-wheel Electric Vehicle Based on Two-Degree-of-Freedom Control,” The 24th Electric Vehicle Symposium, Stavanger, Norway, 2009.05

[73] Kanghyun Nam, Fujimoto, H., Hori, Y., “Motion control of electric vehicles based on robust lateral tire force control using lateral tire force sensors,” AIM, 2012 IEEE/ASME International Conference on, pp.526-531, July 2012.

[74] Yoichi Hori, “Comparison of Torsional Vibration Controls based on the Fast and Slow Disturbance Observers,” IPEC'95, Vol.1, pp.440-446, 1995.4, Yokohama.

[75] Sehoon Oh, Hori, Y., “Sensor Free Power Assisting Control Based on Velocity Control and Disturbance Observer,” Industrial Electronics, 2005. ISIE 2005. Proceedings of the IEEE International Symposium on, pp. 1709- 1714, June 20-23, 2005.

[76] K. Kawashima, "Research on Advanced Motion Control for Electric Vehicles," Ph.D. Dissertation, The University of Tokyo, 2009.

[77] Ando, N., Fujimoto, H., "Yaw-rate control for electric vehicle with active front/rear steering and driving/braking force distribution of rear wheels," Advanced Motion Control, 2010 11th IEEE International Workshop on, pp.726-731, 21-24 March 2010.

[78] Hiroshi Fujimoto, Akio Tsumasaka, Toshihiko Noguchi, “Direct Yaw-moment Control of Electric Vehicle Based on Cornering Stiffness Estimation,” in Proc. Annual Conference of the IEEE Industrial Electronics Society, North Carolina, pp.2626--2631, 2005.

[79] Luenberger, D. G., “Observing the State of a Linear System,” IEEE Transactions on Military Electronics, 8, pp. 74 – 80, 1964.

[80] Kalman, R. E., “Mathematical Description of Linear Dynamical Systems,” Journal Society for Industrial and Applied Mathematics, Control Series, 2, pp. 152-192, 1963.

[81] Greg Welch, Gary Bishop, An Introduction to the Kalman Filter, University of North Carolina at Chapel Hill, 2006

[82] K. Sasajima, and H. Fujimoto, “6 DOF Multirate Visual Servoing for Quick Moving Objects,” American Control Conference, 2007, ACC '07, pp.1538-1543, Jul. 2007.

[83] D. T. Phan, “The Design and Modeling of Multirate Digital Control Systems for Disk Drive Applications,” in Proceedings of the 1993 Asia-Pacific Workshop on Advances in motion control, pp.189-205, July 1993.

[84] Lewis, Frank L., Applied optimal control & estimation: digital design & implementation, Englewood Cliffs, New Jersey, Prentice Hall, 1992.

[85] Jean-Pierre Corrio, Process Control: Theory and Applications, 1st Edition, Springer, 2004.

[86] L. Kovudhikulrungsri, T. Koseki, “Precise Speed Estimation From a Low-Resolution Encoder by Dual-Sampling-Rate Observer,” IEEE/ASME Transactions on Mechatronics, Vol. 11, No. 6, pp. 661-670, Dec-2006.

[87] Fujimoto, H., Hori, Y., “Visual servoing based on multirate sampling control-application of perfect disturbance rejection control,” Proceedings 2001 ICRA. IEEE International Conference on, pp. 711- 716 vol.1, 2001.

[88] M. Choi, J. Choi, J. Park, W. K. Chung, “State estimation with delayed measurements considering uncertainty of time delay,” Proc. ICRA 2009, pp. 3987–3992, Kobe, Japan, May 2009.

[89] S. Challa, R. Evans, and X. Wang, “A Bayesian solution and its approximations to out-of-sequence measurement problems,” Journal of Information Fusion, vol. 4, issue 3, pp.185-199, Sept. 2003.

[90] J.S. Meditch, Stochastic Optimal Linear Estimation and Control, McGraw-Hill, New York, 1969.

[91] Rudolph van der Merwe, "Sigma-Point Kalman Filters for Probabilistic Inference in Dynamic State-Space Models," Ph.D. Dissertation, Oregon Health & Science University, 2004.

[92] K Nam, H. Fujimoto, Y. Hori, “Lateral Stability Control of In-Wheel-Motor-Driven Electric Vehicles Based on Sideslip Angle Estimation Using Lateral Tire Force Sensors,” IEEE Trans. Veh. Technol., vol. 61, no. 5, pp.1972-1985, Jun. 2012.

[93] K. Nam, S. Oh, H. Fujimoto, Y. Hori, “Estimation of Sideslip and Roll Angles of Electric Vehicles Using Lateral Tire Force Sensors Through RLS and Kalman Filter Approaches,” IEEE Trans. Ind. Electron., 2012, in press.

[94] M. Shino, M. Nagai, “Independent wheel torque control of small-scale electric vehicle for handling and stability improvement,” JSAE Review, vol.24, no.4, pp.449–456, Oct. 2003.

[95] J. Song, and W. S. Che, “Comparison and evaluation of brake yaw motion controllers with an antilock brake system,” Proc. IMechE, Part D: J. Automobile Engineering, vol. 222, no. 7, pp.1273–1288, 2008.

[96] R. Rajamani, “Vehicle dynamics and Control,” Springer-Verlag, Berlin, 2006.

[97] M. Abe, Vehicle Handling Dynamics: Theory and Application, Butterworth-Heinemman, 2009.

[98] Yuya Yamauchi, Hiroshi Fujimoto, “Proposal of Lateral Force Observer with Active Steering for Electric Vehicle,” in Proc. SICE Annual Conference, Japan, pp.788-793, 2008.

[99] M. Bertozzi and A. Broggi, “GOLD: A parallel real-time stereo vision system for generic obstacle and lane detection,” IEEE Trans. Image Process, Vol. 7, pp. 62-81, 1998.

[100] T.W. Kaufmann and F. Bolourchi, “Systems, methods and computer program products for lane change detection and handling of lane keeping torque,” U. S. Patent 7885730, 2008.

[101] T. Saito, S. Kudo and H. Oyama, “Lane keeping assistance equipment for automotive vehicles,” U. S. Patent 7890231, 2007.

[102] Marino, R. and Scalzi, S., “Integrated Control of Active Steering and Electronic Differentials in Four Wheel Drive Vehicles,” SAE Int. J. Passeng. Cars - Electron. Electr. Syst. 2(1):141-149, 2009.

[103] K. Kawashima, T. Uchida, and Y. Hori, “Manufacturing of Small Electric Vehicle driven only by Electric Double Layer Capacitors for Easy Experiment of Vehicle Motion Control,” Electric Vehicle Symposium 21, Apr. 2005.

[104] Muad, A.M. Hussain, A. Samad, S.A. Mustaffa, M.M. Majlis, B.Y., “Implementation of inverse perspective mapping algorithm for the development of an automatic lane tracking system,” TENCON 2004, vol. 1, pp. 207-210, 2004.

[105] Stephen Clark, “Autonomous Land Vehicle Navigation Using Millimetre Wave Radar,” PhD thesis, The University of Sydney, 1999.

[106] J. Kosecka, “Vision-based lateral control of vehicles: lookahead and delay issues,” Internal Memo, Department of EECS, University of California Berkeley, 1997.

[107] J. Kosecka, R. Blasi, C.J. Taylor, and J. Malik, “Vision-based lateral control of vehicles,” Intelligent Transportation System, 1997, IEEE Conference on, pp.900-905, Nov. 1997.

[108] K.J. Astrom, R.M. Murray, Feedback Systems: An Introduction for Scientists and Engineers, Princeton University Press, Princeton, NJ, 2009.

[109] Lilit Kovudhikulrungsri, Takafumi Koseki, “Precise Speed Estimation From a Low-Resolution Encoder by Dual-Sampling-Rate Observer,” Mechatronics, IEEE/ASME Transactions on , vol.11, no.6, pp.661-670, Dec. 2006.

[110] William S . Levine, The Control Handbook, CRC Press, 1996.

[111] Y. Sebsadji, S. Glaser, S. Mammar, J. Dakhlallah, “Road slope and vehicle dynamics estimation,” American Control Conference, 2008, pp.4603-4608, Jun. 2008.

[112] Bae, H. S., J. Ruy and J. Gerdes, “Road grade and vehicle parameter estimation for longitudinal control using GPS,” IEEE Conference on Intelligent Transportation Systems. San Francisco, CA, 2001.

List of Publications

[Journal Papers]

1. Y. Wang, B.M. Nguyen, P. Kotchapansompote, H. Fujimoto, and Y. Hori, "Image Processing-Based State Estimation for Vehicle Lateral Control using Multi-rate Kalman Filter," Recent Patents on Signal Processing, Vol. 2, No. 2, 2012.

2. Y. Wang, B.M. Nguyen, H. Fujimoto, and Y. Hori, "Multi-rate Estimation and Control of Body Slip Angle for Electric Vehicles Based on On-board Vision System," IEEE Transaction on Industrial Electronics. (Accepted)

3. Y. Wang, B.M. Nguyen, H. Fujimoto, and Y. Hori, "Vision-based Multi-rate State Estimation for Vehicle Stability Control Considering Random Measurement Delay," IEEE/ASME Transaction on Mechatronics. (To be submitted)

4. B.M. Nguyen, Y. Wang, H. Fujimoto, and Y.Hori, "Lateral Stability Control of Electric Vehicle Based on Disturbance Accommodating Multi-rate Kalman Filter Using Single Antenna GPS," Journal of Electrical Engineering & Technology. (Accepted)

[Conference Papers]

1. Y. Wang, B. M. Nguyen, P. Kotchapansompote, H. Fujimoto, Y. Hori, "Vision-based Vehicle Body Slip Angle Estimation with Multi-rate Kalman Filter considering Time Delay," IEEE ISIE 2012, Hangzhou, China.

2. Y. Wang, K. Nam, H. Fujimoto, Y. Hori, "Proposal of Multi-rate Controller for Vehicle Body Slip Angle based on Real-time Lane Detection," International Symposium on Advanced Vehicle Control (AVEC) 2012, Seoul, South Korea.

3. Y. Wang, B. M. Nguyen, H. Fujimoto, Y. Hori, "Multi-rate Estimation and Control of Body Slip Angle for Electric Vehicles," IEEE IECON2012, Canada.

4. Y. Wang, B. M. Nguyen, H. Fujimoto and Y. Hori, "Multi-rate Kalman Filter Design for Electric Vehicles Control based on Onboard Vision System with Uneven Time," IFAC Mechatronics 2013. (Accepted)

5. Y. Wang, B. M. Nguyen, H. Fujimoto and Y. Hori, “Vision-based Integrated Lateral Control System for Electric Vehicles with Multi-rate Kalman Filter Considering Uneven Time Delay,” IEEE ISIE 2013. (Accepted)

6. P. Kotchapansompote, Y. Wang, T. Imura, H. Fujimoto, Y. Hori, "Electric vehicle automatic stop using wireless power transfer antennas," IEEE IECON 2011, Nov. 2011, pp.3840-3845.

7. B. M. Nguyen, Y. Wang, S. Oh, H. Fujimoto, and Y. Hori, “GPS Based Estimation of Vehicle Sideslip Angle Using Multi-rate Kalman Filter with Prediction of Course Angle Measurement Residual,” FISITA 2012 World Automotive Congress, 2012.

8. B. M. Nguyen, Y. Wang, H. Fujimoto, and Y. Hori, “Sideslip Angle Estimation Using Multi-rate Kalman Filter with Model Error and Disturbance Compensation for Electric Vehicle Stability Control,” 8th IEEE Vehicle Power and Propulsion Conference, 2012.

9. B. M. Nguyen, Y. Wang, H. Fujimoto, and Y. Hori, “Robust Stability Control of Electric Vehicles Based on Multi-rate Disturbance Accommodating Control Using GPS,” ICM, 2013.

10. B. M. Nguyen, Y. Wang, H. Fujimoto, and Y. Hori, “Design of Double Layer State Estimator for Electric Vehicle Using Single Antenna GPS and Advanced Multi-rate Kalman Filter,” IFAC Mechatronics 2013. (Accepted)

[Proceeding Papers]

1. Y. Wang, H. Fujimoto and Y. Hori, “Integrated Lateral State Estimation and Control for Electric Vehicles using Onboard Vision System,” SNU-UT Joint Seminar 2013, Seoul, Korea.

2. Y. Wang, P. Kotchapansompote, H. Fujimoto and Y. Hori, “Multi-rate estimation for vehicle body slip angle using onboard vision system,” SNU-UT Joint Seminar 2011, Kashiwa, Japan.

3. Y. Wang, K. Nam, H. Fujimoto, Y. Hori, “Robust roll and yaw integrated control using 4 wheel steering based on yaw moment and lateral force observers,” IEEJ Technical Report, No. IIC-11-138, pp.25-30, 2011, Chiba, Japan.

The End